



Establishment of a gastrointestinal epithelial organoid assay to assess bowel toxicity in response to chemoradiation treatment

Gabrielle Price

Balliol College

Master of Science by Research in Oncology
Supervisor: Prof Anne Kiltie
Word count: 18,152

CRUK/MRC Oxford Institute for Radiation Oncology Department of Oncology University of Oxford

June 2019

Acknowledgements

I would like to express immense appreciation to my thesis advisor, Professor Anne Kiltie, for extending the offer to be a member of her lab and allowing me to conduct cutting-edge research under her tutelage. Prof Kiltie was very encouraging and reassuring when helping me along this journey. Her passion for conducting research that can impact and improve the lives of the patients is very commendable. I am grateful for the many intriguing scientific discussions we have had and the guidance she has provided, which have shaped me as a future physician-scientist.

I am extremely grateful to Dr Jia-Ling Ruan, a postdoctoral fellow in the Kiltie lab who provided direct and close mentorship. Jia-Ling is an esteemed and incredibly knowledgeable scientist who was always present to provide support, assistance and feedback. Jia-Ling was always very encouraging and imparted wisdom when I needed help with my project. She challenged me to think critically and independently about my experimental process. The project was made possible by the grants that Jia-Ling and Anne drafted and submitted.

I would like to extend thanks to the rest of the members of the Kiltie lab; they provided a constructive and encouraging lab environment and were always helpful in providing feedback. Their motivation and encouragement that contributed to my growth as a budding researcher. I hope that the lab and all of the members are prosperous and successful in their future endeavours.

Lastly, I would like to thank my family for their emotional support and for providing me with the opportunity to study for this degree.

Declaration

This dissertation is submitted for the degree of Master by Research in Oncology. I hereby declare that the results presented in this thesis are my own, except where individuals are acknowledged in the figure legends. The dissertation does not exceed the prescribed word limit.

Table of Contents

1. INTRODUCTION 12
1.1 Muscle-invasive bladder cancer (MIBC) 12
The function and biology of the bladder 12
The origin of MIBC 12
Epidemiology and aetiology of bladder cancer 13
Staging of bladder cancer 13
1.2 Treatment modalities for MIBC 15
Clinical relevance of chemoradiation treatment for MIBC 15
Chemoradiation drugs 16
1.3 Radiation-induced DNA damage response 19
1.4 Sensitivity to radiation of the bladder 20
Underlying mechanisms 20
Side effects 21
1.5 Toxicities from administration 21
Gastrointestinal toxicity 22
1.6 Sensitivity to radiation of the small intestine 22
Underlying mechanisms 22
Side effects 23
1.7 Cellular regulation of the intestine 23
1.8 Intestinal organoids as a physiologically suitable 3D model of cellular proliferation and differentiation 28
1.9 Previous applications of organoids to assess toxicity 30
1.10 Aims of the thesis 31
2. MATERIALS AND METHODS 33
2.1 Maintenance and culture of gastrointestinal organoids 33
Isolation of mouse gastrointestinal organoids 33
Passaging of mouse gastrointestinal organoids 35
Freezing of cryopreserved mouse gastrointestinal organoids 38
Thawing of cryopreserved mouse gastrointestinal organoids 38
2.2 Imaging 39
2.3 Image analysis 39
ImageJ 39

Manual imageJ scoring using the wand tracing tool 40
Manual scoring by outlining 40
2.5 Organoid drug treatment 41
2.6 Organoid irradiation 42
2.7 Organoid chemoradiation treatment 42
2.8 Statistical analysis 43
3. RESULTS 44
3.1 Refinement of murine small intestinal organoid culture system 44
3.1.1 Optimising the Matrigel concentration and seeding density 44
3.1.2 Phenotype of intestinal organoids 45
3.1.3 Relationship between organoid size and budding 48
3.1.4 Optimal centrifugation conditions for passaging organoids 50
3.1.5 Organoid expansion potential 52
3.1.6 Recovery of cryopreserved organoids 53
3.1.7 Comparing expansion of fresh and frozen organoids 57
3.2 Assay development 59
3.2.1 Evaluating passage efficiency for organoid imaging and growth 59
3.3 Assay implementation 61
3.3.1 Organoid growth and budding is halted at doses of radiation above 2 Gy 61
3.3.2 Gemcitabine and panobinostat have the potential to induce organoid drug toxicity 63
3.3.3 Gemcitabine impedes organoid growth at 25 nM concentration 64
3.3.4 Panobinostat impedes organoid growth at 50 nM concentration 66
3.3.5 Pilot experiment: organoid growth assay showed no difference between a combination of panobinostat and irradiation versus irradiation alone 67
3.3.6 The chemoradiation assay with combinations of panobinostat, gemcitabine, and irradiation showed that gemcitabine and panobinostat minimally reduces growth at low doses 70
3.3.7 Gemcitabine minimally reduces growth at low radiation doses 70
3.3.8 Panobinostat minimally reduces growth at low radiation doses 73
3.3.9 Gemcitabine and panobinostat at low radiation doses cause a similar decrease in organoid growth compared to IR alone 75
4. DISCUSSION 77
4.1 Refinement of organoid culturing and cryopreservation method 77

Rho kinase (ROCK) inhibitor is essential for the cryopreservation of gastrointestinal organoids 79
4.2 Development of organoid assay 81
Rationale for evaluating the efficiency of organoid fragment seeding 81
4.3 Intestinal organoids under radiation or chemoradiation conditions 83
4.4 Comparing response to chemoradiotherapy to that of *in vivo* and 2D cell models 84
4.5 Limitations of the research 85
4.6 Future directions 88
5. CONCLUSION 89
6. REFERENCES 90
7. APPENDIX 102

List of Figures

Figure **Page**

1. Bladder composition and tumour invasion by stage 14
2. Mechanism of action of gemcitabine 17
3. The intestinal crypt 24
4. Adaptation of passaging protocol to obtain 50 organoids per well 37
5. Morphological characterisation of murine gastrointestinal organoid cultures 46
6. Most organoids have matured phenotypical characteristics by day six post-isolation and post-passage 48
7. Correlation between mean organoid area and number of buds on an organoid 49
8. The effect of centrifugation speed on passaging efficiency and organoid retainment 52
9. Model growth rate as measured by expansion factor 53
10. Enhanced recovery of cryopreserved intestinal organoids is dependent on culturing conditions 56
11. Recovery of cryopreserved organoids post-passage 57
12. Evaluation of organoid fragment seeding number on expansion factor 59
13. Passage efficiency for fresh organoids is best for imaging and growth when seeded at 50 organoid fragments in a matrix composition of 1:1.5 medium to Matrigel 61
14. Mean organoid area and budding after doses of irradiation up to five days post-irradiation 63
15. Mean organoid area after gemcitabine treatment up to five days post-treatment 65
16. Mean organoid area after panobinostat treatment up to five days post-treatment.. 67
17. Response to panobinostat at different radiation doses three days post-treatment (pilot experiment) 69
18. Response to gemcitabine at different radiation doses three days post-treatment 72
19. Response to panobinostat at different radiation doses three days post-treatment 74

20. Comparison organoid response to irradiation alone and gemcitabine and panobinostat at different radiation doses 76

List of Tables

Table **Page**

1. Tumour, Node, Metastasis (TNM) Classification System for bladder cancer 15
2. Number of titrations of intestinal tissue for each PBS wash during organoid isolation 34
3. Number of titrations of intestinal tissue with 1% BSA in PBS for collection of each organoid fragment fraction during organoid isolation 34
4. Composition of organoid growth medium 35
5. Total volume added to each well of a 24-well plate to achieve respective gemcitabine concentrations 41
6. Total volume added to each well of a 24-well plate to achieve respective panobinostat concentrations 41
7. Total dose given to each well of a 24-well plate during organoid irradiation experiments 42
8. Doses given to each column of the 24-well plate to deliver the required total dose 43

Abstract

Introduction

Chemoradiation is the most common non-surgical treatment for MIBC. However, chemoradiation is associated with acute and late intestinal toxicity, as irradiation (IR) of the surrounding small bowel and rectum is virtually inevitable. In the search for new, less toxic radiosensitisers, it is important to have an assay to determine normal intestinal toxicity. To meet this need, we have investigated whether gastrointestinal toxicity can be predicted *ex vivo* through the use of organoids. Particularly, we determined a range of doses that are safe to the gastrointestinal tract in order to study bowel toxicity to chemoradiation. The ultimate aim is to develop an assay that determines organoid response to irradiation/radiosensitiser combinations, which can recapitulate the *in vivo* normal tissue toxicity assay from animals.

Methodology

Crypts were isolated from the small intestine of mice and cultured in organoid medium containing growth factors. For subculture, organoids cultured on day 7 were passaged. Undissociated organoids were cryopreserved by resuspension in freezing medium. One month after cryopreservation, organoids were thawed with or without Rho kinase inhibitor and subjected to different seeding conditions. The protocol for passaging was modified to achieve optimal organoid formation efficiency. Efficiency of organoid fragment seeding was quantified based on variable Matrigel concentrations and densities of organoid fragment seeding. The assay was tested by irradiating organoids at doses between 0.5 Gy to 6 Gy and treating organoids with variable concentrations of radiosensitisers gemcitabine and panobinostat. Irradiation and drugs were combined to assess whether the organoid response to chemoradiotherapy treatment recapitulated *in vivo* results.

Results

Organoid cryopreservation techniques were refined such that a collection of murine intestinal organoids has been established (n=32). Organoids were successfully cryopreserved and had good freeze-thaw efficiency with 86% survival. Recovery and subsequent growth of cryopreserved organoids was significantly improved by adding Rho-kinase inhibitor to the freezing medium and after thawing procedures. During assay development, seeding 50 organoid fragments per well in a 24-well plate was found to result in the optimum organoid density that allowed for adequate growth and imaging. More favourable organoid formation efficiencies were seen using Matrigel concentrations 1.5 times that of the organoid fragment-suspension medium volume, compared to a one-to-one ratio of medium and Matrigel ($p=0.03$).

When testing the assay, organoid growth and budding was not affected by radiation doses lower than 2 Gy. For organoids that received 2 Gy radiation, budding was halted and there was premature disaggregation (10-15%), where epithelial cells had shed into the lumen, by day 3 post-irradiation. Administration of doses higher than 2 Gy resulted in significant disaggregation (>80%) as soon as 24 hours after irradiation.

For organoids exposed to gemcitabine and panobinostat, significant disaggregation began at doses of 25 nM and 50 nM respectively. Decreased organoid growth was seen when combining the drugs with radiation that was indicated by a decrease in organoid size.

Conclusion

The development of this assay could present a promising modality for assessing the outcome of chemoradiation combinations on the small intestine. This assay is being adapted for use in patient-derived intestinal organoids.

1. INTRODUCTION

1.1 Muscle-invasive bladder cancer

The function and biology of the bladder

The bladder is a muscular organ composed of individual tissue layers. It is responsible for holding concentrated urine secreted by the kidneys. The kidneys filter out potentially hazardous ions and solutes from the bloodstream and metabolic waste ends up in the urine which then is held in the bladder until voiding (Khandelwal et al., 2009). The exchange of compounds and water between the urine, tissue and bloodstream is physically restricted by the urothelium, a mucosal lining composed of 5-7 stratified epithelial layers containing basal, intermediate, and luminal cells (Khandelwal et al., 2009). The urothelium covers the urinary system including the pelvis, ureter, bladder and urethra. It provides a tight barrier due to the specialised umbrella cells that are made up of a membrane containing urothelial plaques, which are composed of highly ordered transmembrane uroplakin proteins (Kreplak et al., 2007). These specialised cells in combination with tight junction proteins and an apical glycan layer act as a barrier to water, toxic compounds, and solutes in the urine (Hurst et al., 1987). The urothelium is recycled by the division of progenitor cells in the basal layer beneath the umbrella cells (Wu, 2009). The frequency of proliferation in the urothelium is dependent on whether the urothelium has been subjected to injury or inflammation. Damage to the urothelium causes an increase in tumour rate (Michaud, 2007).

The origin of MIBC

Muscle-invasive bladder cancer (MIBC) is a malignancy that has invaded the muscle of the bladder wall (National Institute for Health and Care Excellence, 2015) and affects a significant number of individuals. It is the ninth most common cancer worldwide, with an estimated 430,000 new cases every year (Antoni et al., 2017). Most bladder cancers are described as urothelial carcinoma (UC) cases because they originate from the urothelial cell layer. Tumours of the bladder arise from

urothelial abnormalities such as non-invasive papillary lesions and carcinoma in situ-like lesions (Batavia, 2014).

Epidemiology and aetiology of bladder cancer

Smoking is the primary risk factor for bladder cancer, and individuals who smoke are three times as likely to develop bladder cancer compared to non-smokers (van Osch et al., 2016). Moreover, approximately one-quarter of bladder cancers in women and half of bladder cancers in men have been linked to smoking. A meta-analysis has concluded that an individual's occupational environment is the second most common risk factor for bladder cancer and has linked occupational hazards to 5% of all bladder cancers (van Osch et al., 2016). Specifically, workers that are exposed to carcinogens such as aromatic amines, polycyclic aromatic hydrocarbons, combustion products or heavy metals have an increased risk of developing bladder cancer (Cumberbatch et al., 2015). There is a gender disparity associated with bladder cancer, as men are more likely to be diagnosed with the disease (70% of cases). This discrepancy is most likely attributed to biological factors such as anatomy and sex hormone composition, because gender-specific risk differences persists even after adjusting for major risk factors including smoking and occupational hazards (Zhang, 2013).

Staging of bladder cancer

Bladder cancer is categorised based on invasion and spread of the tumour. The tumour stage describes how deeply the tumour has grown into the bladder wall and whether it has extended to other organs. Non muscle-invasive bladder cancer (NMIBC) comprises stages Ta, Tis, and T1, and MIBC comprises stages T2-T4 (Figure 1, Table 1). If a tumour invades the muscle layer of the bladder it is stage T2 or higher, depending on the extent of invasiveness. T2 tumours extends into the muscle layer, whereas T3 tumours show perivesical spread, and T4 tumours show outgrowth

to surrounding tissues such as the prostate, uterus, vagina, or the pelvic or abdominal wall (Brierley et al., 2017).

The 5 year survival rate for patients with organ-confined disease without node metastasis was 89% for T2 and 78% for T3a staged tumours, decreasing to 50% and 41% respectively if nodal metastasis were present, in a highly selected surgical series (Stein et al., 2001). Approximately 50% MIBC patients develop metastasis, predominantly spreading to nearby tissues, lymph nodes, lungs, bones and more rarely brain and liver (Stein et al., 2001). For patients whose MIBC was not confined to the bladder wall (stage T3b and T4) and node negative, the 5 year survival ate was 58%, decreasing to 30% if nodes were involved (Stein et al., 2001). The prevalence and deleterious effects of MIBC, such as impaired bladder storage and incontinence (Ritchey et al., 2009) warrant the discovery of new therapeutic treatments.

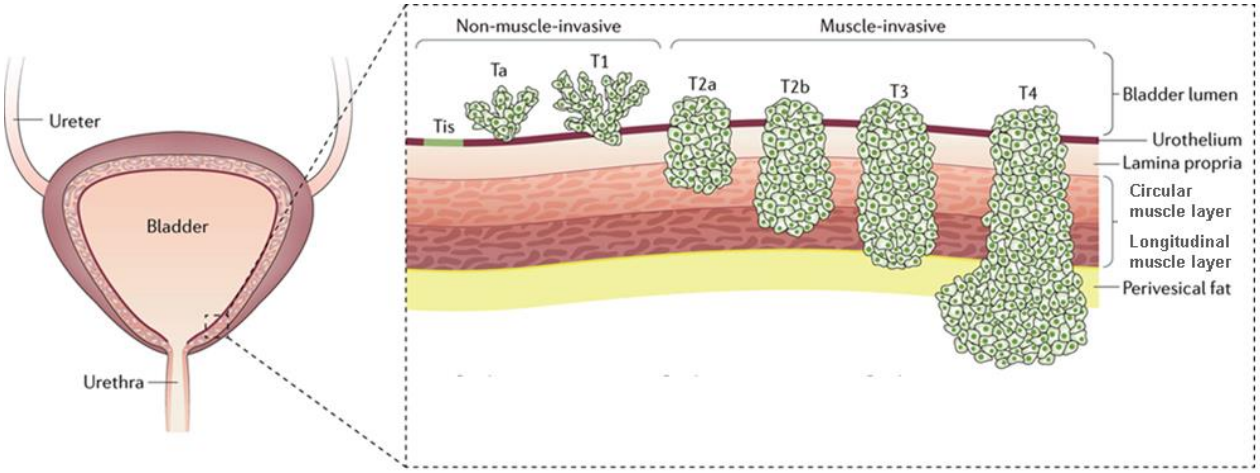

Figure 1. Bladder composition and tumour invasion by stage. Bladder cancer typically originates from the epithelium of the bladder (urothelial carcinoma). Papillary tumours seen within the mucosa or having infiltrated the lamina propria are classified as Ta and T1, respectively. Tis, also known as carcinoma in situ, is a flat, poorly differentiated tumour confined to the mucosa. Stage 2 tumours have invaded the muscle layer either superficially (T2a) or deeply (T2b). T3 tumours have invaded beyond the muscularis propria into perivesical fat. T4 tumours invade the prostate, uterus, vagina, bowel and abdominal wall. Modified from Sanli et al. 2017.

Table 1. Tumour, Node, Metastasis (TNM) Classification System for bladder cancer. Modified from Brierley et al. 2017.

T-Primary tumour	
T1	**tumour invades subepithelial connective tissue**
T2	**tumour invades muscle**
T2a	tumour invades superficial muscle (inner half)
T2b	tumour invades deep muscle (outer half)
T3	**tumour invades perivesical tissue:**
T3a	microscopically
T3b	macroscopically (extravesical mass)
T4	**tumour invades any of the following: prostate stroma, seminal vesicles, uterus, vagina, pelvic wall, abdominal wall**
T4a	tumour invades prostate stroma, seminal vesicles, uterus or vagina
T4b	tumour invades pelvic wall or abdominal wall

1.2 Treatment modalities for MIBC

Clinical relevance of chemoradiation treatment for MIBC

The standard of care treatment for MIBC involves cisplatin-based adjuvant chemotherapy followed by radical cystectomy (Dall'Era et al., 2012). Although common, this treatment regimen is associated with side effects including kidney failure and injury from urinary diversion. For those who are unable to withstand the rigours of radical cystectomy or who do not wish surgery, either due to age, fitness, or reluctance to risk surgery morbidities, chemoradiation therapy (CRT) is the most common treatment modality for non-metastatic MIBC (Gofrit et al., 2015). The aging population of bladder cancer patients, with a mean age at diagnosis of 72 (Smith et al., 2014), coupled with the prevalence of smoking, increases the likelihood that patients are likely to have

additional coexisting diseases. Many of these diseases pose risks for cystectomy, thus, underscoring the importance of non-surgical treatments such as chemoradiation therapy (Grossman et al., 2003). Cystectomy and radiotherapy patients have comparable outcomes (Kotwal et al., 2008) and often, patients who undergo radiotherapy have a better quality of life with normal bladder function. A manuscript comparing the outcomes of MIBC patients who received either radical cystectomy or radiotherapy treatment found that there was no significant difference in recurrence free survival at 5 years between patients who received radiotherapy versus cystectomy (Kotwal et al., 2008). Particularly, the 5-year cancer-specific survival rates for the radical radiotherapy and radical cystectomy group were 56.8% and 53.4%, respectively, and the 8-year CSS rates were 54.9% and 53.4%, respectively. Additionally, increased local control and survival have been associated with concomitant chemoradiotherapy compared to radiotherapy alone (James et al., 2012).

Chemoradiation drugs

Chemoradiotherapy treatment for MIBC involves the delivery of radiation to the bladder along with concomitant chemotherapy. Radiation damages the cell's genetic material (DNA) by inducing double-strand breaks in the cells and blocking the cell's ability to divide and proliferate. In addition, transcription factors such as p53 can cause apoptosis or cell cycle arrest. Radiotherapy treatments are delivered as 64 Gy in 20 fractions over 6.5 weeks or 52.5-55 Gy in 20 fractions over 4 weeks. Optimal rates of local control include a total dose of between 55 and 70 Gy delivered to the bladder tumour bed (Moonen et al., 1998).

Chemotherapeutic agents sensitise neoplasms of the bladder and increase tumour response but can add to normal tissue toxicity. The histone deacetylase inhibitor (HDAC) panobinostat and the anticancer agent gemcitabine are two radiosensitisers of interest for MIBC. Gemcitabine is a

nucleoside analogue that is used clinically and it is an attractive radiosensitising agent because it can be given to one-tenth standard dose (100 mg/m^2) with minimal bowel toxicity (Choudhury, 2011). As an analogue of deoxycytidine, gemcitabine (dFdC) is metabolised to the active triphosphate form of gemcitabine (Mackey et al., 1998) (Figure 2).

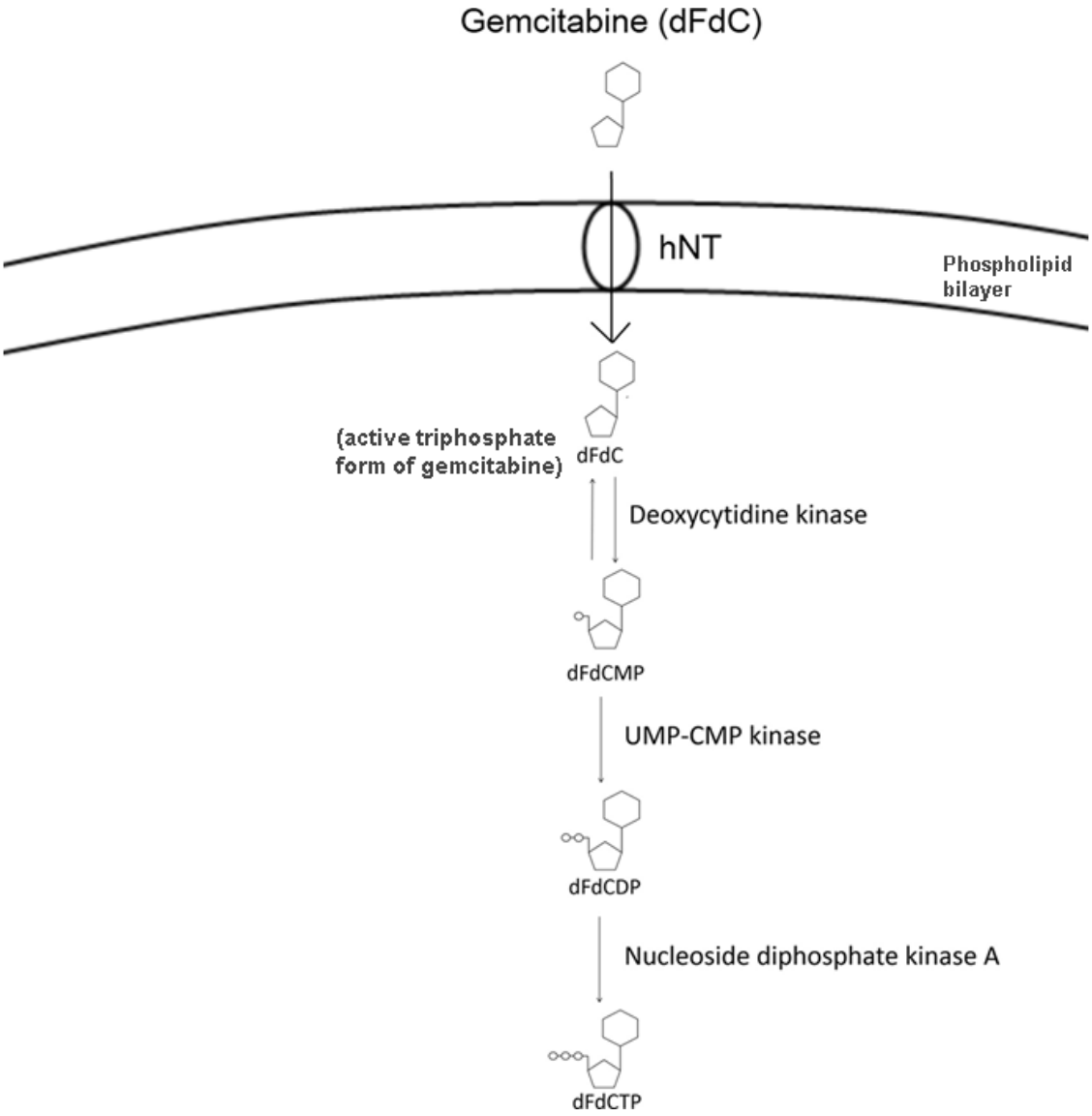

Figure 2. Mechanism of action of gemcitabine. Gemcitabine is metabolised into the active triphosphate form of gemcitabine (dFdCTP). Integral membrane proteins hNTs facilitate the cellular uptake of gemcitabine. Once inside the cell, gemcitabine is phosphorylated in the cytoplasm by deoxycytidine kinase to the monophosphate dFdCMP and then phosphorylated again by pyrimidine nucleoside monophosphate kinase UMP-CMP kinase to result in dFdCDP. For the last step, dFdCDP is phosphorylated into the active metabolite dFdCTP through nucleoside diphosphate kinase A. **Abbreviations:** hNP, human nucleoside transporter; dFdCMP, gemcitabine monophosphate; dFdCDP, gemcitabine diphosphate; dFdCTP, 20, 20-difluoro-20-deoxycytidine triphosphate; UMP-CMP, pyrimidine nucleoside monophosphate. Modified from Calvacante et al. 2014.

Human nucleoside transporters, a family of integral membrane proteins, facilitate the uptake of gemcitabine by overcoming the inherent barrier to diffusion imposed by the hydrophilic nature of nucleosides and nucleoside analogs (Bouffard et al.,1993). Once gemcitabine is inside the cell, it is phosphorylated by deoxycytidine kinase (dCK) in the cytoplasm (Heinemann et al.,1988). Gemcitabine is phosphorylated the second time by pyrimidine nucleoside monophosphate kinase (UMP-CMP kinase) to give gemcitabine diphosphate (dFdCDP) and tri- phosphate (dFdCTP) (Hatzis et al.,1998). Gemcitabine diphosphate (dFdCDP) is an inhibitor of ribonucleotide reductase 1 (RRM1) that leads to the depletion the cell's pools of deoxyribonucleotide (dNTP). RRM1 is an enzyme sub-unit of an enzyme that catalyzes the deoxyribonucleotide (dNTP) to ribonucleotide (rNTP) transition as apart of the nucleoside salvage pathway (Huang et al., 1991; Ciccolini et al., 2010). Gemcitabine prevents the integration of endogenous deoxycytidine triphosphate into newly synthesised DNA in a competitive manner (Huang et al., 1991). The incorporation of gemcitabine triphosphate into DNA enables the addition of one single nucleotide before DNA polymerase is completely obstructed and unable to add more nucleotides to the DNA strand, which is often referred to as masked chain termination (Plunkett et al., 1995). This results in stalling of the replication fork and eventual DNA double-strand break formation Therefore, the gemcitabine nucleotide is not tagged as being misincorporated. (Plunkett et al., 1995).

HDAC inhibitors are a particularly promising category of radiosensitisers, and the lab has previously shown that the pan-HDACi panobinostat (PAN) does not increase normal tissue toxicity when given with radiotherapy *in vivo* (Groselj et al., 2018). The mechanism of action involves downregulating MRE11 and NBS1 signalling proteins. These proteins are responsible for detecting DNA damage (Figure 3) (Groselj et al., 2013).

Panobinostat induces anti-tumour effects through epigenetic modulation of gene expression and preventing protein metabolism (Laubach et al., 2015). Panobinostat also targets histones and transcription factors, namely p53 by increasing protein levels (Atadja, 2009). It assists in activating epigenetically silenced tumour suppressor genes and alters gene expression by inhibiting Akt, a signal transducer, and hypoxia-inducible factor 1a, an activator of transcription (Atadja, 2009). Panobinostat has not yet been used for bladder cancer treatment in the clinic but has been used to treat myeloma.

1.3 Radiation-induced DNA damage responses

Ionising radiation (IR) is a DNA damaging agent that induces a range of DNA lesions, including base damage, single strand breaks (SSB), and double strand breaks (DSBs) (Santivasi et al., 2014).

IR can cause modified bases to pair with the wrong base, which upon DNA replication, gets fixed in the genome. The repair of modified bases most often occurs by a system called base excision repair (Chaudhry et al., 2014). Glycosylases that recognise unnatural bases in DNA help to repair the genome by cutting the bond between the base and the 1'C of the ribose sugar to create an abasic site. This is recognized by other enzymes, the abasic nucleotide is removed, and the correct nucleotide is filled in (Barsky et al., 2000). Methylated bases can also be repaired by a "direct reversal" protein, which binds to the methylated base and transfers the methyl group to a cysteine residue in its active site (Wyatt and Pittman, 2006).

DSBs can be directly repaired by NHEJ. The first step in NHEJ is DSB recognition that involves a number of mechanisms (Lieber et al., 2010). Two DNA-end binding proteins Ku70 and Ku80 recruit DNA-dependent protein kinase (DNA-PKcs), ataxia telangiectasia mutated (ATM), and ataxia telangiectasia and Rad3 related (ATR) to the break site (Davis et al., 2013). The MRN

complex (NBS1, MRE11, Rad50) is brought to the DSB site to facilitate 3'-5' exonuclease activity to trim strand edges. If there are no errors and none of the sequences have been lost in the repair process, the reading frame of the site is repaired and DNA ligase interacts with proteins to rejoin the break (Lamarche et al., 2010). Because NHEJ is error-prone, it is possible for sequences to be lost in the repair process causing an imperfect repair (Lamarche et al., 2010).

In S and G2 phase of the cell cycle after IR, ATR regulates cell cycle checkpoint arrest and HR. First, the MRN complex is recruited, which displaces the Ku complex. Double strand breaks are identified by the MRN complex and 3'-5' exonuclease activity of MRE11 leads to end-trimming close to the site of the break. DNA is resected in the 5' to 3' direction by CtBP-interacting protein, which creates 3' single-strand overhangs (Mimitou and Symington., 2009). Long ssDNA is created from succeeding end-resection by 5'-3' exonucleases EXO1 and Bloom syndrome protein- DNA2. The long single stranded DNA is bound and protected by replication protein A (RPA) (Liu and Haung, 2016). An interaction between breast cancer type 2 susceptibility protein (BRCA2) and RPA is followed by replacement of BRCA2 with Rad51. After the replacement of BRCA2, Rad51 bound to the new ssDNA, searches for the homologous sequence and performs strand invasion (Holloman et al., 2011). Displacement loop formation indicates the point at which the sDNA has identified the homologous sequence and formed heteroduplex DNA (hDNA). Following, synthesis of the strand and Rad54-mediated removal of Rad51 from hDNA occurs (Wright et al., 2014).

1.4 Sensitivity to radiation of the bladder

Underlying mechanisms

The bladder epithelium comprises of a basal layer. This layer is formed from diploid cells that are covered by transitional cells, and these transitional cells are overlaid with polyploid cells that are seen at the surface of the bladder. (Hall and Giaccia, 2017).

Irradiation of the bladder causes senescence of these differentiated functional cells followed by latent damage seen in the basal layer of the bladder. The surface cells of the bladder are lost causing irritation of the deep cellular layers when voiding. This stimulates cellular proliferation that can cause fibrosis and decrease in bladder filling capacities (Hall and Giaccia, 2017).

Side effects

Acute side effects of radiotherapy to the bladder include increased frequency of bladder and bowel, diarrhea, blood in the stool and fatigue. Late side effects include altered bowel habits (30%), rectal bleeding (2%), bladder bleeding (1%), incontinence (1%), and vaginal stenosis in women and impotence in men (30%) (Lieberman et al., 2014; Elliot and Malaeb, 2011).

1.5 Toxicities from administration

Studies have noted that the addition of radiosensitising chemotherapeutic agents to radiotherapy regimen improve locoregional disease-free survival without significant toxicity for MIBC (James et al., 2012). One study involving a treatment plan of concurrent gemcitabine-based chemoradiotherapy recorded 46 out of 50 patients (92%) being able to withstand all cycles of the combinational therapy without acute toxicity. Acute toxicity is described as adverse effects

occurring following administration of radiation doses within 24 hours (Cox et al., 1995). Of the 46 patients who successfully completed the treatment, only one patient experienced late toxicity 30 months after radical chemoradiotherapy. There was no significant late toxicity seen two years post-treatment, and patients appeared to have normal sexual, bladder, and bowel function (James et al., 2012).

The late effects of toxicity from radiotherapy with or without chemotherapy include vascular injury and fibrosis. Historically, radiation injury to the vascular compartment can be an important factor in the pathological processes of intestinal radiation and a driver of acute and late effects after radiotherapy (Hauer-Jensen et al., 2007). This vascular injury is key in the initiation, progression and maintenance of delayed intestinal tissue damage and enhanced fibrosis which lead to loss of mucosal function (Bentzen, 2006).

Gastrointestinal toxicity

The primary dose limiting factor for bladder chemoradiation treatment involves normal tissue toxicity, most notably that of the small intestine. Five percent of patients display grade 3 or higher acute bowel toxicity because of radiotherapy (Majewski and Tarnawski, 2009). The small intestine is comprised of crypt domains and is the gastrointestinal organ that is most sensitive to chemoradiation. Gamma-irradiation doses between 8 and 15 Gy have the propensity to induce intestinal epithelial injury in mice in addition to the damage that may be caused by bone marrow failure if the whole mouse is irradiated (Kim et al., 2018). The mouse intestinal epithelium can be regenerated, particularly when irradiation doses are below 14 Gy. Conversely, when doses above 15 Gy are administered, gastrointestinal acute radiation syndrome is common (Kim et al., 2017).

1.6 Sensitivity to radiation of the small intestine

Underlying Mechanisms

Radiation makes the gastrointestinal epithelium more susceptible to p53-induced apoptosis (Kirsch et al., 2010). Specifically, p53-induces p21, a cyclin-dependent kinase inhibitor, or PUMA, a proapoptotic BH3-only Bcl-2 family protein. P21 prevents a number of cyclin-dependent kinases (CDK) from activating the G_1 cell-cycle checkpoint and maintains the G_2/M checkpoint in some cells (Leibowitz et al., 2011). PUMA kills the cell via the intrinsic pathway of apoptosis where promotion of Bax/Bak Bcl-2 family members causes mitochondria-dependent apoptosis (Yu et al., 2003).

Additionally, radiation induces vascular damage and breakdown of intestinal epithelium which causes mechanical irritation and bacterial infection. This infection stimulates acute inflammatory responses, including the release of inflammatory cytokines leading to shrinking of the mucosa. Incomplete development of epithelial tissue results, depleting the number of intestinal epithelial cells and inhibiting proliferation of intestinal crypts. Loss of normal functions in the epithelium and villi are characteristic (Hall and Giaccia, 2017).

Side effects

As a result of epithelial tissue loss and impairment epithelial cell proliferation, water electrolytes and proteins are expelled into the lumen and depleted. This process is followed by diarrhea. Late effects of radiation to the intestine includes chronic ulcers based on a physiological response from intestinal wall components and mechanical/chemical stress from infections. Fibrotic remodeling is also a potential late side effect that may result in constricting/narrowing of the intestine and

intestinal obstruction from food material. Frequently, vascular lesions are found in the intestine, which potentially results in bleeding (Joyner and Kogel, 2019).

1.7 Cellular regulation of the intestine

The ways in which intestinal cellular proliferation and differentiation are impacted by radiation can be studied easily because of the high turnover rate of the intestine. The small intestine consists of villi, which are finger-like projections, and crypts, which are protruding invaginations (Figure 3). A crypt and villus in the small intestine consists of approximately 250 and 3,500 cells respectively (Crosnier et al., 2006). Crypts are constantly replenished, as approximately 200 crypts are produced on a daily basis from stem cells in the mucosal layer (Reya and Clevers, 2005). The stem cell compartment, proliferative region, and differentiated region are the three components of the intestine based on cell type (Kosinski et al., 2007). Consequently, the intestinal epithelium systematically undergoes proliferation, differentiation, and shedding processes.

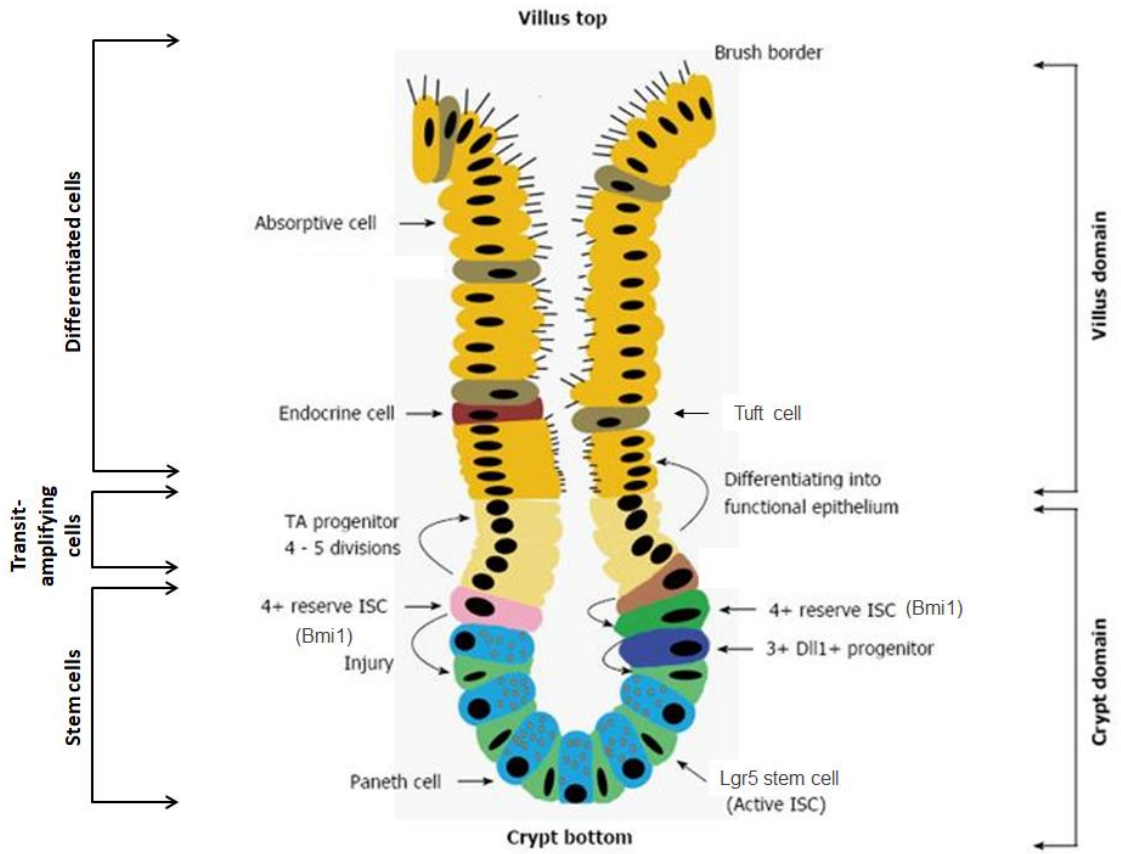

Figure 3. The intestinal crypt. Crypt base columnar (CBC) stem cells and reserved +4 intestinal stem cells (ISCs) are the two stem cell types that can be found in the intestine. CBC ISCs closely interact with Paneth cells. The intestinal stem cells proliferate and differentiate into various cell types that make up the intestinal epithelium. Modified from Cui and Chang, 2016.

The entire gastrointestinal tract is organised into four concentric layers: mucosa, submucosa, muscularis externa, and serosa. The mucosa is the mucous membrane and is further subdivided into epithelium, lamina propria, and muscularis mucosae. The epithelium lines the lumen. It is supported by a layer of delicate connective tissue, the lamina propria, which contains vessels and nerves. Beneath the lamina propria is a thin layer of smooth muscle, the muscularis mucosae (the muscle of the mucosa), separating the mucosa from the submucosa (Young et al., 2019). The submucosa is a supporting layer of connective tissue. It contains large vessels and nerves, and the cell bodies of autonomic ganglia. The muscularis externa contains two layers of smooth muscle: an inner layer (circular layer of myofibers) and an outer layer that is longitudinally arranged (Young et al., 2019).

The lining of the small intestine, like the lining of most of the gut, is a single layered epithelium. The epithelial cells (enterocytes) help absorb nutrients from the lumen of the gut or absorb water from the intestinal contents. In the small intestine the surface of the lining of the gut is increased by the many villi that protrude into the lumen (Crosnier et al., 2006). The surface of the villus is covered by a single layer of enterocytes which extend down into the crypt below.

Intestinal stem cells (ISCs) at the bottom of the crypt located between Paneth cells divide and make copies of themselves (Umar, 2010). ISCs contribute to the high cell turnover rate of the intestine (Barker, 2014). After ISC proliferation, these cells produce transit amplifying cells. The transit amplifying cells proliferate rapidly and move up the walls of the crypt. These cells divide four to five times before undergoing terminal differentiation (Snippert et al., 2010). The ISC is multipotent and its progeny includes a range of cell types including mucus-secreting goblet cells, tuft cells, enteroendocrine cells, enterocytes, transit-amplifying cells, and lysozyme-containing Paneth cells (Umar, 2010).

The ISCs begin to differentiate into various cell types as they migrate upwards towards the villus. While the cells are moving up the sides of the villus they carry out the essential functions of the small intestine (Bjerknes & Cheng, 1981). Enterocytes assist with digestion, absorption, and barrier function. Goblet cells secrete mucous for cytoprotection and lubrication. Enteroendocrine cells secrete several hormones such as secretin, CCK, somatostatin, and enteroglucagon (Chang et al., 1974). Tuft cells are chemosensory cells that detect parasites and other pathogens (Howitt et al., 2016). Transit-amplifying cells (TACs) are undifferentiated cells that convert from stem cells to differentiated cells. When the differentiated cells reach the tip of the villus they undergo apoptosis and are shed into the lumen of the small intestine (Van Der Flier and Clevers, 2009).

In addition to epithelial cells, the intestine is also composed of smooth muscle tissue and fibroblasts. Fibroblasts are mesenchymal cells derived from the embryonic mesoderm that synthesize the extracellular matrix and growth factors. These synthesis processes maintain the structural framework and tissue homeostasis (Bitar et al., 2003). Smooth muscle tissue generates folds that improves the absorptive surface area of the mucosa and induces mechanical contractions that shortens the muscle in order to churn the bolus along the gastrointestinal tract (Bitar et al., 2003).

Vasculature is also an important component of the gastrointestinal system. Digested nutrients diffuse into blood vessels in the gastrointestinal wall. The absorbed nutrients are then transported via the blood vessels to different organs of the body where they are used to build proteins and other essential macromolecules (Geboes et al., 2001).

The celiac, superior mesenteric, and inferior mesenteric arteries are the major arteries of the gastrointestinal tract. The celiac provides blood to the duodenum, the superior mesenteric provides blood to the small intestine and proximal colon, and the inferior mesenteric provides blood to the distal colon (Kachlik et al., 2010). There are arcades and smaller arteries along the mesenteric border that anastomose and provide collateral blood flow. For this reason it is difficult to distinguish the areas supplied by the three major arteries. Stemming from the arcades is the vasa recta, whose branches circle around the musculature of the intestine and form an arterial plexus within the submucosa (Kachlik et al., 2010).

The intestine readily regenerates tissue, with an epithelial replacement time including migration and cell death of between two to five days (Barker et al., 2007) and an average cell cycle time of

12 hours (Al-Dewachi, 1979). The cell lineages, with the exception of Paneth cells, are maintained in the intestine for five to seven days until they are shed into the lumen (Marshman et al., 2002). Paneth cells have a survival rate of three to six weeks (Clevers and Bevins, 2013). The main function of Paneth cells is to make, package, and transport a number of antimicrobial proteins.

The ability of the intestinal epithelium to regenerate is largely dependent on the self-renewing ISCs that reside in the crypt domain. The two types of ISCs, +4 and crypt base columnar (CBC), are located in different regions of the intestine (Barkeret al., 2012). +4 ISCs are spatially located above the Paneth cells. CBC ISCs are situated between the Paneth cells and it has been demonstrated that Lgr5+ is a marker for these cells in the small intestine and colon (Figure 5) (Barker et al., 2007). One crypt contains a total of 15 Lgr5+ CBC stem cells. Lgr5+ CBC stem cells, in combination with growth factors R-spondin, Noggin, and EGF, give rise to "mini-guts" or organoids in a 3D extracellular matrix (Clevers, 2013).

The gene *Bmi1* also serves as a marker for a subset population of ISCs. In the absence of Lgr5+ stem cells, crypt architecture is consistently maintained (Tian et al., 2011). Thus, an alternative stem cell pool exists. A seminal experiment conducted by Tian et al. involved lineage-tracing experiments that studied how the loss of Lgr5+ CBC stem cells, another stem cell population, which is marked with Bmi1, can give rise to new Lgr5+ CBC stem cells (Tian et al., 2011). Similar to +4 ISCs, Bmi1+ ISCs are located above Paneth cells. These stem cells remain quiescent unless they are activated during injury. Unlike Lgr5+ CBC stem cells, Bmi1 stem cells are radioresistant (Yan et al., 2012).

1.8 Intestinal organoids as a physiologically suitable 3D model of cellular proliferation and differentiation

Radiotherapy-induced bowel toxicity in MIBC has previously been studied. However, there remains a need to understand the link between chemoradiotherapy for MIBC and gastrointestinal toxicity. Furthermore, the absence of a cell line model that recapitulates the diversity of the epithelium limits our knowledge about the pathogenesis of radiation-induced intestinal dysfunction and limits our understanding about normal tissue toxicity.

Limitations of standard two-dimensional (2D) culturing practices have been increasingly identified. The monolayer culture model neglects the complexity and heterogeneity of the intestinal epithelium (Nakamura, 2019). Furthermore, 2D intestinal cultures grow flat on rigid substrates by adhering to plastic surfaces, thus failing to recapitulate the architecture of the three-dimensional (3D) cellular environment and the interplay with the extracellular matrix, which is crucial to regulating stem cell growth and differentiation (Edmondson et al., 2014). As a result, 2D culture methods sometimes report findings that are misleading and inaccurate for *in vivo* responses (Kapałczyńska et al., 2016). Funding bodies in the field of cancer biology have begun to focus on allocating monies to 3D modelling because of its potential.

Organoid models are becoming widely used because of their ability to recapitulate the complex cellular environment of the tissue of origin, including parenchymal components (Lin and Chen, 2018). Three-dimensional (3D) cell cultures are suitable models for studying normal tissue toxicity in that they promote epithelial cell polarisation and differentiation and recapitulate the complexity of human tissue and the microenvironment of the native intestine (Torras et al., 2018).

Organoid or mini gut culture began in 2009 when Clevers and Sato first published about their methodology for culturing mouse intestinal crypts in a 3D system *ex vivo* (Sato et al., 2009). With organoid culturing, isolated intestinal crypts or individual Lgr5+ cells are embedded in Matrigel (composed of extracellular membrane components including collagen IV, lamina and entactin) (Kleinman et al., 1982). The following growth factors in the medium aid in maintaining stem cell activity. R-Spondin is a secreted protein that is a Wnt agonist, binding to Lgr5 (de Lau et al., 2011; Kaushik et al., 2018). Epidermal growth factor (EGF) helps to promote ISC growth and differentiation (de Lau et al., 2014). Noggin inhibits differentiation through the modulation of BMP signalling and enables the maintenance and passage of the organoids *in vitro* (Biteau and Jasper, 2011). In contrast to 2D cultures, organoid cultures preserve the tissue diversity that is often seen in the intestinal epithelium. Furthermore, it has been proposed that proliferative and differentiated regions identified in organoid cultures represent *in vivo* conditions of the compartments along the crypt-villus in the small intestine (Wang et al., 2017). Organoids can be subcultured or passaged *in vitro* for at least one and a half years while maintaining an intact karyotype (Leushacke and Barker, 2014).

1.8 Previous applications of organoids to assess toxicity

Organoid models typically involve growing organoids from tumours to study mechanisms of intestinal diseases or are used in gene editing studies to understand disease aetiology. Thus, the application of normal intestinal organoid cultures to study the impact of chemoradiation therapy on normal tissue toxicity is novel and has gained traction within the last year. Most recently, efforts have been centered around the use of organoids to predict chemoradiation response, particularly

as it relates to colorectal cancer. For locally advanced rectal cancer, it has been found that rectal cancer organoids (RCOs) recapitulate the pathophysiology and genetic changes of the original tumor. Specifically, RCO chemoradiation response is consistent with that of the tumour, with 84.43% accuracy, 78.01% sensitivity, and 91.97% specificity (Yao et al., 2019). Organoids have also been used to study chemoradiation for metastatic colorectal cancer. There has been the establishment of a test predicting the sensitivity to chemotherapy in patient-derived lesions resulting in the correct classification of 80 % of patients who would be responsive to chemotherapy (Ooft et al., 2019). The benefit of non-cancerous organoid cultures includes their potential ability to predict a patient's response to drugs and radiation pre-treatment and in a personalised manner.

Previously, the lab assessed intestinal crypt integrity using a Swiss roll technique for mouse intestine. The swiss roll is a well-established method of preparing the mouse intestine for histological study (Moolenbeek et al., 1981). Intestinal integrity/crypt regeneration was investigated at 3.75 days following irradiation to the bladder and surrounding intestine, in response to 10 Gy, 12 Gy, and 14 Gy irradiation, in combination with radiosensitisers gemcitabine and panobinostat. Whilst addition of panobinostat did not increase of the effect of 12 Gy on crypt regeneration, gemcitabine with 12 Gy yielded intestinal damage that was equivalent to 14 Gy irradiation (Groselj et al., 2018). Assessing crypt loss using this technique provided a direct comparison between the two drugs, but the use of mice is costly and low-throughput. In contrast, organoids can be grown in a timely manner and, once a stock has been established, negate the need for further mice.

A former Master's student previously began working with mouse intestinal organoid cultures and determined optimal passaging methods in the lab. She found that 50 organoids per well is optimal for Brightfield imaging at 4x magnification, with precise scoring for mean organoid size using an

ImageJ platform. Additionally, she established immunofluorescence conditions for detection of Lgr5, Bmi, villin, Muc2, and lysozyme.

1.9 Aims of the thesis

Our group is interested in identifying chemoradiotherapeutic treatment strategies in MIBC which are minimally toxic to normal tissue. The lab has been identifying drugs which both kill tumour cells and have minimal toxicity effects. The mechanisms underlying their radiosensitising properties have also been studied. The HDACi panobinostat was an effective radiosensitiser *in vivo* in bladder cancer without increasing early normal tissue radiation toxicity (Groselj et al., 2018). These former projects have provided the basis for my work.

Here, I set out to investigate gastrointestinal response to radiosensitisers using organoids derived from mouse small intestine. The thesis focuses on titrating the dose for toxicity in healthy small intestinal organoids with the hopes that we can next determine if the equivalent dose is effective in killing MIBC. Development and refinement of this assay is important to eventually determining whether equivalent nontoxic doses are effective in killing MIBC and capable of being translated into a clinical setting.

Specifically, the aims of this thesis were to:

1. enhance passaging and cryopreservation techniques to ensure that minimal resources are used in organoid expansion
2. finding safe chemoradiation dose with minimal intestinal toxicity that could in future be confirmed as effective in killing MIBC

2. MATERIALS AND METHODS

All animal research was conducted in accordance with United Kingdom Home Office Guidelines and institutional guidelines, under University of Oxford project licences P4B738A3B and P8484EDAE. Animal experiments were conducted by PIL holders in the lab.

2.1 Maintenance and culture of gastrointestinal organoids

Isolation of mouse gastrointestinal organoids

Gastrointestinal crypts were isolated from mouse small intestine and colon as published in Sato *et al.* 2009. Most of the experiments conducted in the lab involved the use of CD-1 nude mice and thus organoids were derived from these mice. CD1-nude mice were culled according to applicable ethical regulations, and the duodenum to colon (approx. 20 cm) were harvested from each CD1-nude mouse. Most of the experiments conducted in the lab involved the use of CD-1 nude mice, an immunodeficient mouse strain, and thus, organoids were derived from these mice. The intestinal tract was segmented into four pieces and labelled segments 1, 2, 3, and 4, which approximately correspond to the duodenum/proximal jejunum, distal jejunum, ileum and colon respectively. Each segment was individually inflated with ice-cold Dulbecco's phosphate-buffered saline (PBS). Faecal contents were removed, and the sections were agitated with additional cold PBS and cut into 2-4 mm pieces. Tissue fragments were then transferred into 50 mL conical tubes with 15 mL cold PBS. Using a 10 mL serological pipette, tissue fragments were washed with 10 mL PBS for a different number of times, depending on the section of the gastrointestinal tract being washed. Washing consisted of agitating the segments by pipetting up and down the required number of times with PBS (Table 2), removing the supernatant of PBS, and replacing with fresh PBS. After the intestinal pieces had sunk by gravity, PBS was removed, and the washing process was repeated, by pipetting up and down for the respective number of times.

Table 2. Number of titrations of intestinal tissue for each PBS wash during organoid isolation

Wash number	**Number of times pipetted up and down**
1	10
2	7
3	5
4	3

5	3

Segments were then placed on a rocking platform at 20 rpm for 25 minutes at room temperature with 25 mL of 5 mM EDTA in PBS. Then EDTA solution was removed from each segment and replaced with 1% bovine serum albumin (BSA) in PBS. The segments were incubated in the BSA solution for three to four minutes. The number of times the pieces were pipetted up and down was incrementally increased for each wash (Table 3). The supernatant was removed and strained through a 70 μm filter into designated conical tubes labelled by segment and fraction number.

Table 3. Number of titrations of intestinal tissue with 1% BSA in PBS for collection of each crypt fraction during organoid isolation.

Fraction number	**Number of times pipetted up and down**
1	3
2	5
3	7
4	10

Upon completion of all fractions, the crypt-containing supernatant was centrifuged at 290 x g for 3 minutes. The supernatant (containing the BSA solution) was removed and the pellet was re-suspended in 1% BSA in PBS for re-washing. Following the mixing of the pellet and BSA reagent, the mixture was centrifuged (at 200 x g at 4°C for 5 minutes). After subsequent washing with DMEM/HEPES, the crypt pellet was re-suspended in 80 μL organoid growth medium (Stem Cell Therapeutics) and 120 μL Matrigel (Corning) by gently pipetting up and down 10 times. The 50 μL mixture was dispensed into the centre of a pre-warmed 24 well plate. The plate was inverted and placed in a 37°C, 5% CO_2 humidified incubator for 15 minutes to polymerise the droplets and facilitate the formation of domes. Approximately 500 μL of organoid growth medium was added

to each well and returned to the incubator (Table 4). Medium changes were performed every 2-4 days depending on how long the medium retained the original colour.

Table 4. Composition of organoid growth medium

Component	**Company**	**Volume**
IntestiCult™ OGM Basal Medium	Stem Cell Technologies	90 mL
IntestiCult™ OGM Supplement 1	Stem Cell Technologies	5 mL
IntestiCult™ OGM Supplement 2	Stem Cell Technologies	5 mL
100x Pen/Strep (added fresh before feeding)	Life Technologies	1 mL

Passaging of mouse gastrointestinal organoids

Organoids were passaged once they were mature and exhibited a dark central lumen and multiple organoid fragment domains, which was typically seven days after isolation and seven days after passage. Passaging involved adding 1 mL of cold 15 mM EDTA in PBS to the organoid-containing wells and pipetting up and down ten times. Fifteen millimolar EDTA was used to isolate organoids in the lab because it efficiently disassociates organoids from fibroblast and muscle tissue without damaging cell membranes and killing the cells, while being more cost-efficient than commercialised disassociation medium.

Next, the fragmented Matrigel domes were removed and placed into a 15 mL conical tube. This step was done for all wells and repeated to ensure all organoids were removed from each well. The content of all wells for the respective segment were combined. The conical tubes were then incubated on a rocker at 25 rpm for 10 minutes at room temperature and centrifuged at 290 rpm at

4°C for 5 minutes. The supernatant was then discarded, and the pellet was re-suspended in 10 mL DMEM/HEPES for washing. After the subsequent washing, the organoid fragment pellet was re-suspended in Matrigel (Corning Life Sciences) and organoid growth medium (BD Biosciences) by gently pipetting up and down 10 times. Fifty microlitres of mixture was dispensed into the centre of a pre-warmed 24 well plate in a dome-like structure, ensuring that the circular shape was retained. The plate was inverted and placed in a 37°C, 5% CO_2 humid incubator for 15 minutes to polymerise the droplets and facilitate the formation of domes. Five hundred microlitres of organoid growth medium was added to each well and returned to the incubator. Medium changes were performed every two to four days depending on how long the medium retained the original colour. Initially, the organoids were maintained by passage at a one-to-two split ratio every seven days. However, approximately 50 organoid fragments per well were eventually counted from the suspension and seeded (Figure 4).

The process to obtain approximately 50 organoids per well involved suspending the pellet of organoid fragments in 5 mL DMEM/HEPES after removing supernatant that consisted of EDTA and organoid medium. Ten microlitres of the organoid fragment mixture were pipetted onto the gridded part of a haemocytometer and the number of organoids in the aliquot was counted. Based on the quantity of organoid fragments that were counted, the amount of Matrigel and medium that was needed to seed approximately 50 organoids per well was calculated. Afterwards, similar to the original passaging procedure, the mixture was centrifuged and the pellet was re-suspended in the desired volumes of Matrigel and medium, and the organoid fragment suspension was plated.

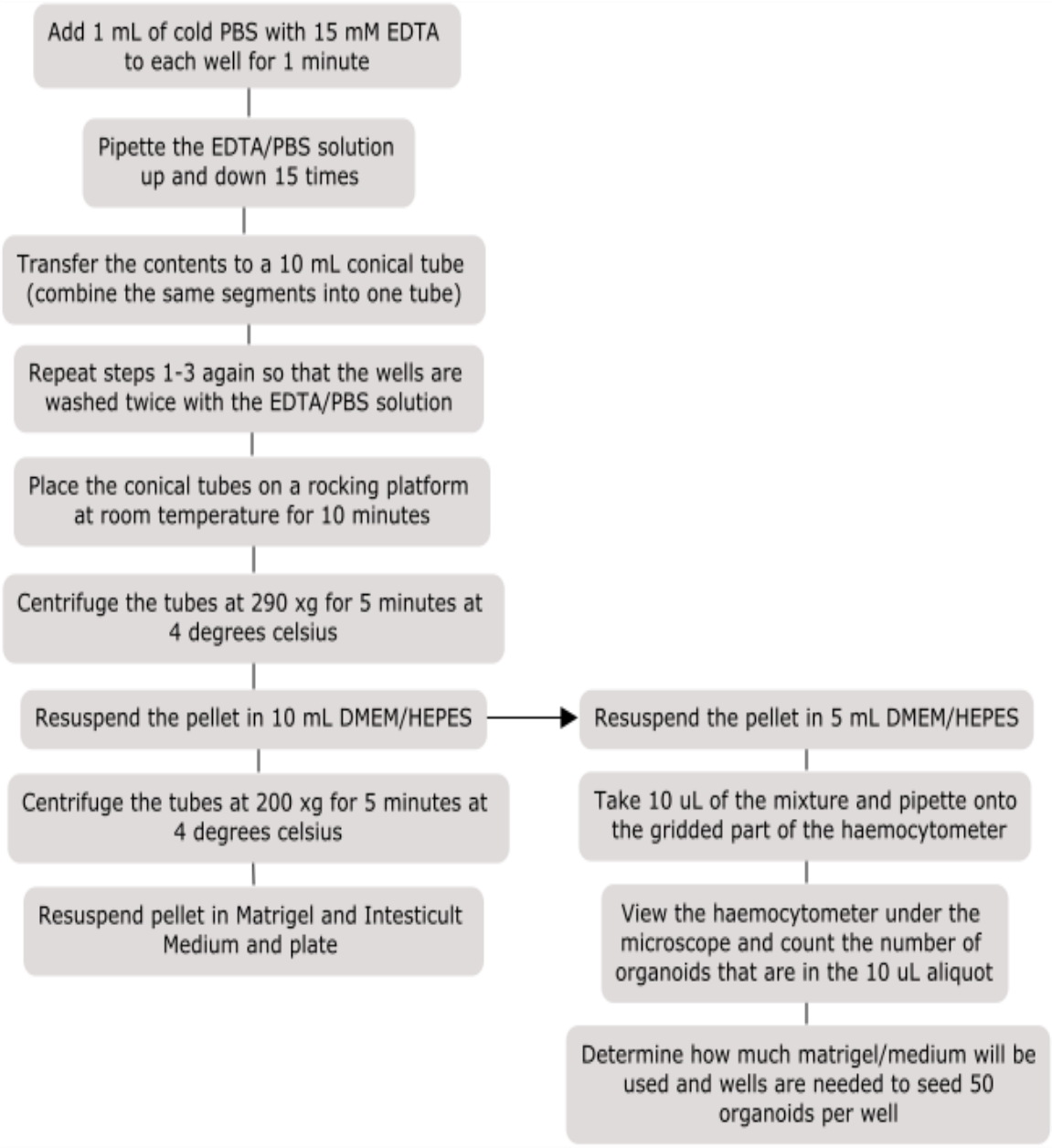

Figure 4. Adaptation of passaging protocol to obtain 50 organoids per well. Steps 1-9 describe the original passaging protocol. Steps 10-14 detail modifications made to the protocol to achieve a quantity of 50 organoids per well.

Freezing of cryopreserved mouse gastrointestinal organoids

Medium was aspirated from wells containing the organoids to be cryopreserved. Approximately 300 µL of organoids were pooled and processed simultaneously. One mL of 5 mM EDTA in PBS was added to the wells to be frozen, and pipetted up and down fifteen times to break up the domes before transferring the mixture to a 15 mL conical tube. The fragmented domes were transferred to 15 mL conical tubes and centrifuged at 300 x g for 5 minutes at 4°C. The supernatant was removed and the pellet was re-suspended in 10 mL DMEM/HEPES and centrifuged at 300 x g for 5 minutes at 4°C. The pellet was re-suspended in 1 mL CryoStor® CS10 freezing medium and placed in a freezing container with 500 mL of isopropyl alcohol and placed in a -80 ºC freezer for one month. To test the effects of Y-27632, a specific inhibitor of ROCK, on freezing organoid cultures, 10 µM ROCK inhibitor was directly added into the freezing medium for some of the cryovials.

Thawing of cryopreserved mouse gastrointestinal organoids

Frozen organoids were retrieved from the -80ºC freezer and placed in a water bath at 37ºC. The cryovial was rapidly thawed by placing it in a 37ºC water bath for approximately 2 minutes. The vial was wiped with 70% ethanol before opening. The inside of the vial was rinsed with 1 mL of cold 1% BSA in DMEM/F12 by pipetting up and down five times. The contents were transferred to the same conical tube containing 2 mL of 1% BSA in DMEM/F12. This process was repeated twice more to ensure that all of organoids were removed from the cryovial. Following centrifugation of the tube at 290 x g at 4ºC for 5 minutes, the supernatant was carefully aspirated and re-suspended in 120 µL Matrigel and 80 µL organoid growth medium by gently pipetting up and down 10 times. Fifty microliters of the mixture was dispensed into the centre of a pre-warmed 24 well plate in a dome like structure, ensuring that they retained their shape. The plate was inverted and placed in a 37°C, 5% CO_2 humid incubator for 15 minutes to polymerise the droplets and facilitate the formation of domes. Five hundred microlitres of organoid growth medium was

added to each well and returned to the incubator. Medium changes were performed every 2-4 days depending on how long the medium retained the original colour. To test the effects of Y-27632 on growing cryopreserved organoid cultures, thawed organoid cultures were grown in the presence and the absence of ROCK inhibition following thawing. Organoids that were tested with ROCK inhibitor were submerged in organoid growth medium containing 10 μM ROCK inhibitor. The organoids were treated with ROCK inhibitor for three days after thawing before being replaced with fresh growth medium.

2.2 Imaging

To visualise organoids and observe the effects of radiosensitisation and irradiation, brightfield images of the organoids were obtained using an inverted microscope (Nikon-TiE), with 4x, 10x, and 20x objectives and magnifications of 40x, 100x, and 200x respectively.

2.3 Image Analysis

ImageJ

Organoid size was analysed using an ImageJ platform. There were two different image analysis packages/plugins for images that were used to measure organoid size: Nikon ND2 Reader and Adaptive Threshold. These plugins were downloaded using a 64-bit Mac platform-dependent library file. Scale bars were burned on to images to set the image to scale. The image was set to scale through the “analyse” function and “set scale” tab. Most images were set to a scale of 0.6 pixel/unit. Colour graphics were compacted by using the “converting image” function and converting the image type to an 8-bit image. The brightness and contrast were adjusted by using the “image and adjust” tab. The image was sharpened and smoothed through the “process” tab. For ImageJ, smoothing was achieved by sharpening the raw image with “Sharpen”, median filtering with Median (radius=1), opening by reconstruction with Maximum (radius=5) followed

by Morphological Reconstruction (marker=eroded image, mask=non-eroded image), and closing by reconstruction with Minimum (radius=5) followed by Morphological Reconstruction (marker = dilated image, mask = non-dilated image). The image was further processed by converting it to "binary". Adaptive thresholding of the smoothed image was performed with the "adaptiveTr" plugin (parameter=weighted-mean, window size=250). The "analyse particles" function was used (under the analyse tab) with particle size set to $\geq$ 9,500 um^2. Results were displayed and summarised, organoids on edges were excluded and organoids were added to ROI manager.

Disaggregated or combined organoids were removed by using the ROI manager once a list of organoids and their sizes had been generated. Each number in the manager represented an organoid. The numbers that corresponded to disaggregated or clumped organoids were deleted from the tabulated list using a button in the ROI manager. Clicking the "Summarise" button allowed for recalculation of the parameter size.

Manual ImageJ Scoring Using the Wand Tracing Tool

Colour graphics were compacted by using the converting image function and converting the type to 8-bit image and the image was processed by converting to binary. The wand tracing tool was used to select the individual organoid of interest and then the organoids were measured using the "analyse" tab.

Manual scoring by outlining

Organoids that were outside of the automated scorable parameter when the image was converted to binary or was not accurately calculated automatically were outlined by hand. Scale bars were burned on to images to set the image to scale. The image was set to scale via the 'analyse' function and 'set scale' tab. Most images were set to a scale of 0.6 pixel/unit. The image brightness was

adjusted until the organoids were clearly visible. The freehand selection was used, and organoids were individually outlined by their distinctive border and then measured using the "analyse" tab.

2.5 Organoid drug treatment

Organoids were treated with panobinostat (Selleck Chemicals) and gemcitabine (Eli Lilly) 3 days after passaging (Tables 5 and 6). Organoid medium was changed 24 hours following radiosensitiser treatment.

Table 5. Total volume added to each well of a 24-well plate to achieve respective gemcitabine concentrations. The initial concentration of gemcitabine was 1 mg/L. Gemcitabine was diluted with culture medium 1:10,000 to a final concentration of 0.1 µg/L.

Desired Concentrations	50 nM	25 nM	10 nM	5 nM	2.5 nM
Volume of drug used	10 µL	5 µL	2 µL	1 µL	0.5 µL

Table 6. Total volume added to each well of a 24-well plate to achieve respective panobinostat concentrations. The initial concentration of panobinostat was 1 mg/L. Panobinostat was diluted with culture medium 1:10,000 to a final concentration of 0.1 µg/L.

Desired Concentrations	100 nM	50 nM	25 nM	12.5 nM	6.25 nM
Volume of drug used	20 µL	10 µL	5 µL	2.5 µL	1.25 µL

2.6 Organoid irradiation

Organoids were irradiated 3 days after passaging using a 24-well plate. Organoids were irradiated with x-rays generated from a Comet MXR-321 X-ray set operating at 225 kV and 17 mA with a copper uniformity filter. Organoid medium was changed to drug-free medium immediately following irradiation and the plates were placed back in the 37 °C incubator. Plates were irradiated according to the following set up, with each column of the plate irradiated separately (Table 7):

Table 7. Total dose given to each well of a 24-well plate during organoid irradiation experiments.

	1	**2**	**3**	**4**	**5**	**6**
A	0 Gy	0.5 Gy	1 Gy	2 Gy	4 Gy	6 Gy
B	0 Gy	0.5 Gy	1 Gy	2 Gy	4 Gy	6 Gy
C	0 Gy	0.5 Gy	1 Gy	2 Gy	4 Gy	6 Gy
D	0 Gy	0.5 Gy	1 Gy	2 Gy	4 Gy	6 Gy

2.7 Organoid chemoradiation treatment

Organoids were treated with radiosensitisers panobinostat and gemcitabine 3 days after passage. Six hours after drug treatment, organoids were irradiated according to the following set up, with each column of the plate irradiated separately. Organoid medium was changed to drug-free medium immediately following irradiation and then the plate was placed back in the 37 °C incubator. The timeline for this experiment can be found in the appendix (S6) (Table 8):

Table 8. Doses given to each column of the 24-well plate to deliver the required total dose. Individual doses are cumulative to give the total dose.

Total dose	0 Gy	0.5 Gy	1 Gy	2 Gy	4 Gy	6 Gy
Individual Dose	0 Gy	0.5 Gy	0.5 Gy	1 Gy	2 Gy	2 Gy
Time	0 s	21 s	21 s	42 s	1 m 24 s	1 m 24 s

2.8 Statistical Analysis

All statistical analysis was performed using GraphPad. Multiple comparison of means test, Brown-Forsythe test, and regression analysis was used with the p-values as indicated in the figures. Pearson's correlation coefficient was calculated with the r-value that is indicated in the figure. Unless noted, values were plotted as mean ± SEM.

3. RESULTS

3. 1 Refinement of murine small intestinal organoid culture system

3.1.1 Optimising the Matrigel concentration and seeding density

In order to determine the seeding density and matrix composition that leads to the most efficient organoid formation from organoid fragments, the passage efficiency of organoids was measured under different conditions. In an attempt to generate the optimal matrix for culturing organoids, different combinations of medium/Matrigel were tested to see which best supported organoid growth. Organoids were isolated and passaged over a period of 7 days and a second passage was completed 6 days later. The seeded organoid fragments that were then imaged for seven consecutive days, and the number of organoids counted for each condition at five days post-passage. After dissociating the organoids, 10 μL of the suspension was removed and the number of organoid fragments calculated using a haemocytometer (Figure 13A). The specific number of organoid fragment per well was plated. The medium with the desired organoid fragment number was combined with various concentrations of medium/Matrigel. The medium-to-Matrigel ratios that were used for the matrix were 1:1.5, 1:1.2, 1:1, and pure Matrigel. Pure Matrigel involved adding Matrigel directly to the pellet. With the 24-well conditions, each well had 50 μL of the medium/Matrigel combination. Therefore, pure Matrigel was composed of 50 μL of Matrigel. The ratio of 1:1.5 was composed of 30 μL of Matrigel and 20 μL of medium. The 1:1.2 ratio was composed of 27.3 μL of Matrigel and 22.7 μL of medium. Lastly, the 1:1 ratio was composed of 25 μL of Matrigel and 25 μL of medium. A ratio of 1:1.5 medium to Matrigel (M/MG) resulted in the highest percentage of seeded organoid fragments that formed organoids (Figure 13B), a statistically significant increase compared to a one-to-one ratio of medium and Matrigel ($p=0.0299$). In order to obtain 50 organoids per well, no more than 50 organoid fragments were seeded in a matrix composed of 1:1.5 M/MG mixture. This particular Matrigel matrix had enough basement membrane extract (BME) to provide the biological signals for organoid formation while providing significant mechanical support and allowing for good imaging. The mean percentage of

seeded organoid fragments which formed organoids was 90.67, 117.33, 100, 163.33, and 136.67 % for seeding numbers 100, 50, 40, 20 and 10, respectively. Confirming what was previously established (Gorrill et al., 2018), organoids could be best visualised and counted at 50 organoids per well. Using a medium to Matrigel concentration of 1:1.5 was best overall for organoid formation and imaging. The medium to Matrigel concentration of 1:1.5 was used for subsequent experiments.

3.1.2 Phenotype of intestinal organoids

Intestinal epithelial organoid isolation, passage, and maintenance protocols, as previously described in Stem Cell Technologies were used to establish the cultures. These protocols are based on the 2009 3D "mini-gut" culturing technique (Sato et al., 2009). Isolation of intestinal organoids serves as an *ex vivo* model to maintain intestinal stem cells in a system anatomically resembling the gut architecture. This process, involving the isolation and passaging of intestinal epithelial crypts, is not possible without the use of a culture composed of specified cell culture serum-free medium containing the growth factors EGF, R-Spondin, and Noggin.

The growth and phenotypical characteristics of organoids grown from CD1-nude mice were evaluated by light microscopy using a brightfield microscope. The purpose of the experiment was to establish a system of defining intestinal organoid morphology. In addition, it was crucial to determine at what days key signs of organoid growth were displayed during the organoid formation processes post-isolation and post-passage.

To investigate the quality of organoids seen in cultures, brightfield images of organoids were taken at different timepoints. Once budding began, intestinal organoids had a grape-like shape (Figure 5A), as previously noted (Sato et al., 2009). Non-budding crypts without a visible lumen were also

seen in gastrointestinal organoid cultures. These crypts had a circular or oval shape (Figure 5B). However, these organoids were slower growing and began to bud over time. Non-budding organoids with a large lumen were also characteristically seen in intestinal organoid cultures. These rounded structures of different sizes and were seen in no more than approximately 5% of all of the cultures (Figure 5C). Disaggregated organoids were seen in cultures if organoids were not passaged on a weekly basis. As organoids began to disaggregate after day 7 organoids were consistently passaged once a week (Figure 5D).

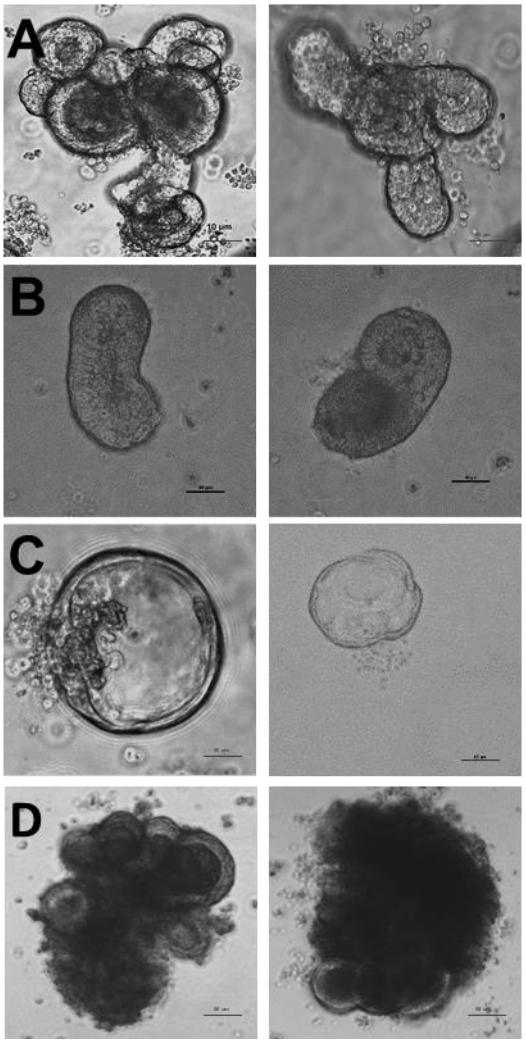

Figure 5. Morphological characterisation of murine gastrointestinal organoid cultures. A. Examples of budding organoids. Images taken on day 2 post-passage. B. Examples of non-budding organoids without a visible lumen. Images re taken on day 3 post-passage. C. Examples of non-budding organoids with a visible lumen. Images taken on day 2 post-passage. D. Examples of disaggregated organoids. Images taken on day 9 post-passage. Images are from different isolations. Scale bars are 50 μm.

During the isolation process, intestinal tissue was split into four segments with segments 1, 2, 3, and 4 corresponding to the duodenum/proximal jejunum, distal jejunum, ileum and colon respectively (Figure 6A). A small amount of variance was noted between organoid structures and cultures when comparing segments 1, 2, and 3. However, the growth of segment 4 was difficult because of the large amounts of debris present from the fibrous tissue structures that are characteristic of the colon.

To assess organoid morphology, brightfield images are depicted for each timepoint. These images were taken from a single isolation. Images are the same organoid and well from a single isolation, with approximately 125 organoids per well. On day 1, crypts formed a round shape, called an enterosphere, and these structures became larger over time. Robust budding was observed on day 6, demonstrating a mature morphology typical of small intestinal organoids with a crypt-villus structure.

At day 3 post-isolation organoids began budding (Figure 6B). After the first passage, organoids had begun to bud at day 3 similar to post-isolation (Figure 6B). Growth and increase in size of intestinal organoids was seen during the first week of culture.

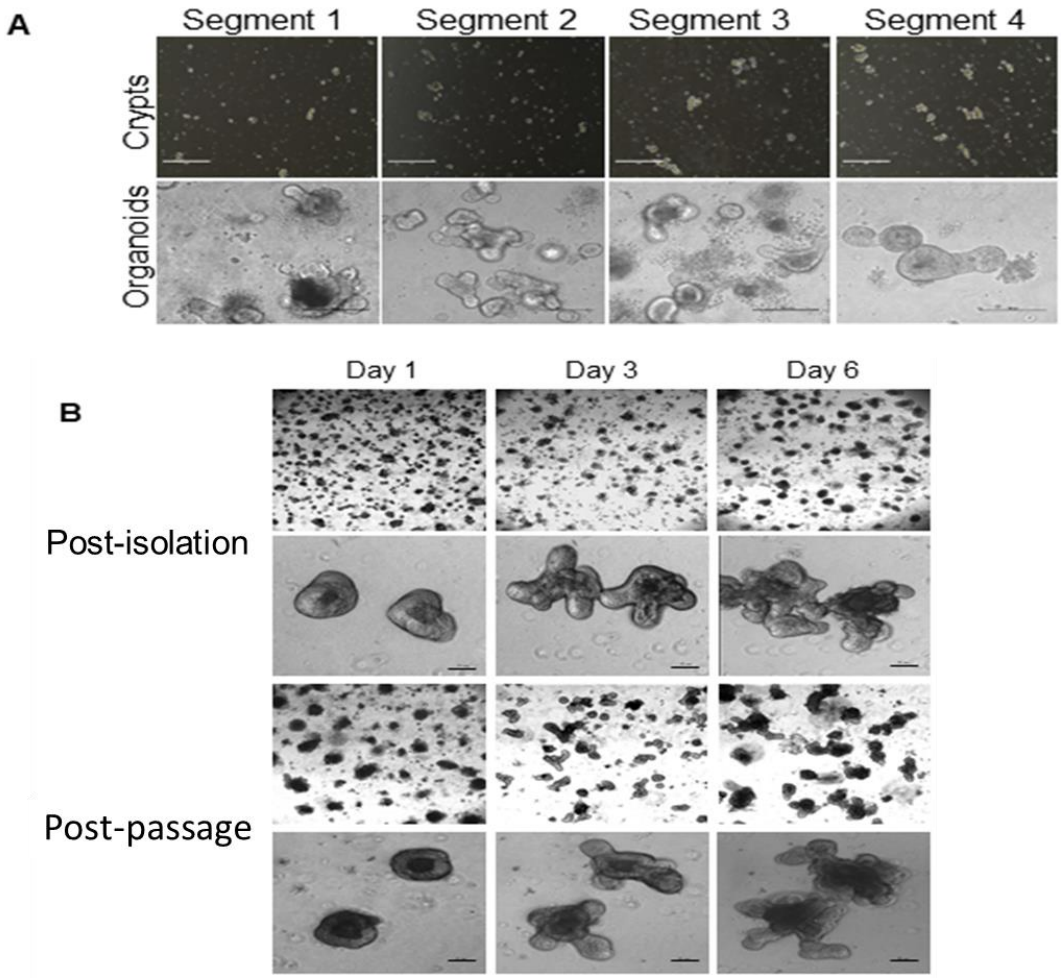

Figure 6. Most organoids have mature phenotypical characteristics by day six post-isolation and post-passage. A. Phenotype for organoid fragments and organoids of the duodenum (segment 1), jejunum (segment 2), ileum (segment 3), and colon (segment 4). B. Representative morphology of CD1-nude organoids cultured on days 1, 3, and 6 upon isolation and passaging. Scale bars for Figure 6A and 6B are 500 μm and 100 respectively.

3.1.3 Relationship between organoid size and budding

In order to evaluate the relationship between organoid area and the number of organoid buds, the number of buds per organoid has and the organoid size were determined using imageJ plugins (Figure 7A-B). Organoid images were taken on day 4 because budded and non-budded organoids were seen in cultures and there was no disaggregation that could impede the accurate organoid size from being determined.

There was a direct, statistically significant, linear relationship ($p<0.0001$) between the number of buds and mean organoid area. This finding validates the use of mean organoid size as a method to study organoid response to drug treatments and irradiation.

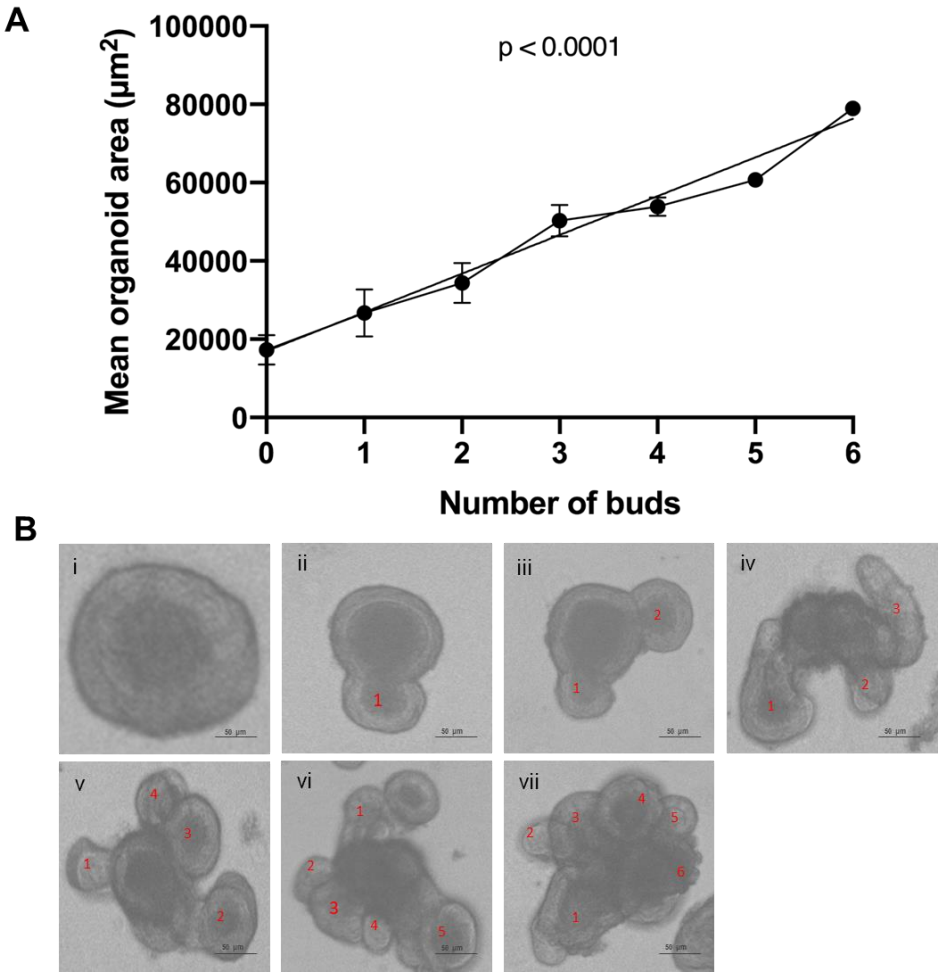

Figure 7. Correlation between mean organoid area and number of buds on organoid. A. Line graph of the relationship between mean organoid area and number of buds with linear regression (N=1-10 for each point, $p<0.0001$). Error bars show standard error of the mean. B. Representative images of organoids that have i. zero. ii. one. iii. two. iv. three v. four vi. five vii. six. Buds are counted in red. Scale bars are 50 µm.

3.1.4 Optimal centrifugation conditions for passaging organoids

There has been some inconsistency in the literature regarding passaging techniques, specifically the centrifugation speed that results in the optimal retainment of organoids (Moorefield et al., 2018; Pastula et al., 2016). The reported speeds ranged from 100 x g to 500 x g, which led to the testing of centrifugation speeds to investigate the most favourable speed for passaging that would result in the purest cultures, while retaining as many organoids as possible. If the centrifugation speed was too high, the passaged cultures may retain tissue debris that affects the organoid growth. If the centrifugation speed was not enough, smaller organoids may not be pelleted and will remain suspended in the supernatant, which would eventually reduce the organoid yield.

For this experiment, organoids were passaged twice, passaging every 7 days. The third passage involved the use of different centrifugation speeds and times. The wells of cultured organoids were imaged and counted for each centrifugation condition on day 5 post-passage.

During the passaging process, intestinal organoids were centrifuged twice. The organoids were first centrifuged with the matrix for organoid dissociation with 15 mM EDTA in PBS. Subsequently, organoids were centrifuged with DMEM/HEPES as part of the washing process. Extremely high centrifugation speeds can lead to damage of organoids whereas very low centrifugation speeds can lead to formation of a loose pellet that is inseparable from the supernatant. The centrifugation speeds of 200 x g, 290 x g and 500 x g were tested in the first and second centrifugation steps. The organoid pellet could be visualised at all centrifugation speeds. However, at the lower speeds of 200 x g and 290 x g, there was a significant decrease in the passage efficiency (the number of organoids that grow after seeding the organoid fragment pellet for passaging) since the organoid number was approximately 30% less than that of the passage using a centrifugation speed of 500 x g (Figure 8A). By using a passaging speed of 500 x g, nearly full

retainment of organoids was accomplished. Centrifugation time were also tested in the organoid passaging protocol. If the organoid suspension was centrifuged for a long period of time, it could impede the ability of a pellet to re-suspend in the culture medium. Contrastingly, short centrifugation times could reduce the passaging efficiency by preventing organoids from properly forming a pellet. All centrifugation speeds were tested at three and five minutes to determine how these combinations could impact organoid culture retainment and purity. It was deduced that there was a negligible difference between centrifuging the suspension for three minutes versus five minutes. Organoids could be seen at a centrifugation speed of 500 x g using a Brightfield microscope while maintaining a high passaging yield (Figure 8B). It was also concluded that the aforementioned centrifugation speeds do not have an impact on the size or purity of the organoid cultures (Figure 8C). Therefore, using a centrifugation speed of 500 x g is optimal for passaging and would allow one to retain the highest number of organoids while having minimal debris in the culture.

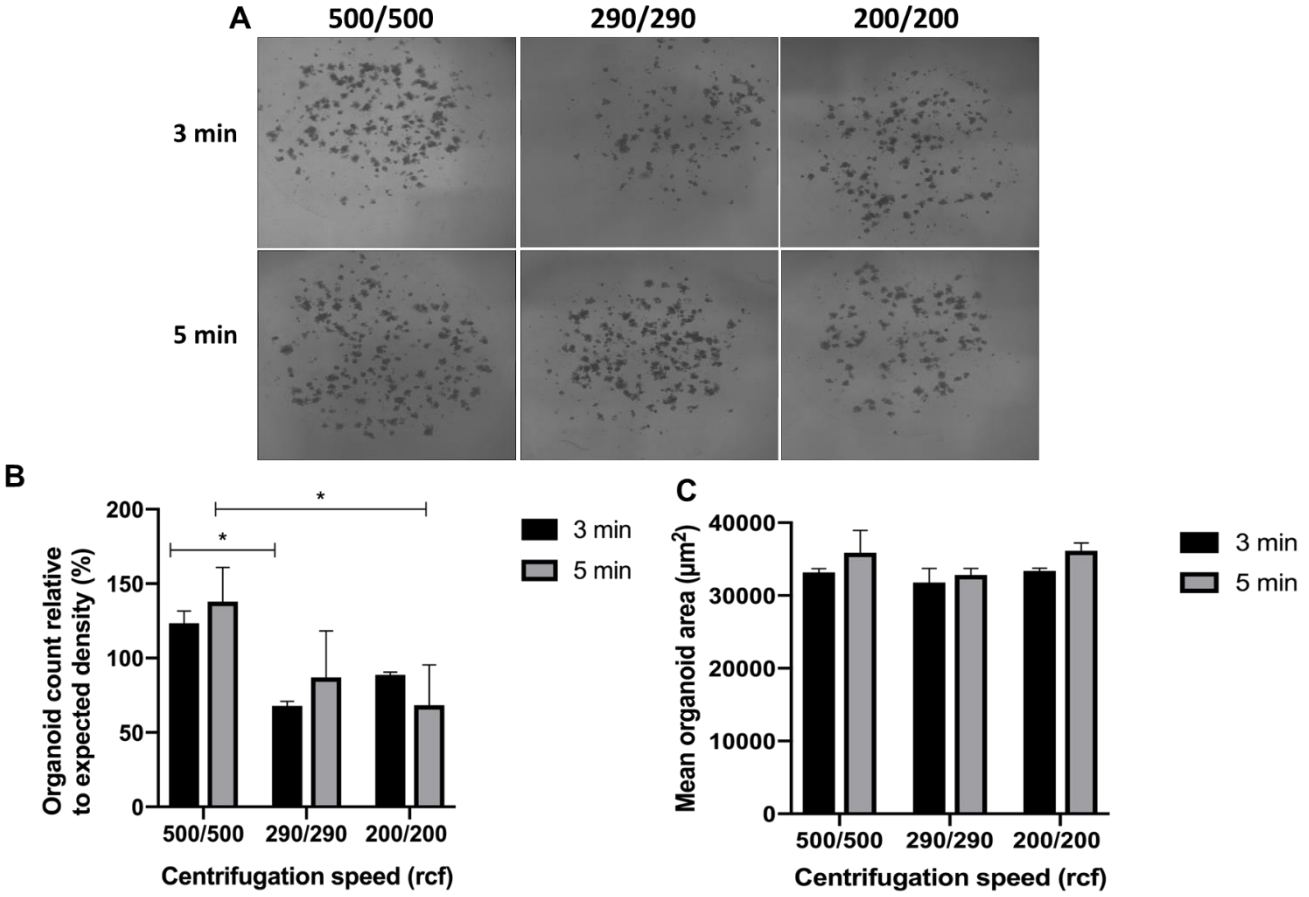

Figure 8. The effect of centrifugation speed and time on passaging efficiency and organoid retainment. A. Brightfield images of organoids that were passaged using centrifugations speeds 500 x g, 290 x g, and 200 x g. Images were taken on day 5. B. The centrifugation speed of 500 x g leads to an increase in organoid retainment (the number of organoids that grow after seeding the organoid fragment pellet for passaging) post-passage by approximately 30%. Using the centrifugation speed of 500 x g resulted in the highest retainment of organoids while having minimal debris in organoid cultures. There was very little difference between centrifugation times of 3 and 5 minutes. C. There was a negligible difference in mean organoid size when testing different centrifugation speeds on day 5. The timeline for this experiment can be found in the appendix (S1). Error bars show standard error of the mean. N=2. *$p<0.05$.

3.1.5 Organoid expansion potential

In order to evaluate the potential for expansion of organoid cultures, organoids were passaged three times for expansion after organoid fragment isolation. The organoids were counted 5 days after passage. The expansion factor was quantified as the organoid number after passage dividing by the organoid number before passage. Organoids continued to expand after each passage, and it was concluded that organoids have the greatest expansion factor after the first passage (Figure 9A-B).

A

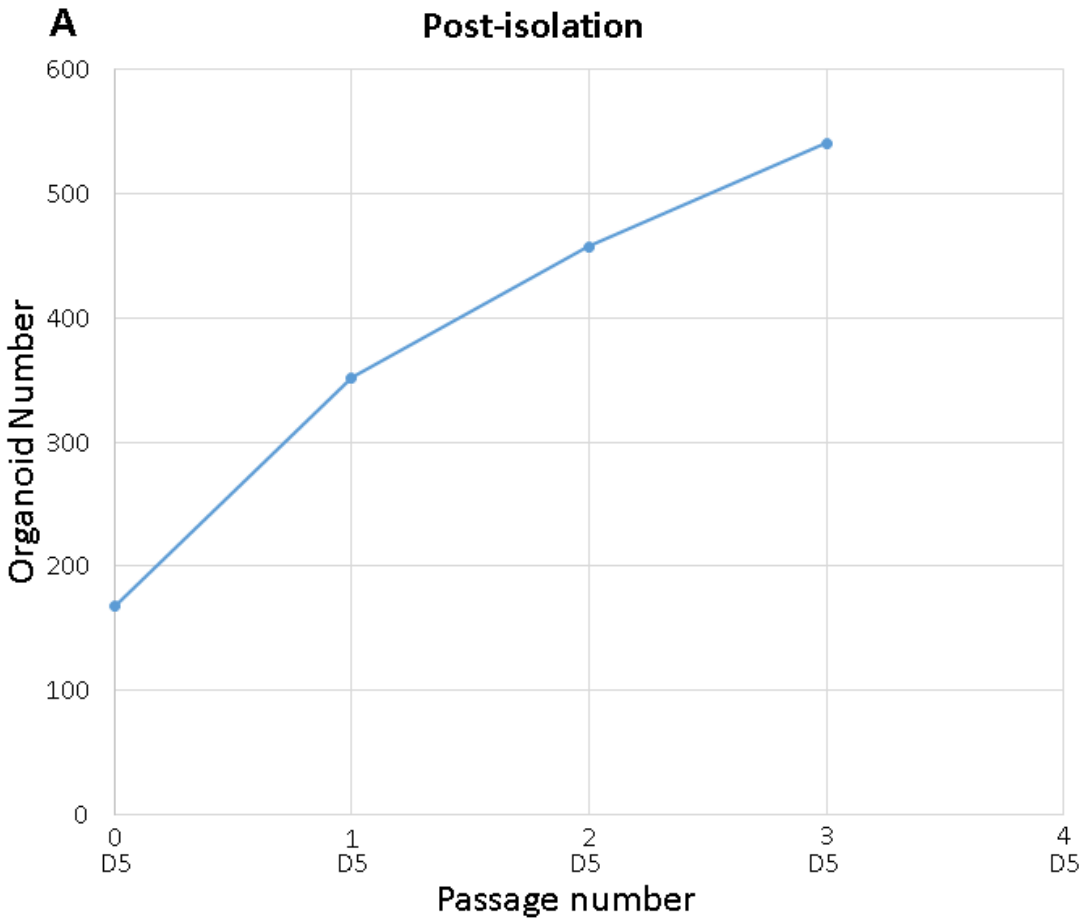

B

	Isolation	Passage #1	Expansion factor	Passage #2	Expansion factor	Passage #3	Expansion factor
Organoid Count	168	352	2.0952	457	1.2983	540	1.1816

Figure 9. Model growth rate as measured by expansion factor. A. Line graph of organoid expansion over the course of three passages. B. Expansion factor was calculated by dividing the organoid number after passage by the organoid number before passage. The expansion factor ranged from 1.3 – 2.1. Organoids had the greatest expansion factor after the first passage. The timeline for this experiment can be found in the appendix (S2).

3.1.6 Recovery of cryopreserved organoids

The aim of the experiment was to improve post-thaw recovery of organoids so that maximum thawing yield is achieved. Proper freezing and thawing methods are needed in order to generate an intestinal collection for future assays and reduce the resources used in maintaining the culture. As such, improvements to the thawing of cultured organoids was tested by the addition of a ROCK

inhibitor. The other condition tested for this experiment was to optimise the plating conditions to see if using a 6-well plate or 24-well plate was better. Though most of the protocols worked on 24-well plates, one of the cryopreservation protocols reported using 6-well plates could help to improve nutrient and gas exchange, make manipulation of organoids easier, and improve polymerisation of the matrix (Clinton and Koeppen, 2019). For the 6-well seeding condition, approximately 8-10 droplets, with 10-15 µL per droplet, were placed into each well of the pre-warmed 6-well plate (Figure 10A). The volume of medium that was required for each well in the 6-well plate was 1.5 mL. For the 24-well seeding conditions, one 50 µL droplet was dispensed into each well asnd 400 µL of medium was required for each well. The objective of this experiment was to replicate an alternative protocol that is used where organoids are seeded in 6-well plates (Clinton and Koeppen, 2019) to determine if this method is more cost-effective and uses fewer resources. Seeding the same number of cells is not a requirement under this condition. Note that for every experiment, the same organoid, Matrigel, and medium suspension was used for both the 6-well and 24-well experiment. For this experiment, the different seeding conditions were solely tested (Figure 10B).

The experiment involved thawing organoids that were cryopreserved for one month. Organoids were thawed with or without ROCK inhibitor treatment. For this experiment, ROCK inhibitor was not added in the freezing medium. Throughout the thesis project, a single experiment was conducted with ROCK inhibitor in freezing medium and post-thawing, however, because of limited time, the effect of using ROCK inhibitor in the freezing medium and when thawing could not be concluded.

For those that were thawed with ROCK inhibitor, organoid growth medium was replaced three days after incubation. Organoids were imaged and counted five days after thawing. One week after

thawing, organoids were passaged, and images were taken five days post-passage. It has been observed that thawed organoids initially were growing slower than organoids that were recently isolated but growth increased after 7-10 days post-passage (Ruchinskas and Clinton, 2018). Mature morphology was seen in all cultures five days after thawing; however, debris were seen in all cultures (Figure 10D). There was minimal debris seen in the 24 well plate culture with ROCK inhibitor, and there were more growing organoids with 86% viability. By evaluating the densities of mature organoids after thawing, it was found that the addition of ROCK inhibitor into growth medium after thawing resulted in superior recovery compared to cultures where there was no ROCK inhibitor present (Figure 10C). Additionally, higher viability of organoids was seen when using the 24-well seeding conditions compared to the 6-well seeding conditions. Thawed organoids cultured using the 24-well method with the addition of ROCK inhibitor had almost full recovery.

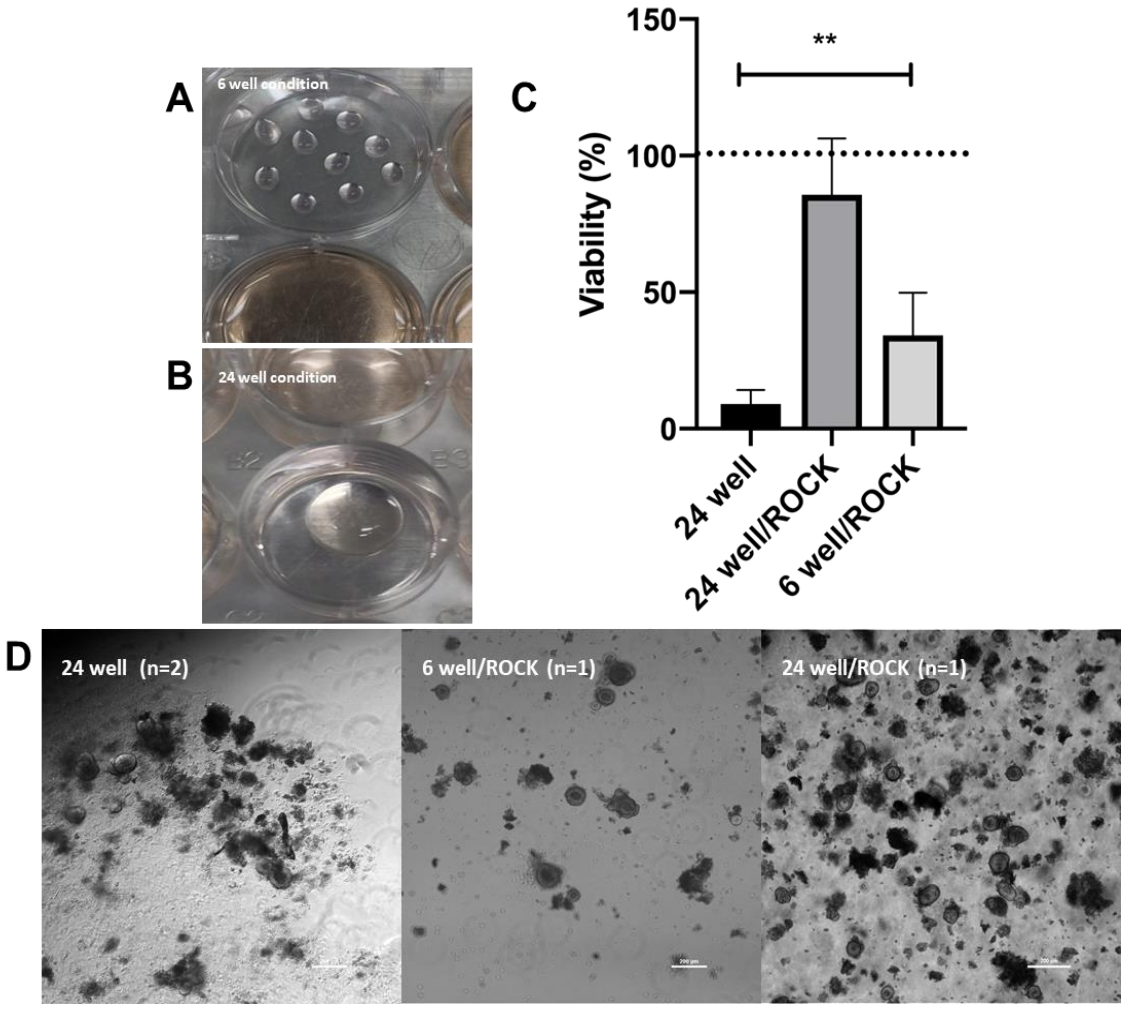

Figure 10. Enhanced recovery of cryopreserved intestinal organoids is dependent on culturing conditions. Organoids were treated with ROCK inhibitor for 3 days immediately following thawing. A. One well of a 6-well plate containing eight cell matrix domes after polymerisation and before overlay with medium. B. One well of a 24-well plate containing single matrix dome after polymerisation and before overlay with medium. C. Quantification of recovery from cryopreserved organoids. Dotted line (100%) represents no change in organoid quantity post-thawing. It was estimated that 300 organoids were frozen in each cryovial. D. Representative morphology of cryopreserved organoids cultured on day 5. The timeline for this experiment can be found in the appendix (S3). Error bars show standard error of the mean. Scale bars are 200 μm. N=3. **p<0.005.

Much cleaner cultures with large budded organoids and mature morphology were seen after post-thawing organoids were passaged (Figure 11A-B). Very few organoids developed post-passage without ROCK inhibitor treatment. However, adequate passage efficiency was seen for those cultures treated with ROCK inhibitor. Moreover, organoid growth characteristics were fully restored after two passages from the frozen state.

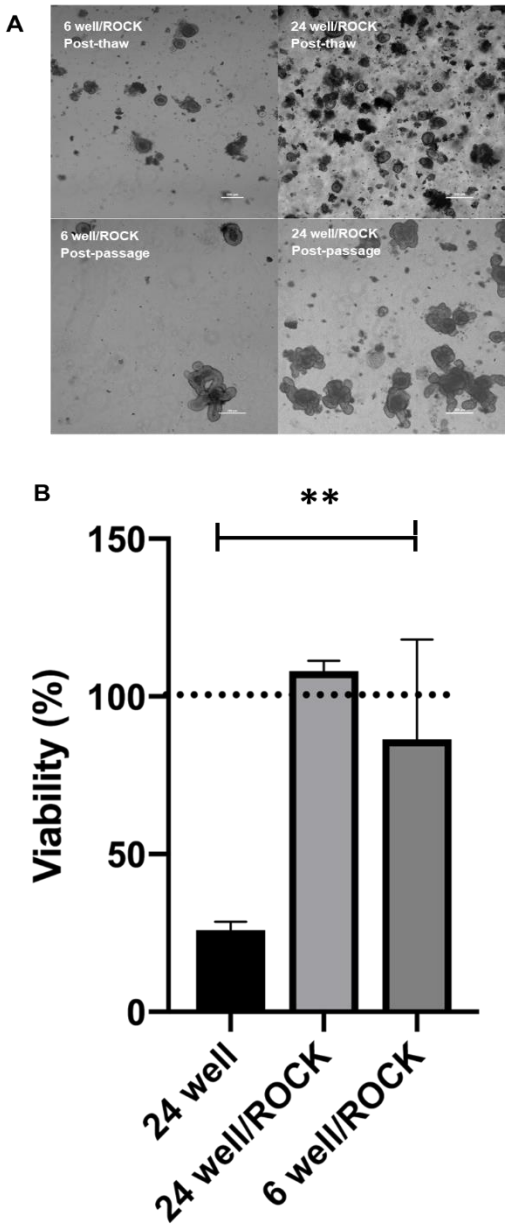

Figure 11. Recovery of cryopreserved organoids post-passage. A. Representative morphology of cryopreserved organoids on day 5 after passage compared to cryopreserved organoids cultured on day 5. Addition of ROCK inhibitor after passage increased organoid viability and there was no difference between seeding conditions from a 24-well or a 6-well plate. Scale bars are 200 μm. B. Quantification of cryopreserved organoids retained after passage. Dotted line (100%) represents no change in organoid quantity post-passage. Error bars show standard error of the mean. 24-well condition: N=2. 24-well/ROCK and 6-well /ROCK: N=3. **p<0.005.

3.1.7 Comparing Expansion of Fresh and Frozen Organoids

In order to evaluate how organoid expansion could be affected by cryopreservation and the number of times organoids were previously passaged, expansion of fresh and cryopreserved organoids was assessed on the third and sixth passages using different seeding numbers. Cryopreserved organoids

were frozen and thawed with ROCK inhibitor. Fresh organoids were grown without the ROCK inhibitor treatment. Organoids were passaged on a weekly basis and organoid numbers were counted five days after passaging. A splitting ratio of two was used for each well (Figure 12A). The organoid number increased after passaging. It was concluded that fresh organoids on the third and sixth passage (Figure 12B & 12D) and frozen organoids on the third passage (Figure 12C) had the greatest expansion at organoid fragment seeding numbers below 100. There was negligible change in expansion across all numbers for frozen organoids on their sixth passage (Figure 12E). Therefore, if aiming to obtain large quantities of organoids, it is important to seed fewer organoid fragments (below 100 organoid fragments) during the first few passages. Particularly, if organoids have been recently isolated, passaging the organoids using a organoid fragment seeding number of 50 would result in the greatest organoid expansion. To grow organoids that were cryopreserved and have been thawed, it would be best to use a organoid fragment seeding number of 75 so the maximum organoid yield can be obtained after passaging.

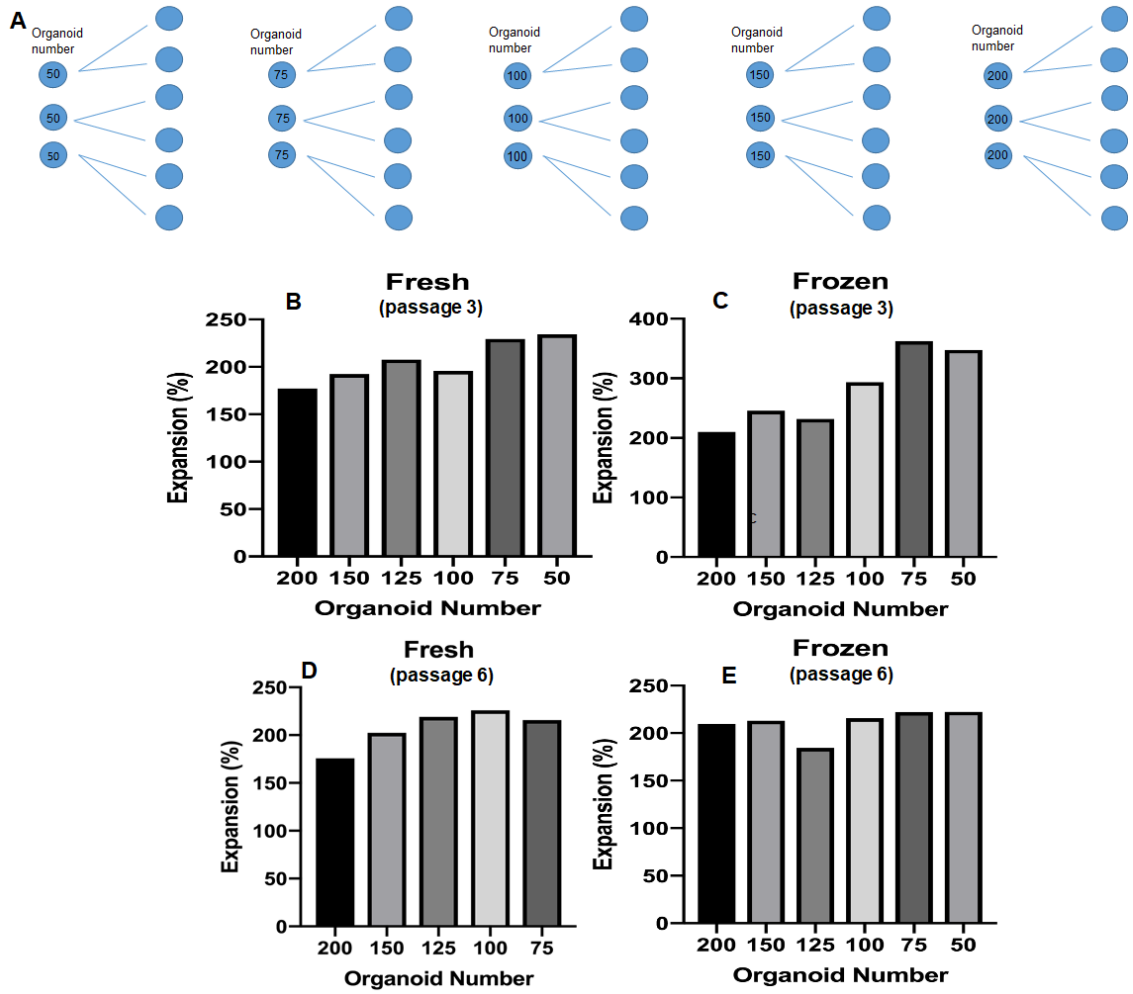

Figure 12. Evaluation of organoid fragment seeding number on expansion factor. A. Schematic of organoid expansion experiment. When passaging, 50, 75, 100, 125, and 150 organoids were seeded in triplicate. Organoids were seeded in a 24 well plate and passage every seven days Five days after passage 3 and 6, organoids from the three wells for each condition were counted and the total organoid number was calculated by adding the quantities from the three wells. The expansion was calculated by dividing the organoid number after passage by the organoid number before passage and multiplying the quantity by 100. B. Expansion for fresh organoids being passaged for the third time. C. Expansion for cryopreserved organoids being passaged for the third time. D. Expansion for fresh organoids being passaged for the sixth time. E. Expansion for cryopreserved organoids being passaged for the sixth time. The timeline for this experiment can be found in the appendix (S4). N=1.

3.2 Assay development

3.2.1 Evaluating passaging efficiency for organoid imaging and growth

In order to determine the seeding density and matrix composition that leads to the most efficient organoid formation from organoid fragments, the passage efficiency of organoids was measured

under different conditions. In an attempt to generate the optimal matrix for culturing organoids, different combinations of medium/Matrigel were tested to see which best supported organoid growth. Organoids were isolated and passaged over a period of 7 days and a second passage was completed 6 days later. The seeded organoid fragments that were then imaged for seven consecutive days, and the number of organoids counted for each condition at five days post-passage. After dissociating the organoids, 10 μL of the suspension was removed and the number of organoid fragments calculated using a haemocytometer (Figure 13A). The specific number of organoid fragments per well was plated. The medium with the desired organoid fragment number was combined with various concentrations of medium/Matrigel. The medium-to-Matrigel ratios that were used for the matrix were 1:1.5, 1:1.2, 1:1, and pure Matrigel. Pure Matrigel involved adding Matrigel directly to the pellet. The seeding was conducted in the 24-well conditions, and each well had 50 μL of the medium/Matrigel combination to form the Matrigel dome. Therefore, pure Matrigel was composed of 50 μL of Matrigel. The ratio of 1:1.5 was composed of 30 μL of Matrigel and 20 μL of medium. The 1:1.2 ratio was composed of 27.3 μL of Matrigel and 22.7 μL of medium. Lastly, the 1:1 ratio was composed of 25 μL of Matrigel and 25 μL of medium. A ratio of 1:1.5 medium to Matrigel (M/MG) resulted in the highest percentage of seeded organoid fragments that formed organoids (Figure 13B), a statistically significant increase compared to a one-to-one ratio of medium and Matrigel ($p=0.0299$). In order to obtain 50 organoids per well, no more than 50 organoid fragments were seeded in a matrix composed of 1:1.5 M/MG mixture. This particular Matrigel matrix had enough basement membrane extract (BME) to provide the biological signals for organoid formation while providing significant mechanical support and allowing for good imaging. The mean percentage of seeded organoid fragments which formed organoids was 90.67, 117.33, 100, 163.33, and 136.67 % for seeding numbers 100, 50, 40, 20 and 10, respectively. Confirming what was previously established (Gorrill et al., 2018), organoids

could be best visualised and counted at 50 organoids per well. Using a medium to Matrigel concentration of 1:1.5 was best overall for organoid formation and imaging.

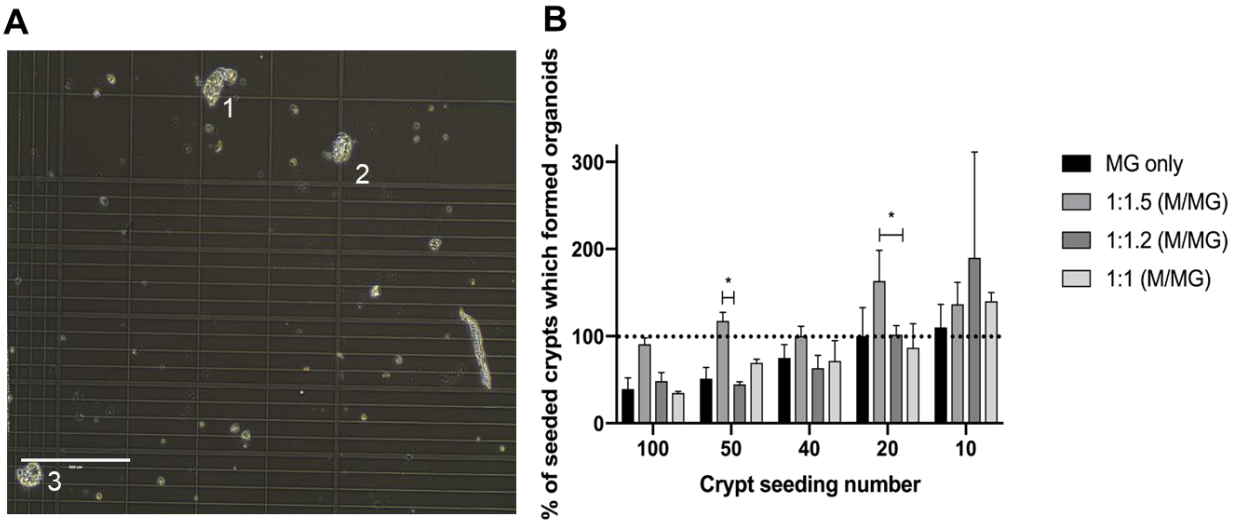

Figure 13. Passage efficiency for fresh organoids is best for imaging and growth when seeded at 50 organoid fragments in a matrix composition of 1:1.5 medium to Matrigel. A. Image of organoid fragment visualisation with a haemocytometer. Organoid fragments are counted in this image. B. Quantification of organoids formed post-passage relative to the organoid fragment seeding number. Dotted line (100%) represents where the number of organoids formed was the same as the organoid fragment seeding number. The timeline for this experiment can be found in the appendix (S5). Error bars show standard error of the mean. Scale bar is 100 μm. N=3. *p<0.05.

3.3 Assay implementation

3.3.1 Organoid growth and budding is halted at doses of radiation above 2 Gy

Implementation of the assay involved assessing organoid response to a range of radiation doses. Organoids were irradiated with 0.5 Gy, 1 Gy, 2 Gy, 4 Gy, and 6 Gy and imaged every day over a five-day period. Radiation doses were determined based on results from previously (Gorrill, 2018) showing that 10 Gy resulted in significant organoid dissociation post-irradiation. Thus, to survey a broader range of radiation doses, lower values were used. Organoids were irradiated three days after passaging because most passaged organoids begin to exhibit budding morphology by day 3 and at that time point organoid dissociation is not seen. Both mean organoid size and the ratio of budding-to-total organoids were determined. The ratio of budding-to-total organoids was

calculated by dividing the number of budding organoids in a culture by the total number of intact organoids seen in cultures (excluding the disaggregated organoids).

There was a significant increase in the mean organoid size and budding-to-total organoid ratio (budding ratio) for the control organoids between day 0 and day 1 (post-IR) (Figure 14A-B). Additionally, there was a steady increase in the mean organoid size and budding-to-total organoid ratio for the control organoids after day 1 (post-IR) (Figure 14C). The control organoids showed the peak budding ratio of 0.8 on day 3 post-IR. These findings are consistent with the previous observation that organoid budding can continue up until 6 days after passage, which will be 3 days after irradiation. Similarly, the organoid budding and size continued to increase for cultures irradiated with 0.5 and 1 Gy, and organoid growth was constant within 5 days post-irradiation. The budding ratio of both doses reached to the peak on day 4 post-IR, which was one day delay compared to the 0 Gy group. For 0.5 Gy, the peak budding ratio was very close to the control. This suggests that most organoids in this dose did not receive significant radiation damage that would impede budding and the organoid size, but the radiation dose might cause some delay of budding. For 1 Gy, the peak budding ratio was about 0.7, which indicate this radiation dose may cause more impedance on budding.

Organoids irradiated with 2 Gy had a minimal increase in mean organoid size, as organoids that remained non-budded enlarged over the course of five days. At 2 Gy, there was minimal increase in the budding-to-total organoid ratio between day 0 and day 1 (and a minimal increase in budding in cultures). Beyond day two, organoid budding was static.

At doses of 4 Gy and 6 Gy, mean organoid size declined, beginning at day 1, because the organoids disaggregated quickly. The mean organoid size steadily decreased as more of the larger, budded

organoids began to disaggregate. After day two, there was no change in the budding-to-total organoid ratio.

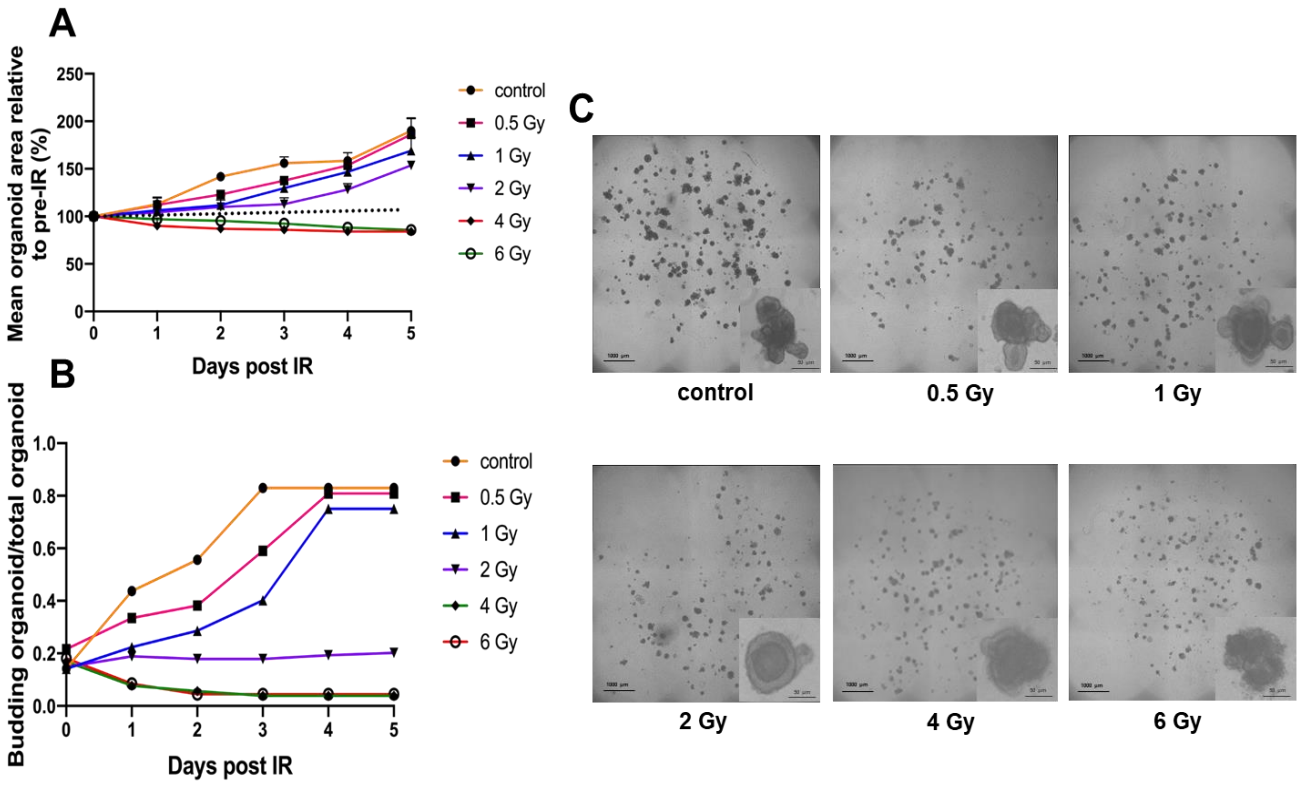

Figure 14. Mean organoid area and budding after doses of irradiation up to five days post-irradiation. The same wells and organoids were used to assess organoid area and budding-to-total organoid ratio after treatment. A. Dotted line (100%) represents no change in organoid size relative to pre-IR. Below the dotted line represents a decrease in organoid size and above represents an increase in organoid size relative to size pre-IR. At doses above 2 Gy, organoid growth is halted, while doses lower than 2 Gy showed continuous growth. B. At 2 Gy, organoid budding is static. For doses above 2 Gy, the organoid budding-to total organoid ratio decreases. For doses below 2 Gy, organoid budding-to-total organoid ratio increases and reached a plateau 4 days post-IR. On the other hand, the control organoids reached the highest budding on day 3 post-IR. This suggests the potential growth delay effect from radiation. C. Representative images five days post-IR showcasing the organoid disaggregation and not decrease in organoid size. At the higher doses (4 Gy and 6 Gy), disaggregation of organoids was present and organoids display minimal budding. Enlarged individual organoids are shown in the right-hand corners. The average number of organoids per well, average and standard deviation can be found in the appendix (S1.1, S1.2). Error bars show standard error of the mean. For some values the error bars are smaller than the symbol. N=3 from one individual isolation. Scale bar shows 50 µm for magnified organoids and 1000 µm for each well.

3.3.2 Gemcitabine and panobinostat have the potential to induce organoid drug toxicity

Previous studies from the lab showed that gemcitabine, when using as a chemoradiation agent, could increase the severity of acute intestinal tissue toxicity *in vivo*, while panobinostat showed no signs of intestinal deterioration and thus no toxic effect (Groselj et al., 2018). Therefore, gemcitabine and panobinostat are chosen as our modelled chemoradiation drugs to test if the organoid system can reflect the *in vivo* conditions. However, due to the drug's metabolic difference between *in vitro* and *in vivo* conditions, it is necessary to determine the concentrations of panobinostat and gemcitabine to be used for future assays.

Organoids were passaged and three days post-passage, drugs were given to organoids for 24 hours. Then the medium containing the drug was removed and replaced with fresh organoid growth medium. Images were taken before drug administration and five consecutive days after treatment. The drug concentration ranges were determined from the concentrations that have previously been used in cell culture experiments for cancer cell toxicity.

3.3.3 Gemcitabine impedes organoid growth at 25 nm concentration

For gemcitabine, organoid growth was seen until the drug concentration reached 25 nM or more (Figure 15A). The administration of gemcitabine concentrations below 25 nM did not have an effect on organoid morphology. A reduction in organoid size was seen for drug concentrations of 25 and 50 nM. Gemcitabine toxicity was noticeable because many of the organoids that once exhibited mature morphology would disaggregate at 25 and 50 nM (Figure 15C).

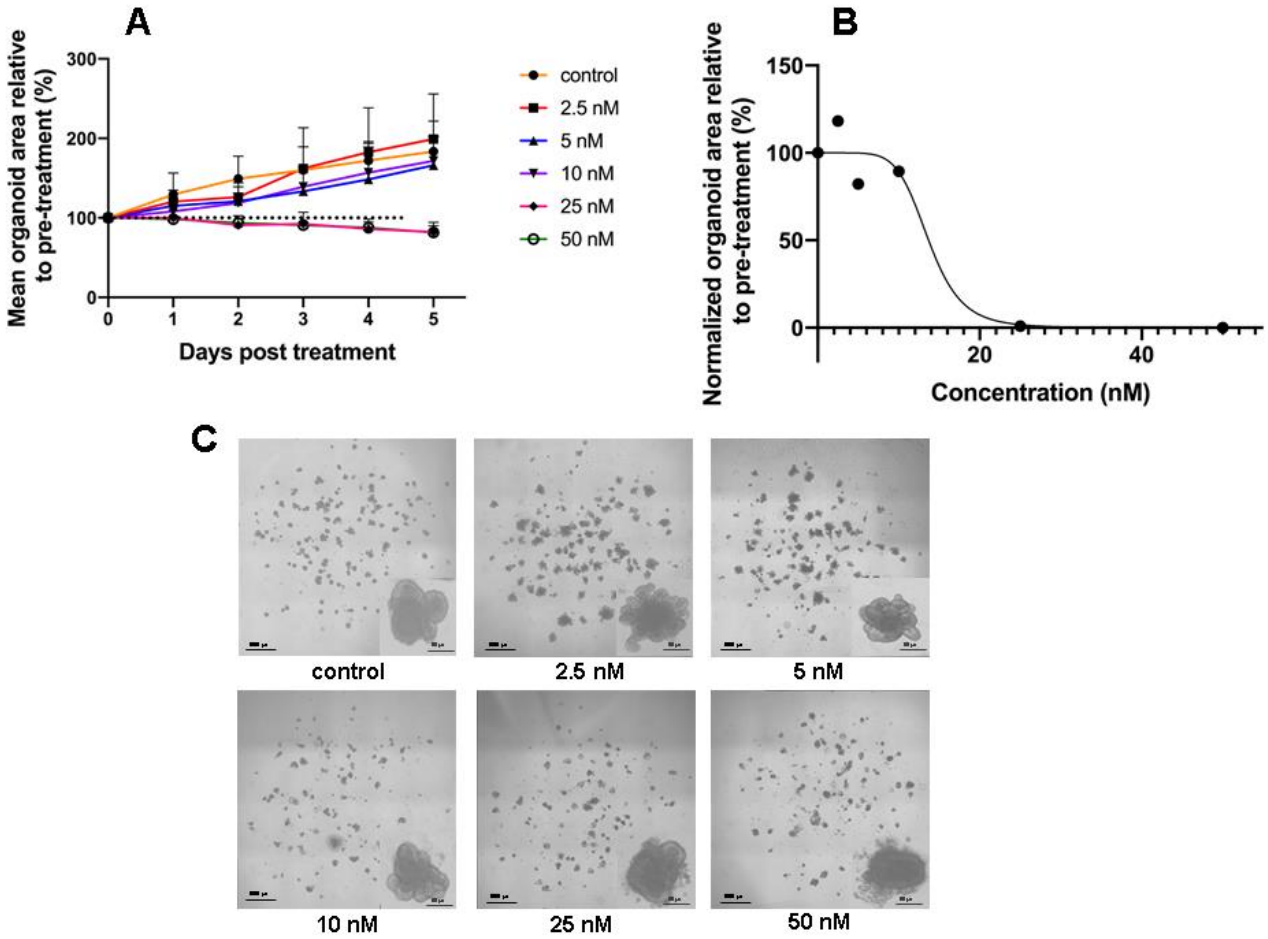

Figure 15. Mean organoid area after gemcitabine treatment up to five days post-treatment. A. At 25 nM and above, organoid growth is halted. Dotted line (100%) represents no change in organoid size relative to pre-treatment. Below the dotted line represents a decrease in organoid size and above represents an increase in organoid size relative to size pre-IR (day 0). Error bars show standard error of the mean. For some values the error bars are smaller than the symbol. B. The half-maximal half inhibitory concentration (IC50) of gemcitabine for organoid size is 13.7 nM at 5 days post-treatment. C. At 5 days post-treatment, at higher doses of 25 nM and 50 nM disaggregation of organoids is present. Organoids also display minimal budding. Magnified individual organoids are shown in the right-hand corners. The average number of organoids per well, average and standard deviation can be found in the appendix (S2.1, S2.2). N=9 from three biological independent repeats. Scale bar shows 50 μm for magnified organoids and 1000 μm for each well.

The results suggest that the drug is toxic to intestinal organoids at 25 nM or more. Thus, a gemcitabine concentration below 25 nM should be administered during future chemoradiation experiments. The day 5 post-IR change in organoid size relative to pre-treatment was used to create a dose-response curve (Figure 15B). The half-maximal half inhibitory concentration (IC50) of gemcitabine for organoid size was 13.7 nM. This was determined by first correcting the baseline

so that it was the value of the control organoids (i.e., organoids that did not receive any gemcitabine treatment). Following, the data points were normalised to the control organoids before being fit with a nonlinear regression line. This IC50 value was used to establish the gemcitabine treatment parameters for use in the experiment testing organoid response to gemcitabine and IR.

3.3.4 Panobinostat impedes organoid growth at 50 nm concentration

For panobinostat, organoids receiving a concentration of 25 nM or less consistently increased in relative size. Specifically, at 6.25 nM and 12.5 nM panobinostat promotes organoid growth to a greater extent than the control organoids (Figure 16A). Doses of panobinostat higher than 50 nM resulted in the halting of organoid growth and reduction in size. Similar to gemcitabine, panobinostat toxicity was identified at 50 and 100 nM dose because many of the organoids that once exhibited mature morphology would disaggregate (Figure 16C). This disaggregation was not observed in the control group or organoids treating with lower drug dose. Based on these findings, panobinostat concentrations greater than 25 nM should not be administered for the future chemoradiation experiments. The day 5 post-IR change in organoid size relative to pre-treatment was used for a dose-response curve (Figure 16B). The half-maximal inhibitory concentration (IC50) of panobinostat for organoid size was 27.5 nM. This was determined by first correcting the baseline so that it was the value of the control organoids (i.e., organoids that did not receive any panobinostat treatment). Following, the data points were normalised to the control organoids before being fit with a nonlinear regression line. The IC50 value was used to establish the panobinostat treatment parameters for the chemoradiation experiment.

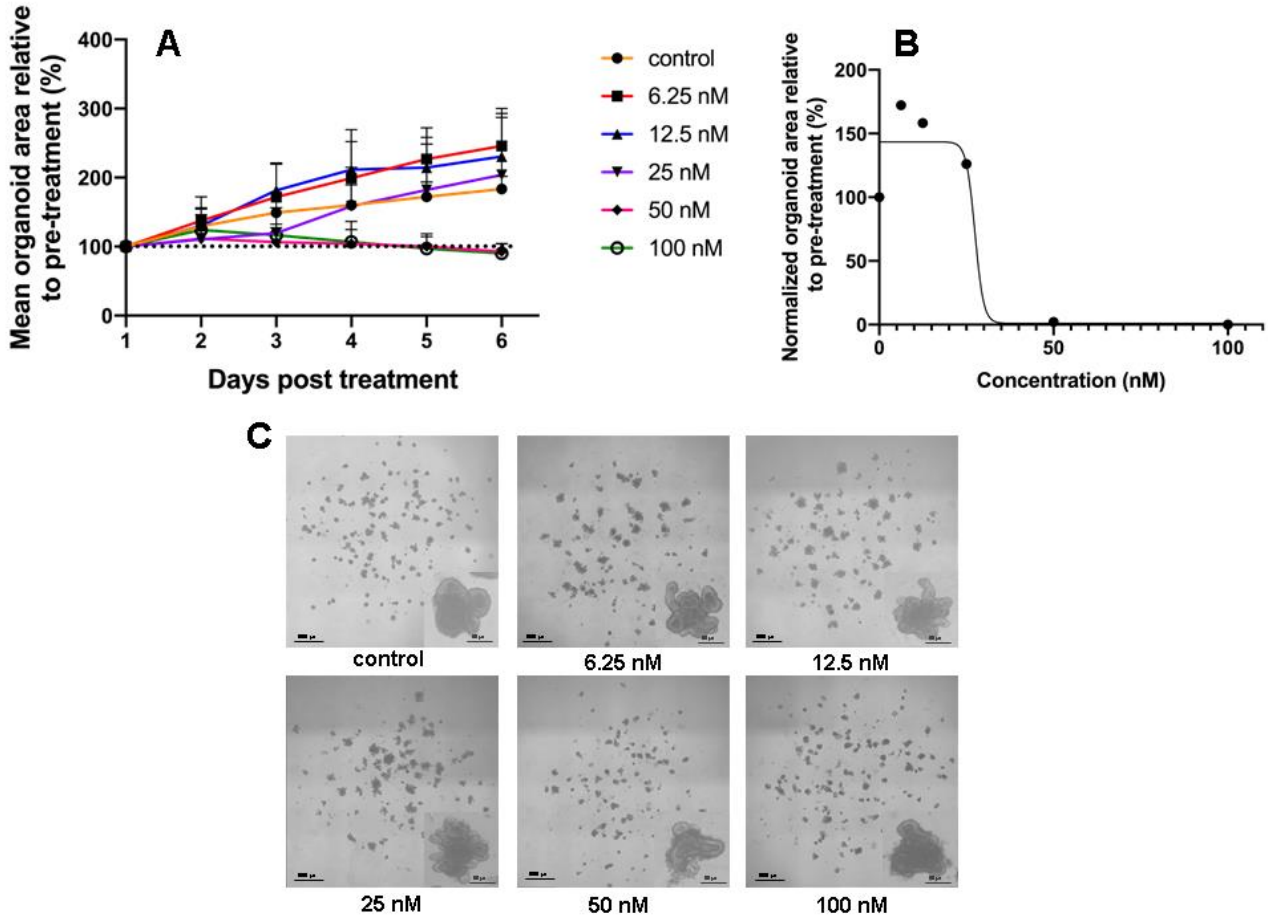

Figure 16. Mean organoid area after panobinostat treatment up to five days post-treatment. A. At 50 nM and above, organoid growth is halted. Dotted line (100%) represents no change in organoid size relative to pre-panobinostat. Below the dotted line represents a decrease in organoid size and above represents an increase in organoid size relative to size pre-treatment (day 0). Error bars show standard error of the mean. For some values the error bars are smaller than the symbol. B. The half-maximal inhibitory concentration (IC50) of gemcitabine for organoid size is 27.5 nM at 5 days post-treatment. C. At 5 days post-panobinostat, at higher doses of 50 nM and 100 nM disaggregation of organoids is present and organoids display minimal budding. Magnified individual organoids are shown in the right-hand corners. The average number of organoids per well, and average/standard deviation of organoid size can be found in the appendix (S3.1, S3.2). N=9 from three biological independent repeats. Scale bar shows 50 µm for magnified organoids and 1000 µm for each well.

3.3.5 Pilot experiment: organoid growth assay showed no difference between a combination of panobinostat and irradiation versus irradiation alone

Following the investigation of irradiation and drug alone, a combined approach involving irradiation and panobinostat was investigated. Organoids were passaged and three days later given panobinostat and IR similarly to the previous experiments. Based on the previously calculated

IC50 of panobinostat alone, 29 nM panobinostat was added 6 hours before IR to match the time of the *in vivo* gastrointestinal Swiss roll experiments that were completed previously in the lab (Groselj et al., 2018). Medium was changed immediately after irradiation.

Radiation doses at 4 Gy and above delivered with 29 nM of panobinostat resulted in organoid disaggregation and a decrease in organoid area at day 3 post-treatment and IR (Figure 17A). Historical data from the irradiation experiment (IR) was compared with panobinostat+IR. Increasing growth (compared to pre-treatment) was observed by radiation doses lower than 2 Gy with 29 nM panobinostat since the organoid area relative to organoids before treated with panobinostat and irradiation was greater than 100%. After 2 Gy radiation and panobinostat, organoid budding was halted and there was premature disaggregation as indicated by the white errors pointing to the shedding of epithelial cells in the figure. Administration of radiation doses higher than 2 Gy with panobinostat resulted in significant disaggregation (Figure 17C).

For consistency, experiments that involve testing organoid response to panobinostat+IR should have an incubation time that is the same as the experiments for panobinostat alone. Therefore, future experiments should involve a 24-hour incubation time for panobinostat prior to irradiation.

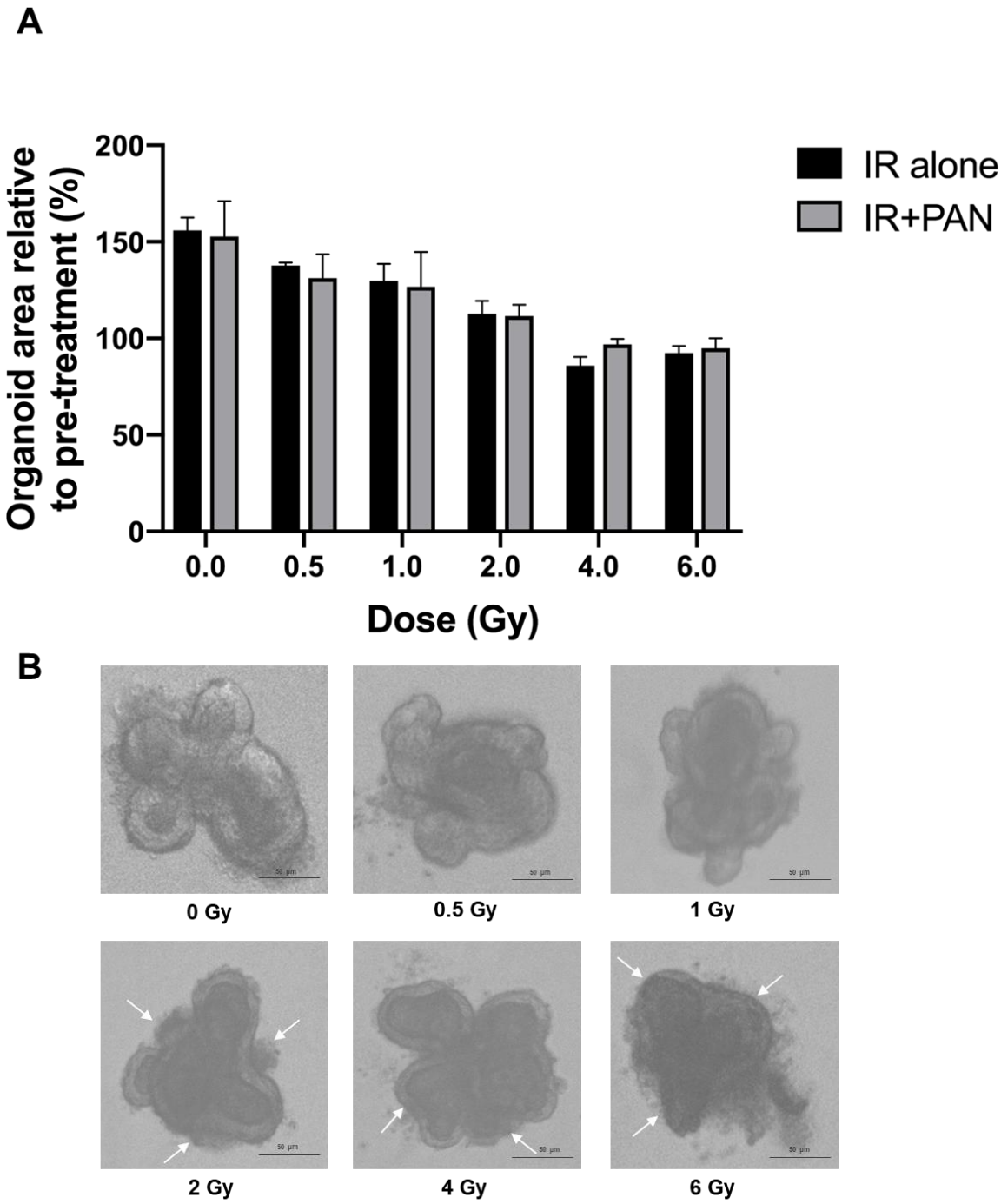

Figure 17. Response to panobinostat/IR at different radiation doses three days post-treatment (pilot experiment). A. Organoid growth response for 29 nM of panobinostat+IR was compared to IR alone. B. Brightfield images of organoids treated with 29 nM panobinostat and irradiation. At 3 days post-drug treatment+IR, disaggregation (as indicated by the white arrows) can be seen at 2 Gy, 4 Gy, and 6 Gy. The average number of organoids per well, and average/standard deviation of organoid size can be found in the appendix (S4.1, S4.2). Error bars show the standard error of the mean. N=3 from one individual isolation. Scale bar shows 50 μm.

3.3.6 The chemoradiation assay with combinations of panobinostat or gemcitabine, and irradiation showed that gemcitabine and panobinostat minimally reduces growth at low doses

Following the results from the pilot experiment involving assessing organoid response to panobinostat and irradiation, parameters were altered to test the IR+drug combination treatments. For this set of experiments, doses between 0 Gy and 2 Gy were used because at radiation doses of 4 Gy and higher there is significant organoid disaggregation, which could affect the quantification of the organoid growth.

The concentrations of gemcitabine and panobinostat were determined based on the IC50 values that were calculated when assessing organoid response to drug alone. Here we chose the concentrations that were slightly below the IC50 values so the additive effect of the drug to the radiation would not cause complete disaggregation of the organoids but allow for organoid response to be observed and compared to radiation alone.

The procedure for this experiment was similar to that of the pilot experiment where organoids were imaged before treatment and then the drugs were administered 6 hours prior to irradiation. The medium was changed immediately after irradiation and organoids were imaged three days after drug treatment and irradiation.

3.3.7 Gemcitabine minimally reduces organoid growth at low radiation doses

Historical data from the irradiation experiment was compared with gemcitabine+IR. (Figure 18A). Organoids that were only exposed to irradiation had an organoid growth between 113% and 138%. Gemcitabine at 10 nM with IR seems to show lower organoid growth compared to gemcitabine at 2.5 nM with IR. At 0.5 Gy and 2.5 nM gemcitabine treatment, organoid growth was increased to

133% compared to pretreatment/IR. At 0.5 Gy and 10 nM gemcitabine treatment, organoid growth was increased to 131% compared to pretreatment/IR. At 1 Gy and 2.5 nM gemcitabine treatment, organoid growth was increased to 134% compared to pretreatment/IR. At 1 Gy and 10 nM gemcitabine treatment, organoid growth was increased to 122% compared to pretreatment/IR. At 2 Gy and 2.5 nM gemcitabine treatment, organoid growth was increased to 115% compared to pretreatment/IR. At 2 Gy and 10 nM gemcitabine treatment, organoid growth was increased to 114% compared to pretreatment. Two-way ANOVA analysis was completed to compare the mean differences between IR alone, IR+ 2.5 nM gemcitabine, and IR+10 nM gemcitabine at radiation doses of 0.5 1 and 2 Gy. Although a small reduction in organoid growth as seen with gemcitabine+IR, changes were not statistically significant upon conducting two-way ANOVA analysis.

For consistency, experiments that involve testing organoid response to gemcitabine+IR should have an incubation time that is the same as the experiments for gemcitabine alone. Therefore, future experiments should involve a 24 hour incubation time for gemcitabine prior to irradiation.

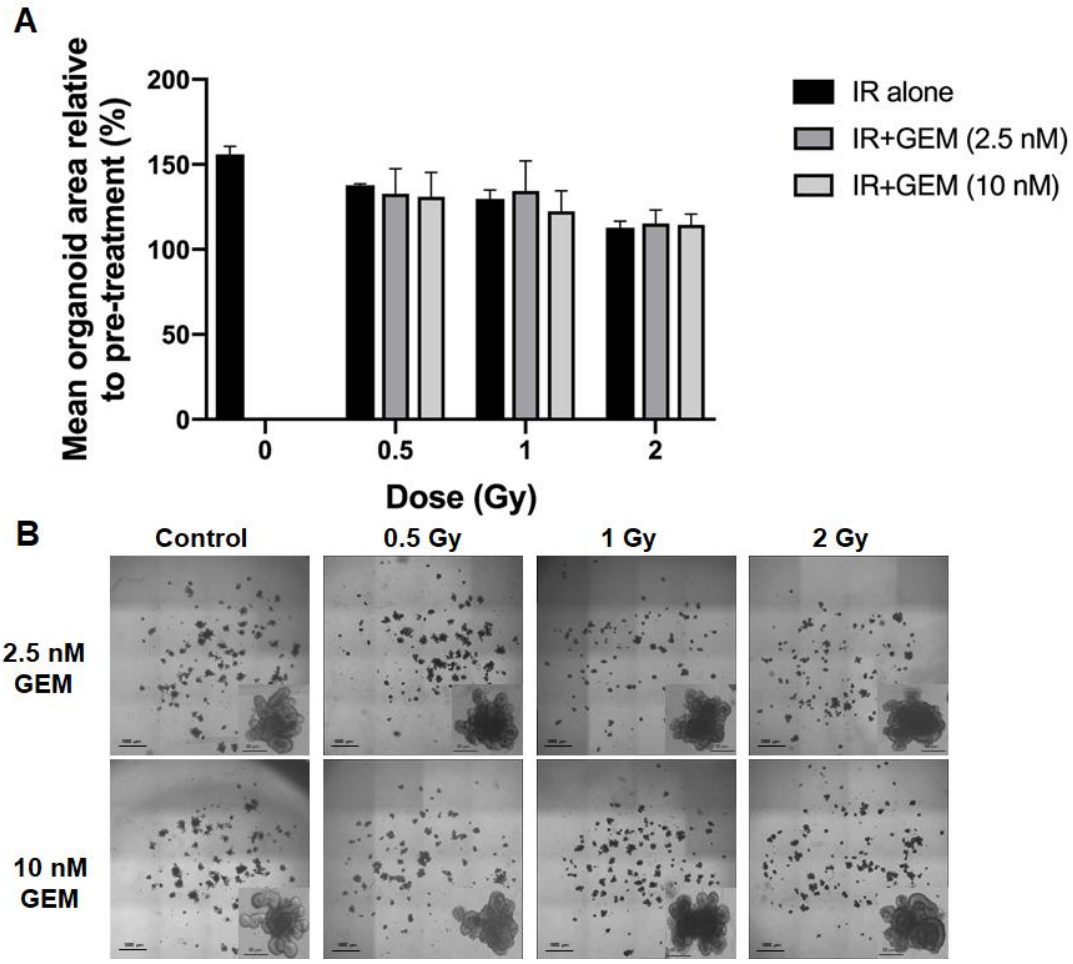

Figure 18. Response to the gemcitabine at different radiation doses three days post-treatment. A. There is negligible difference between gemcitabine concentrations with IR results compared to IR only. Organoid growth response for 2.5 and 10 nM of gemcitabine+IR was compared to IR. B. Brightfield images of organoids treated with gemcitabine and irradiation. At 3 days post-drug treatment+IR, minimal disaggregation can be seen at 2 Gy. Magnified individual organoids are shown in the right-hand corners. The average number of organoids per well, and average/standard deviation of organoid size can be found in the appendix (S5.1, S5.2). Error bars show the standard error of the mean. N=4 from two biological independent repeats. Scale bar shows 50 μm for magnified organoids and 1000 μm for each well.

Gemcitabine and irradiation did not impeded organoid growth since all organoid areas were increased compared to pre-IR when assessing chemoradiotherapy and irradiation. However, gemcitabine toxicity was demonstrated by the disaggregation of organoids showing mature morphology at IR doses of 2.0 Gy at three days post-treatment (Figure 18C). Although a potential radiosensitising effect is observable, it was not significant enough to cause a change in organoid

size. Therefore, conclusions cannot be made about the potential for gemcitabine to induce intestinal organoid toxicity and serve as an additive effect to irradiation.

3.3.8 Panobinostat minimally reduces organoid growth at low radiation doses

Historical data (IR alone) from the irradiation experiment was compared with panobinostat+IR. No statistical significance was found between the control and treatment groups upon conducting two-way ANOVA analysis, although the control groups for the panobinostat+IR seems to be higher than the IR only (Figure 19A). The control groups were the same results as what had been used for the gemcitabine+IR experiment. The growth of organoids that only received radiation was similar to the organoids that received 6.25 nM and 25 nM of panobinostat and differential radiation doses. Though at 0.5 Gy IR with 25 nM panobinostat showed less increase in organoid growth compared to 0.5 Gy IR with 6.25 nM panobinostat, the organoid growth was actually higher in 25 nM panobinostat with higher IR dose compared to 6.25 nM panobinostat with higher IR dose. At 0.5 Gy and 6.25 nM panobinostat treatment, organoid growth was increased to 137% compared to pretreatment/IR. At 0.5 Gy and 25 nM panobinostat treatment, organoid growth was increased to 130% compared to pretreatment/IR. At 1 Gy and 6.25 nM panobinostat treatment, organoid growth was increased to 127% compared to pretreatment/IR. At 1 Gy and 25 nM panobinostat treatment, organoid growth was increased to 128% compared to pretreatment/IR. At 2 Gy and 6.25 nM panobinostat treatment, organoid growth was increased to 110% compared to pretreatment/IR. At 2 Gy and 25 nM gemcitabine treatment, organoid growth was increased to 112% compared to pretreatment/IR. The extent to which organoids grew with chemoradiation was decreased when both concentrations of panobinostat were combined with 2 Gy radiation dose. Minimal panobinostat toxicity was demonstrated by minimal disaggregation of organoids at 2 Gy (Figure 19B). As the lack of panobinostat only group in the experimental design, conclusions cannot be

made about the potential for panobinostat to induce intestinal organoid toxicity and serve as a radiosensitiser to irradiation.

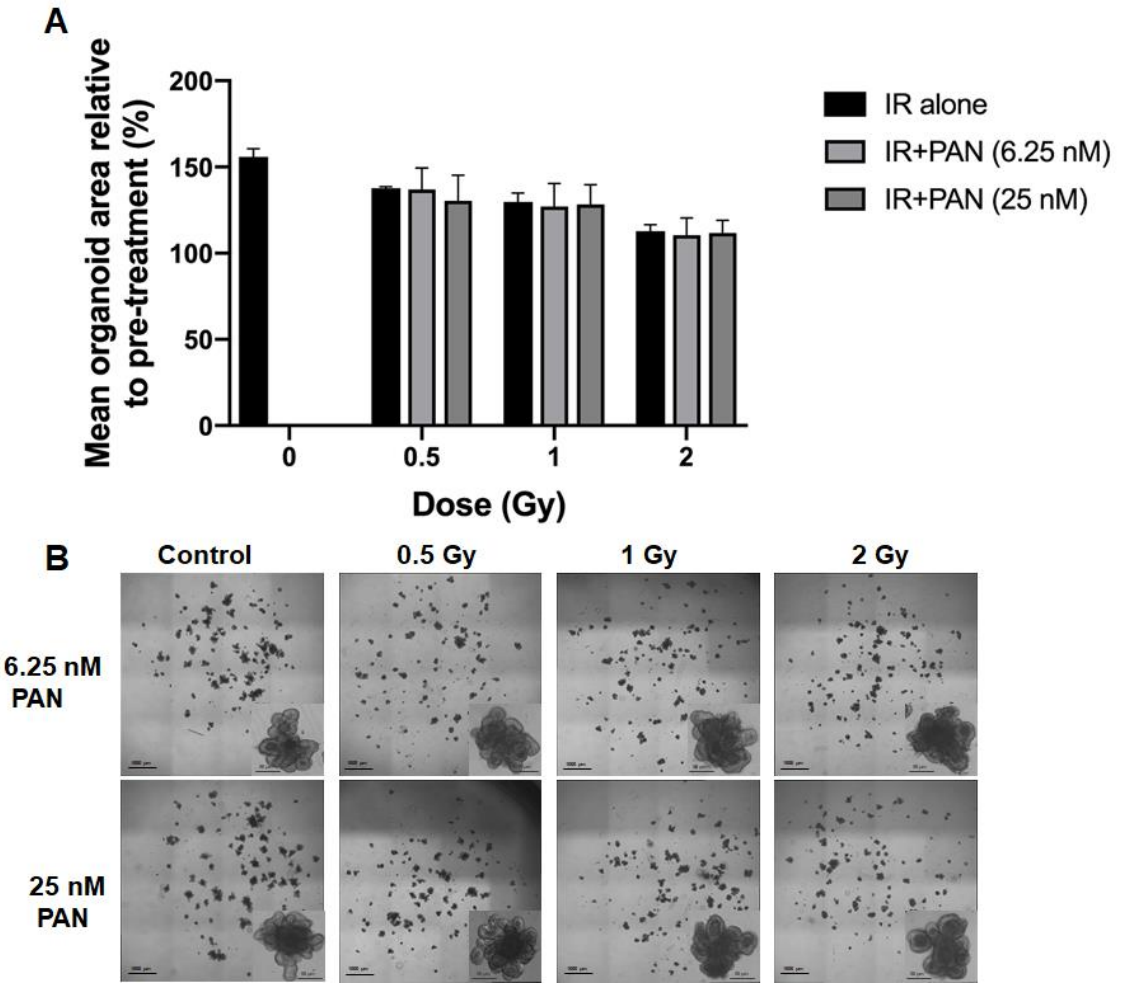

Figure 19. Response to the panobinostat at different radiation doses three days post-treatment. A. Organoid growth response for 6.25 and 25 nM of panobinostat+IR was compared to IR alone. There is negligible difference between panobinostat concentrations with IR results compared to IR only. C. Brightfield images of organoids treated with panobinostat and irradiation. At 3 days post-drug treatment+IR, minimal disaggregation can be seen at 2 Gy. Magnified individual organoids are shown in the right-hand corners. The average number of organoids per well, and average/standard deviation of organoid size can be found in the appendix (S6.1, S6.2). N=4 from two biological independent repeats. Scale bar shows 50 μm for magnified organoids and 1000 μm for each well.

3.3.9 Gemcitabine and panobinostat at low radiation doses cause a similar decrease in organoid growth compared to IR alone

When directly comparing the effects of gemcitabine+IR and panobinostat+IR alone, it is demonstrated that there is negligible difference in organoid growth. However, both drugs caused decreased organoid growth compared to IR alone but findings were not statistically significant. When comparing organoid response for each condition to the control, at 0.5 Gy with 25 nM panobinostat and 10 nM gemcitabine treatment, organoid growth was increased to 130% and 131% respectively, whereas organoid growth was increased to 138% for IR alone (Figure 20A). At 1 Gy with 25 nM panobinostat and 10 nM gemcitabine treatment, organoid growth was reduced to 128% and 122% respectively, whereas organoid growth was reduced to 130% for IR alone (Figure 20B). At 2 Gy with 25nM panobinostat and 10 nM gemcitabine treatment, organoid growth was reduced to 112% and 114% respectively, whereas organoid growth was reduced to 112% for IR alone (Figure 20C). At all radiation doses, gemcitabine and panobinostat had similar effects because there was no more than a 6% difference in organoid growth. At administration of 0.5 Gy, organoid growth was greater for IR alone compared to the combined drug and IR treatment. Based on the analysis of results, gemcitabine and panobinostat do not significant radiosensitising affects at these concentrations that would impact the mean organoid size, however, minimal disaggregation was seen in both culture at 2 Gy.

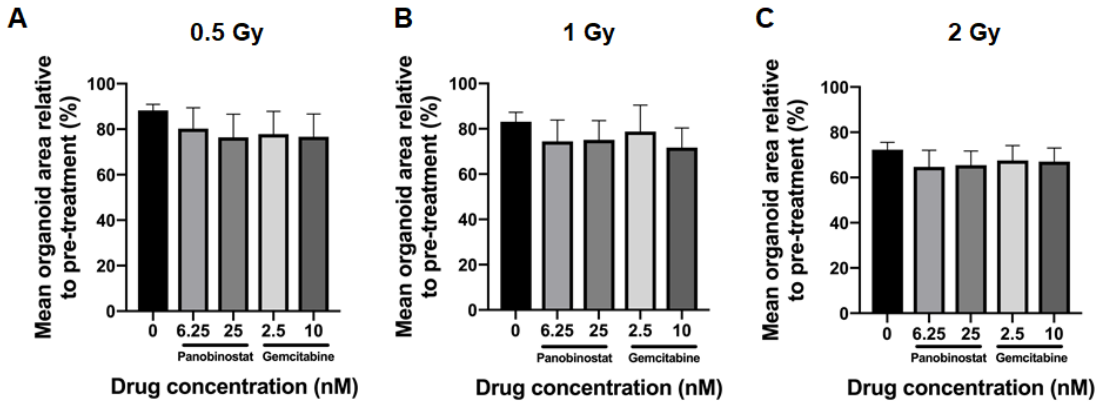

Figure 20. Comparison organoid response to irradiation alone and gemcitabine and panobinostat at different radiation doses. There is negligible difference in organoid response when comparing GEM+IR and PAN+IR. A. At 0.5 Gy, organoid growth response for gemcitabine+IR and panobinostat+IR was compared to IR alone by normalising the data points to the individual 0 Gy. B. At 1 Gy, organoid growth response for gemcitabine+IR and panobinostat+IR was compared to IR alone by normalising the data points to the individual 0 Gy. C. At 2 Gy, organoid growth response for panobinostat+IR and panobinostat+IR was compared to IR alone by normalising the data points to the individual 0 Gy. Error bars show the standard error of the mean.

4. DISCUSSION

Although the mechanisms by which chemoradiation therapy impacts normal intestinal tissue has been studied at the cellular and molecular level (Shadad et al., 2013) a systematic approach to study chemoradiation therapy-induced intestinal toxicity is still lacking in the development pipeline for new radiosensitisers. Chemoradiation therapy is often what is used to treat relatively fit elderly patients with MIBC who are unable to withstand surgery. However, there are sequelae associated with chemoradiation therapy involving gastrointestinal tissue toxicity. This is due to the high turnover rate of intestinal epithelial cells that are ablated when irradiated.

Previous research studying the radiation response of the intestine has involved using preclinical animal models. However, these models are difficult to translate into clinical practice due to the difference between human and animal and cannot be used to personalise treatment based on the patient's needs. Therefore, further development in the current preclinical research models is required to understand the impact of varying levels of irradiation and radiosensitisers on the intestine. The first aim of this project involved establishing a 3D *in vitro* tool using gastrointestinal organoids. As patient-derived human intestinal organoids are harder to come by, murine organoids were used here to optimise the potential assay conditions. Optimisation of the protocols resulted in increased efficiency of organoid generation. The response of gastrointestinal organoids to irradiation and radiosensitising drugs could be studied by conducting assays where the size and budding organoid-to-total organoid ratio after treatment was recorded.

4.1 Refinement of organoid culturing and cryopreservation method

Upon determining the most time and cost effective procedures to isolate and maintain the gastrointestinal organoid assay, there were some techniques that deviated from standardized organoid isolation and maintenance protocol (Sato et al., 2011). Particularly, a ratio of 3:2

Matrigel-to-medium was used to culture organoids compared to the standard of suspending organoids in 100% Matrigel. This was done to reduce the cost associated with replenishing expensive Matrigel. Additionally, upon dispensing the mixture consisting of organoids, Matrigel, and medium, organoids were unconventionally inverted and placed in the incubator for 10 minutes before turning the plate right side up (commonly referred to as the hanging drop method). Because there was a lower concentration of Matrigel in the Matrigel/medium/organoid domes compared to the standard protocol, the mixture was not as dense and were inverted to ensure polymerization and solidification of the domes. Lastly, passaging organoids entailed adding 1 mL of cold 15 mM EDTA in PBS to the organoid-containing wells and pipetting up and down ten times and incubating for 10 minutes instead of using trypsin-EDTA/TrypLE to disassociate the organoids. This use of 15 mM EDTA in PBS to disassociate organoids was established from a previous lab protocol and was more cost-effective than purchasing the commercialized dissociation reagent. .

Establishing effective thawing and freezing protocols was key to refinement of the assay and creation of an intestinal organoid collection that could be cryopreserved.

Unlike general tissue culture, cryopreservation of intestinal organoids is challenging due to poor crypt survival. Poor crypt survival may be linked to the difficulties with maintaining intestinal epithelial cells when cryopreserved. During the process, intestinal epithelial cells begin to shed, undergo DNA fragmentation and demonstrate morphological features of apoptosis (Grossman et al., 1998).

Low crypt viability may also be due to the disrupted basement membrane that is characteristic of organoids, as configuration of the basement membrane can create conditions that induce “anoikis”. Anoikis is a form of apoptosis involving the detachment of anchorage-dependent cells from the

surrounding extracellular matrix, which has been known to cause low organoid numbers from loss of intestinal epithelial cells post-cryopreservation (Frisch and Francis, 1994).

Another explanation for low organoid yield post-preservation is the breakdown in blood supply and thermoregulation that has an additive effect with the disruption of cell-cell and cell-matrix interactions during isolation (Fang et al., 2017). These problems, in addition to anoikis, make the organoid model unstable and unable to independently withstand freeze and thaw cycles like normal cell cultures.

ROCK inhibitor is essential for the cryopreservation of gastrointestinal organoids

Establishing effective thawing and freezing protocols was key to refinement of the assay and creation of an intestinal organoid collection. Unlike general tissue culture, cryopreservation of intestinal organoids is challenging due to poor crypt survival. Poor crypt survival may be linked to the difficulties with maintaining intestinal epithelial cells when cryopreserved. During the process, intestinal epithelial cells begin to shed, undergo DNA fragmentation and demonstrate morphological features of apoptosis (Grossman et al., 1998).

Low crypt viability may also be due to the disrupted basement membrane, which may induce “anoikis”. Anoikis is a form of apoptosis due to the detachment of anchorage-dependent cells from the surrounding extracellular matrix, which has been known to cause low organoid numbers from lost of intestinal epithelial cells post-cryopreservation (Fang et al., 2017).

To aid in the survival of various types of stem cells, including ISCs, ROCK inhibitor treatments were employed during subculture. Optimisation of the organoid cryopreservation was achieved by adding the ROCK inhibitor on the thawing organoids. In previously published protocols, ROCK

activity and cytoskeletal phenotypes are almost completely inhibited by 10 μmol/L of ROCK inhibitor (Han et al., 2017). Studies have found that ROCK activation is required for "membrane ruffling", a process involved in apoptosis (Sebbagh, 2005) and ROCK inhibition has demonstrated anti-apoptotic activity by diminishing anoikis-induced apoptosis (Anderson et al., 2002; Honjo et al., 2007). By evaluating the densities of grown organoids after thawing, the addition of ROCK inhibitor into the growth medium while thawing resulted in superior recovery with 86% viability ($p=0.0299$) (Figure 12C).

Plating conditions were also optimised. It has been claimed that culturing organoids in 6-well plates helps to optimise culture vessel space, make manipulation of organoids easier, and improve polymerisation of the matrix (Clinton and Koeppen, 2019). To test this statement, approximately 8-10 droplets (10-15 μL per droplet) were dispensed into each well of the pre-warmed 6-well plate with 1.5 mL of complete growth medium. This "multi-dome" approach was adopted in the hope that gas and nutrient diffusion would be maximised. The standard conditions of 24-well plate were also used as comparison, where each dome contained 50 μL of re-suspended organoids in matrix with 400 μL of complete growth medium. However, contrary to the previous findings, a higher yield (viability) of organoids was seen when using the 24-well seeding conditions compared to the 6-well seeding dish conditions in the post-thawing organoids (Figure 10). On the other hand, cryopreserved organoids that have been passaged at least once showed good viability in both conditions and 6-well seeding seems to produce better yield, but more experiment will need to be done for further validation ($p=0.0038$) (Figure 11).

Overall, establishing an optimal expansion and cryopreservation protocol led to the creation of a collection that was time-efficient in terms of coordinating assay schedules and for reducing expenses.

4.2 Development of organoid assay

Rationale for evaluating the efficiency of organoid fragment seeding

When developing the assay, it is important to establish the organoid fragment seeding number that would be best for not only intestinal growth but also end point analysis. In our assay, we used microscopic imaging as our end point analysis. Thus, organoid seeding densities and matrix compositions (medium/Matrigel ratio) were determined that were optimal for growth, imaging and automated scoring. The former MSc student established that 50 organoids per well was best for imaging and growth, under a 1:1.2 medium/Matrigel ratio (Gorrill, 2018). However, it was necessary to determine how many organoid fragments needed to be seeded in order to achieve that optimal organoid formation number and whether the ratio of medium to Matrigel has an impact on organoid formation.

The matrix in which organoids are embedded includes medium and tumour-derived basement membrane extract (provided as the commercial product Matrigel). This basement membrane extract (BME) enables intestinal stem cells and primary intestinal epithelium to grow and expand *in vitro* following mechanical or enzymatic dissociation. Addition of organoid growth culture medium to BME helps to promote homogeneous distribution of growth factors to the crypt suspended in the matrix. The matrix composition also has an impact on imaging abilities and whether the distribution of organoids resides within suitable focal planes for monolayer imaging. It is important that the maximum number of organoids are in the same plane and are scorable. The result showed that best organoid formation was seen when crypts were suspended in Matrigel concentrations 1.5 times that of the crypt-suspension medium volume, resulting in scorable organoids being evenly distributed throughout the dome (Figure 13).

4.3 Intestinal organoids under radiation or chemoradiation conditions

The irradiation assay was conducted to determine the optimal radiation dose range for intestinal organoids. Compared to the non-irradiated control, irradiation caused more rapid disaggregation for all organoid groups and delayed budding at radiation doses 2 Gy or higher. Although the administration of irradiation below 2 Gy does not impede organoid growth, doses above 2 Gy (4 and 6 Gy) stopped budding and caused disaggregation by the second day post-irradiation (Figure 14). This study gave a preliminary indication of the time points and irradiation doses required for the chemoradiation assay.

To determine the dose required for testing radiosensitisation of intestinal organoids, the drug assay was conducted by treating organoids with gemcitabine or panobinostat at different concentrations for 24 hours. Beginning at day 2, significant disaggregation was seen for organoids that were treated with 25 nM and 50 nM of gemcitabine (Figure 15) and 50 nM and 100 nM of panobinostat (Figure 16) compared to the control organoids and organoids that received lower concentrations of the drugs. By day 5, minimal premature disaggregation was present in cultures that received low drug concentrations whereas disaggregation was rarely seen in the controls.

Overall, 2.5 nM/10 nM gemcitabine or 6.25 nM/25 nM panobinostat in combination with irradiation has no effect on organoid growth and budding compared to IR alone (Figure 20). This is indicated by the increased in organoid size relative to pre-IR for all gemcitabine and panobinostat concentrations. For the combinational treatment, disaggregation of some of the larger organoids was seen 3 days post-treatment/IR in cultures irradiated at 2 Gy however there was not a significant amount of disaggregation to elicit a change in average organoid size for the cultures, This observation suggested that at higher gemcitabine and panobinostat doses, both may enhance radiation toxicity, however, their effect on the organoid area compared to IR alone was minimal.

This can be attributed to the low doses of the drugs that were administered, making it difficult to determine the antagonistic effect of gemcitabine and panobinostat on radiotherapy. Incremental concentrations of drug treatment would have to be tested to discern which doses have the greatest effect on organoid growth without completely disaggregating the organoids.

Intestinal response to panobinostat concentrations differed from our previous *in vivo* study (Groselj et al., 2018). The lab has shown that panobinostat has no effect on apoptosis or cell proliferation within 24 hours of treatment. A previous manuscript published by the lab concluded that there was no panobinostat toxicity in intestinal swiss rolls and panobinostat did not increase acute intestinal toxicity following ionizing radiation. For experiments testing the effects of panobinostat alone, approximately 100-250 nM of panobinostat was administered to the small intestine for the swiss roll experiment and no toxicity was seen. Conversely, minimal toxicity was seen in organoids that received 50 nM and 100 nM of panobinostat (Groselj et al., 2018). The difference in intestinal response to panobinostat could be attributed to the different models used for the two experiments. When a swiss roll is prepared using mouse intestine, the swiss roll has less penetration efficiency and greater surface area compared to mouse intestinal organoids and thus may be more resistant to panobinostat toxicity.

Another consideration that should be made regarding panobinostat involves determining the concentrations that are used in the organoid assay that would be proportional to the concentrations administered to patients as a chemotherapy. Currently, panobinostat has been on clinical trials to treat melanoma patients, however, if panobinostat were implemented in the clinic to treat bladder cancer, integrating the clinical use of panobinostat and the use of panobinostat for the organoid assay must be considered. The same could be said for gemcitabine since the clinical trial for gemcitabine involves administering a weekly intravenous low-dose gemcitabine (75 mg/m^2) to

treat bladder cancer (Atasoy et al., 2014). Perhaps determining the threshold for panobinostat and gemcitabine toxicity in organoids and patients would be a formidable metric to determine radiosensitiser doses for the organoid assay that is consistent with doses that are administered to patients.

Additionally, the understanding intestinal organoids response to IR, radiosensitiser, and chemoradiation damage can be expanded by using quantitative approaches such as cell viability assays. The MTT tetrazolium reduction assay can be used to measure cellular metabolic activity as an indicator of cell viability assays, proliferation, and cytotoxicity. CellTiter-Glo could be used as an alternative cell viability since the assay determines the number of living cells in culture based on the amount of ATP present, which signals the presence of metabolically active cells. If the assay shows decreased cell viability by some combinations, this could be indicative of acute normal tissue effects.

In future experiments, before assessing intestinal organoid response to chemoradiation and chemotherapy we should validate that panobinostat and gemcitabine were taken up into cells and were active. This can be done by histone acetylation and DNA damage. Histone acetylation experiments could involve western blot, ATAC-seq, and CHIP-seq. DNA damage experiments involve Tunel assay and staining for Rad 51.

4.4 Comparing 3D organoid response to chemoradiotherapy to that of *in vivo* and 2D cell models

Research has shown that radiation doses of 8 to 15 Gy are sufficient to induce intestinal epithelial injury in mice (Kim et al., 2017). Previously, when assessing intestinal chemoradiation toxicity using the *in vivo* Swiss roll technique in the lab, between 10 and 14 Gy doses were given to the

abdomen of the mouse (Groselj et al., 2018). The swiss roll technique is a standard method for processing the intestine for histology; however, this method does not reflect the normal structure of the intestine in a mouse. Similar to assessing gastrointestinal organoid toxicity, the drugs were administered six hours prior to irradiation. Significant crypt loss began at 10 Gy for the Swiss roll technique compared to the irradiation of organoids where significant disaggregation was seen at 4 Gy, both with and without drug treatment. There is an apparent difference between the threshold at which the intestine and an intestinal organoid show signs of degradation due to radiation toxicity. This can be attributed to the difference in size of a mouse intestinal organoid compared to a whole mouse intestine and penetration efficiency.

In terms of cell culture, there is very little information regarding the effects of chemoradiotherapy on intestinal cell toxicity in 2D cell lines. Previously, when exploring the radiosensitiser effects of panobinostat , the lab has used clonogenic assays to assess the effects of 6 Gy irradiation and panobinostat (25 nM) and other HDAC inhibitors on bladder cancer cell lines (Groselj et al., 2018). A similar study was done where the toxicity from 5 Gy irradiation and gemcitabine (10 nM) was assessed in a panel of bladder cancer cell lines (Kerr et al., 2014). Although the reported gemcitabine and panobinostat concentration from both publications matched our current testing concentration for chemoradiation assay, the cell lines were treated for 24 hours, instead of incubating the cell lines with the drugs for 6 hours, as done in the *in vivo* and the current organoid experiments. It is possible that incubation the organoids with drugs for only 6 hours was not be sufficient for the uptake of these drugs in 3D culture condition.

4.5 Limitations of the research

The goal of this study was to develop a gastrointestinal organoid assay to screen the optimal combination of radiosensitising drugs with radiotherapy in studying the gastrointestinal normal

tissue toxicity from chemoradiation therapy. Here the organoid size was used as our primary end point analysis and the budding to total organoid ratio was assessed on day 4 post-passage and showed a positive linear correlation with the organoid size. However, in addition, other markers such as Bmi1 and Lgr5+ should also be studied to identify the potential change in cellular composition in organoids.

One major limitation of the organoid model is that organoids are exclusively comprised of epithelial cells and therefore lack associated fibroblast and muscle tissue. Fibroblasts are mesenchymal cells derived from the embryonic mesoderm (McCauley and Wells, 2007). They contribute to the maintenance of a structural intestinal framework and of tissue homeostasis with their ability to synthesise many extracellular matrix and growth factors. Fibroblast also play an important role in foetal development, wound healing, and cancer progression (Higuchi et al., 2015). This lack of regulatory environment in organoid cultures disregards an important crosstalk that is important for stability of intestinal epithelial cells.

Smooth muscle comprises of folds that increase the absorptive surface area of the mucosa and produces tonic contractions that maintain organ dimensions against boluses, as well as dynamic contractions that produce the condensing of muscles to propel the bolus along the gastrointestinal tract (Silverthorn et al., 2018). Therefore the mechanical abilities of the intestine cannot be considered when using an organoid assay to assess irradiation and radiosensitiser response.

Additionally, MIBC patients receive fractionated radiation while single doses were used here. This may lead to difference in organoid response. This assay should be adapted to test fractionated radiotherapy. By conducting experiments involving this mode of radiotherapy, we would be able

to assess whether single dose administration significantly differs from fractionated dose and determine the best method to use.

Moreover, the organoid model lacks vasculature and associated immune cells that might be contributed to the pathological outcome of radiation injury. Radiation injury to the vascular compartment is thought to be a key feature in the pathological processes of intestinal radiation injury as well as an important determinant of both acute and chronic effects after radiotherapy (Molla, 2007). Apoptosis and acquisition of a pro-inflammatory, prothrombotic, and antifibrinolytic phenotype is commonly associated with an irradiated endothelium. These phenotypes can be characterised by increased secretion of soluble mediators such as cytokines, chemokines, and growth factors (Wang et al., 2007).

Activated endothelial cells express adhesion molecule markers, such as VCAM-1, ICAM-1, PECAM-1, E and P selectins (Mollà et al., 2003), and cytokine-favouring immune cells that are recruited to the site of injury. These adhesion molecules, cytokine-favoring immune cells, and pro-inflammatory soluble mediators of irradiated endothelial cells activate resident macrophages and favour the early recruitment of polymorphonuclear neutrophils from the bloodstream. Neutrophils are recruited almost immediately after trauma to tissues, and their presence is characteristic of acute inflammation. There is further inflammation at the site of injury from the recruitment of monocytes and activation of resident mast cells. These cells produce pro-inflammatory and pro-fibrosis mediators such as IL-1β, IL-6, IL-8, CXCL-1, CXCL-2, TNF-α, and TGF-β (Blirando et al., 2011). This innate immune response carried out by macrophages, neutrophils, and mast cells is supported by the adaptive immune response assumed by the B and T lymphocytes (François et al., 2013).Thus, future efforts can be focused on the development of a co-culture system that can incorporate other cell components.

Overall, the development of MIBC organoids would be a critical component for subsequent experiments for this project. Although titrating doses for toxicity in healthy gastrointestinal organoids have been established, we have yet to elucidate whether equivalent doses can kill MIBC. In order to fully achieve the aim of screening for safe and effective combinational doses, both healthy intestinal organoids and MIBC organoids should be used to titrate the minimal effective dose that kills MIBC but can be tolerated by healthy intestinal organoids.

4.6 Future directions

This assay has been established using mouse intestinal organoids. The next step for this project is to fully establish and refine the assay in human gastrointestinal organoids using multiple patient-derived samples. Human gastrointestinal organoids will be tested the same way that the murine intestinal organoids were tested and used in a collection setting. This would bring the project one step closer for preclinical findings from this assay to be translatable to the clinic to select chemoradiation treatments that are non-toxic to normal tissue when treating MIBC. Once implemented clinically, it would be best to coordinate organoid response to chemoradiotherapeutics to organ response in a patient. In addition, this assay can also be used to assess the effects of components that have been known to alleviate intestinal toxicity. Drugs such as BCN057, an anti-neoplastic small molecular agent, induce ISC proliferation and promotes intestinal epithelial repair against radiation injury (Bhanja et al., 2018). These could be used to assess the efficacy of the protective effect in our organoid system after radiation treatment.

5. CONCLUSION

In this study, an *in vitro* organoid culture system was established to predict normal intestinal tissue toxicity to radiosensitisers and irradiation. This model involves the isolation of intestinal crypts and grows them into 3D organoids. Studies involving the use of organoids as a tool to assess toxicity of chemoradiation therapy differs from their typical use of studying the cellular microenvironment and creating effective precision medicine for various cancer types. This project has much clinical relevance because gastrointestinal complications are the most prevalent side effects of cancer treatment and is associated with a poor quality of life (Andreyev et al., 2012). From the development of a high-throughput assay, organoids can be integrated into pharmacological studies to aid in the development of drugs that could treat MIBC by efficiently eliminating cancer cells while having minimal side effects on the gastrointestinal tract.

In this project, passaging and cryopreservation protocols were optimized. Additionally, the assay was developed such that organoid fragment seeding resulted in organoid quantities that are best for organoid growth and imaging. Finally, parameters of irradiation and drug concentration were determined for the chemoradiation testing. Mouse intestinal organoids were used here but the established assays should be transferable to patient derived organoids, which would allow personalized chemoradiation treatment. The 3D organoid culture system described in this thesis lays the foundation for this clinical application.

6. REFERENCES

Al-Dewachi HS, Appleton DR, Watson AJ, Wright NA. Variation in the cell cycle time in the crypts of Lieberkuhn of the mouse. Virchows Arch B Cell Pathol Incl Mol Pathol. 1979;31(1):37-44.

Anderson SC, Stone C, Tkach L, SundarRaj N. Rho and Rho-kinase (ROCK) signaling in adherens and gap junction assembly in corneal epithelium. Invest Ophthalmol Vis Sci. 2002;43(4):978-86.

Antoni S, Ferlay J, Soerjomataram I, Znaor A, Jemal A, Bray F. Bladder Cancer Incidence and Mortality: A Global Overview and Recent Trends. Eur Urol. 2017;71(1):96-108.

Atadja P. Development of the pan-DAC inhibitor panobinostat (LBH589): successes and challenges. Cancer Lett. 2009;280(2):233-41.

Barker N. Adult intestinal stem cells: critical drivers of epithelial homeostasis and regeneration. Nat Rev Mol Cell Biol. 2014;15(1):19-33.

Barker N, van Es JH, Kuipers J, Kujala P, van den Born M, Cozijnsen M, et al. Identification of stem cells in small intestine and colon by marker gene Lgr5. Nature. 2007;449(7165):1003-7.

Barker N, van Oudenaarden A, Clevers H. Identifying the stem cell of the intestinal crypt: strategies and pitfalls. Cell Stem Cell. 2012;11(4):452-60.

Barsky, D., Foloppe, N., Ahmadia, S., Wilson, D. M., & MacKerell, A. D. (2000). New insights into the structure of abasic DNA from molecular dynamics simulations. *Nucleic Acids Research, 28*(13), 2613–2626. https://doi.org/10.1093/nar/28.13.2613

Bentzen SM. Preventing or reducing late side effects of radiation therapy: radiobiology meets molecular pathology. Nat Rev Cancer. 2006;6(9):702-13.

Beumer J, Clevers H. Regulation and plasticity of intestinal stem cells during homeostasis and regeneration. Development. 2016;143(20):3639-49.

Bhanja P, Norris A, Gupta-Saraf P, Hoover A, Saha S. BCN057 induces intestinal stem cell repair and mitigates radiation-induced intestinal injury. Stem Cell Res Ther. 2018;9(1):26.

Bitar, K. N. (2003). Function of gastrointestinal smooth muscle: from signaling to contractile proteins. *The American Journal of Medicine, 115*(3), 15–23.

Biteau B, Jasper H. EGF signaling regulates the proliferation of intestinal stem cells in

Drosophila. Development. 2011;138(6):1045-55.

Bjerknes, M., & Cheng, H. (1981). Methods for the isolation of intact epithelium from the mouse intestine. The Anatomical Record, 199(4), 565–574.

Blirando, K., Milliat, F., Martelly, I., Sabourin, J. C., Benderitter, M., & François, A. (2011). Mast cells are an essential component of human radiation proctitis and contribute to experimental colorectal damage in mice. *American Journal of Pathology*, *178*(2), 640–651.

Booth C, Tudor G, Tudor J, Katz BP, MacVittie TJ. Acute gastrointestinal syndrome in high dose irradiated mice. Health Phys. 2012;103(4):383-99.

Bouffard DY, Laliberte J, Momparler RL. Kinetic studies on 2',2'-difluorodeoxycytidine (Gemcitabine) with purified human deoxycytidine kinase and cytidine deaminase. Biochem Pharmacol. 1993;45(9):1857-61.

Brierley JD, Brierley JD, Gospodarowicz MK. TNM Classification of Malignant Tumours, 2016.

Casteleyn C, Rekecki A, Van der Aa A, Simoens P, Van den Broeck W. Surface area assessment of the murine intestinal tract as a prerequisite for oral dose translation from mouse to man. Lab Anim. 2010;44(3):176-83.

Chaudhry, M. A. (2007). Base excision repair of ionizing radiation-induced DNA damage in G1 and G2 cell cycle phases. *Cancer Cell International*, *7*, 1–11.

Chen L, Deng H, Cui H, Fang J, Zuo Z, Deng J, et al. Inflammatory responses andinflammation associated diseases in organs. Oncotarget. 92018. p. 7204-18.

Choudhury A, Swindell R, Logue JP, Elliott PA, Livsey JE, Wise M, et al. Phase II study of conformal hypofractionated radiotherapy with concurrent gemcitabine in muscle invasive bladder cancer. J Clin Oncol. 2011;29(6):733-8.

Ciccia A, Elledge SJ. The DNA Damage Response: Making it safe to play with knives. Mol Cell. 2010;40(2):179-204.

Ciccolini, J., Barbolosi, D., Meille, C., Lombard, A., Serdjebi, C., Giacometti, S., André, N. (2017). Pharmacokinetics and pharmacodynamics-based mathematical modeling identifies an optimal protocol for metronomic chemotherapy. *Cancer Research*, *77*(17), 4723–4733.

Clevers H. The intestinal crypt, a prototype stem cell compartment. Cell. 2013;154(2):274-84.

Clevers HC, Bevins CL. Paneth cells: maestros of the small intestinal crypts. Annu Rev Physiol. 2013;75:289-311.

Clinton J, McWilliams-Koeppen P. Initiation, Expansion, and Cryopreservation ofHuman Primary Tissue-Derived Normal and Diseased Organoids in Embedded Three-Dimensional Culture. Curr Protoc Cell Biol. 2019;82(1):e66.

Cox JD, Stetz J, Pajak TF. Toxicity criteria of the Radiation Therapy Oncology Group (RTOG) and the European Organization for Research and Treatment of Cancer (EORTC). Int J Radiat Oncol Biol Phys. 31. United States1995. p. 1341-6.

Crosnier C, Stamataki D, Lewis J. Organizing cell renewal in the intestine: stem cells, signals and combinatorial control. Nat Rev Genet. 2006;7(5):349-59.

Cui S, Chang PY. Current understanding concerning intestinal stem cells. World J Gastroenterol. 2016;22(31):7099-110.

Cumberbatch MG, Cox A, Teare D, Catto JW. Contemporary Occupational Carcinogen Exposure and Bladder Cancer: A Systematic Review and Meta-analysis. JAMA Oncol. 2015;1(9):1282-90.

Dall'Era MA, Albertsen PC, Bangma C, Carroll PR, Carter HB, Cooperberg MR, et al. Active surveillance for prostate cancer: a systematic review of the literature. Eur Urol. 2012;62(6):976-83.

Davidson LA, Callaway E, Kim E, Weeks BR, Fan YY, Allred CD, et al. Targeted deletion of p53 in Lgr5-expressing intestinal stem cells promotes colon tumorigenesis in a preclinical model of colitis-associated cancer. Cancer Res. 2015;75(24):5392-7.

Davis, A. J., & Chen, D. J. (2013). DNA double strand break repair via non-homologous end joining. *Translational Cancer Research*, *2*(3), 130–143.

de Lau W, Barker N, Low TY, Koo BK, Li VS, Teunissen H, et al. Lgr5 homologues associate with Wnt receptors and mediate R-spondin signalling. Nature. 2011;476(7360):293-7.

de Lau W, Peng WC, Gros P, Clevers H. The R-spondin/Lgr5/Rnf43 module: regulator of Wnt signal strength. Genes Dev. 2014;28(4):305-16.

de Sousa Cavalcante L, Monteiro G. Gemcitabine: metabolism and molecular mechanisms of action, sensitivity and chemoresistance in pancreatic cancer. Eur J Pharmacol. 2014;741:8-16.

Edmondson R, Broglie JJ, Adcock AF, Yang L. Three-Dimensional Cell Culture Systems

and Their Applications in Drug Discovery and Cell-Based Biosensors. Assay Drug Dev Technol. 122014. p. 207-18.

Elphick DA, Mahida YR. Paneth cells: their role in innate immunity and inflammatory disease. Gut. 542005. p. 1802-9.

Farin HF, Karthaus WR, Kujala P, Rakhshandehroo M, Schwank G, Vries RG, et al. Paneth cell extrusion and release of antimicrobial products is directly controlled by immune cell–derived IFN-γ. J Exp Med. 2112014. p. 1393-405.

François, A., Terro, F., Janet, T., Bilan, A. R., Paccalin, M., & Page, G. (2013). Involvement of interleukin-1β in the autophagic process of microglia: Relevance to Alzheimer's disease. Journal of Neuroinflammation, 10. https://doi.org/10.1186/1742-2094-10-151

Frisch SM, Francis H. Disruption of epithelial cell-matrix interactions induces apoptosis. J Cell Biol. 1994;124(4):619-26.

Gao Z, Ye Y, Zhang W, Shen D, Zhong Y, Jiang K, et al. An anatomical, histopathological, and molecular biological function study of the fascias posterior to the interperitoneal colon and its associated mesocolon: their relevance to colonic surgery. J Anat. 2013;223(2):123-32.

Geboes, K., Riddell, R., Ost, A., Jensfelt, B., Persson, T., & Löfberg, R. (2000). A reproducible grading scale for histological assessment of inflammation in ulcerative colitis. *Gut, 47*(3), 404–409.

Gehart H, Clevers H. Tales from the crypt: new insights into intestinal stem cells. Nat Rev Gastroenterol Hepatol. 2019;16(1):19-34.

Gofrit ON, Nof R, Meirovitz A, Pode D, Frank S, Katz R, et al. Radical cystectomy vs. chemoradiation in T2-4aN0M0 bladder cancer: a case-control study. Urol Oncol. 2015;33(1):19.e1-.e5.

Gorrill J. Development of a organoid assay to identify chemoradiation combinations for abdominal and pelvic tumors. 2018.

Groselj B, Ruan JL, Scott H, Gorrill J, Nicholson J, Kelly J, et al. Radiosensitization In Vivo by Histone Deacetylase Inhibition with No Increase in Early Normal Tissue Radiation Toxicity. Mol Cancer Ther. 2018;17(2):381-92.

Groselj B, Sharma NL, Hamdy FC, Kerr M, Kiltie AE. Histone deacetylase inhibitors as radiosensitisers: effects on DNA damage signalling and repair. Br J Cancer. 2013;108(4):748-54.

Grossman HB, Natale RB, Tangen CM, Speights VO, Vogelzang NJ, Trump DL, et al. Neoadjuvant chemotherapy plus cystectomy compared with cystectomy alone for locally advanced bladder cancer. N Engl J Med. 2003;349(9):859-66.

Hall, E. J., & Giaccia, A. J. (2012). *Radiobiology for the radiologist: Seventh edition*. *Radiobiology for the Radiologist: Seventh Edition*.

Han SH, Shim S, Kim MJ, Shin HY, Jang WS, Lee SJ, et al. Long-term culture-induced phenotypic difference and efficient cryopreservation of small intestinal organoids by treatment timing of Rho kinase inhibitor. World J Gastroenterol. 2017;23(6):964-75.

Hatzis P, Al Madhoun A, Jullig M, G Petrakis T, Eriksson S, Talianidis I. The Intracellular Localization of Deoxycytidine Kinase1998. p. 30239-43.

Hauer-Jensen M, Wang J, Boerma M, Fu Q, Denham JW. Radiation damage to the gastrointestinal tract: mechanisms, diagnosis, and management. Curr Opin Support Palliat Care. 2007;1(1):23-9.

Hausmann M, Spottl T, Andus T, Rothe G, Falk W, Scholmerich J, et al. Subtractive screening reveals up-regulation of NADPH oxidase expression in Crohn's disease intestinal macrophages. Clin Exp Immunol. 2001;125(1):48-55.

Higuchi, Y., Kojima, M., Ishii, G., Aoyagi, K., Sasaki, H., & Ochiai, A. (2015). Gastrointestinal fibroblasts have specialized, diverse transcriptional phenotypes: A comprehensive gene expression analysis of human fibroblasts. *PLoS ONE*, *10*(6).

Holloman, William K. “Unraveling the mechanism of BRCA2 in homologous recombination.” *Nature structural & molecular biology* vol. 18,7 748-54.

Honjo M, Tanihara H, Kameda T, Kawaji T, Yoshimura N, Araie M. Potential role of Rho associated protein kinase inhibitor Y-27632 in glaucoma filtration surgery. Invest Ophthalmol Vis Sci. 2007;48(12):5549-57.

Howitt, Michael R, Sydney Lavoie, Monia Michaud, Arthur M Blum, Sara V Tran, Joel V Weinstock, Carey Ann Gallini, Kevin Redding, Robert F Margolskee, Lisa C Osborne, David Artis, and Wendy S Garrett. "Tuft Cells, Taste-chemosensory Cells, Orchestrate Parasite Type 2 Immunity in the Gut." *Science (New York, N.Y.)* 351.6279 (2016): 1329-1333.

Huang, P., Plunkett, W., Grindey, G. B., & Plunkett, W. (1991). Action of 2’,2’-Difluorodeoxycytidine on DNA Synthesis. *Cancer Research*, *51*(22), 6110–6117.

Hurst RE, Rhodes SW, Adamson PB, Parsons CL, Roy JB. Functional and structural characteristics of the glycosaminoglycans of the bladder luminal surface. J Urol. 1987;138(2):433-7.

James ND, Hussain SA, Hall E, Jenkins P, Tremlett J, Rawlings C, et al. Radiotherapy with or without chemotherapy in muscle-invasive bladder cancer. N Engl J Med. 2012;366(16):1477-88.

Kachlik, D., Baca, V., & Stingl, J. (2010). The spatial arrangement of the human large intestinal wall blood circulation. *Journal of Anatomy*, *216*(3), 335–343.

Kapałczyńska M, Kolenda T, Przybyła W, Zajączkowska M, Teresiak A, Filas V, et al. 2D and 3D cell cultures – a comparison of different types of cancer cell cultures2016.

Kaushik G, Ponnusamy MP, Batra SK. Concise Review: Current Status of Three Dimensional Organoids as Preclinical Models. Stem Cells. 2018;36(9):1329-40.

Kerr M, Scott HE, Groselj B, Stratford MR, Karaszi K, Sharma NL, et al. Deoxycytidine kinase expression underpins response to gemcitabine in bladder cancer. Clin Cancer Res. 2014;20(21):5435-45.

Khandelwal P, Abraham SN, Apodaca G. Cell biology and physiology of the uroepithelium. Am J Physiol Renal Physiol. 2972009. p. F1477-501.

Kim CK, Yang VW, Bialkowska AB. The Role of Intestinal Stem Cells in Epithelial Regeneration Following Radiation-Induced Gut Injury. Curr Stem Cell Rep. 32017. p. 320-32.

Kim SJ, Kim EK, Song DH. Effects of bone marrow aspirate concentrate and platelet rich plasma on patients with partial tear of the rotator cuff tendon. J Orthop Surg Res. 2018;13(1):1.

Kirsch, David G et al. “p53 controls radiation-induced gastrointestinal syndrome in mice independent of apoptosis.” *Science (New York, N.Y.)* vol. 327,5965 (2010): 593-6.

Kleinman HK, McGarvey ML, Liotta LA, Robey PG, Tryggvason K, Martin GR. Isolation and characterization of type IV procollagen, laminin, and heparan sulfate proteoglycan from the EHS sarcoma. Biochemistry. 1982;21(24):6188-93.

Kosinski C, Li VS, Chan AS, Zhang J, Ho C, Tsui WY, et al. Gene expression patterns of human colon tops and basal crypts and BMP antagonists as intestinal stem cell niche factors. Proc Natl Acad Sci U S A. 2007;104(39):15418-23.

Kreplak L, Wang H, Aebi U, Kong XP. Atomic force microscopy of Mammalian urothelial

surface. J Mol Biol. 2007;374(2):365-73.

Lamarche, B. J., Orazio, N. I., & Weitzman, M. D. (2010). The MRN complex in double-strand break repair and telomere maintenance. *FEBS Letters*, *584*(17), 3682–3695.

Laubach JP, Moreau P, San-Miguel JF, Richardson PG. Panobinostat for the Treatment of Multiple Myeloma. Clin Cancer Res. 2015;21(21):4767-73.

Leibowitz BJ, Qiu W, Liu H, Cheng T, Zhang L, Yu J. Uncoupling p53 functions in radiation induced intestinal damage via PUMA and p21. *Mol Cancer Res*. 2011;9(5):616–625. doi:10.1158/1541-7786.MCR-11-0052

Leushacke M, Barker N. Ex vivo culture of the intestinal epithelium: strategies and applications. Gut. 2014;63(8):1345-54.

Liberman, D., Mehus, B., & Elliott, S. P. (2014). Urinary adverse effects of pelvic radiotherapy. *Translational Andrology and Urology*, *3*(2), 186–195.

Lieber, M. R. (2011). The mechanism of DSB repair by the NHEJ. *Molecular Microbiology*, (3), 181–211. https://doi.org/10.1146/annurev.biochem.052308.093131.The

Liu Q, Gheorghiu L, Drumm M, Clayman R, Eidelman A, Wszolek MF, et al. PARP-1 inhibition with or without ionizing radiation confers reactive oxygen species mediated cytotoxicity preferentially to cancer cells with mutant TP53. Oncogene. 2018;37(21):2793-805.

Liu, Ting, and Jun Huang. “DNA End Resection: Facts and Mechanisms.” *Genomics, proteomics & bioinformatics* vol. 14,3 (2016): 126-130.

Liu Y, Chen YG. 2D- and 3D-Based Intestinal Stem Cell Cultures for Personalized Medicine. Cells. 2018;7(12).

Mackey JR, Mani RS, Selner M, Mowles D, Young JD, Belt JA, et al. Functional nucleoside transporters are required for gemcitabine influx and manifestation of toxicity in cancer cell lines. Cancer Res. 1998;58(19):4349-57.

Majewski W, Tarnawski R. Acute and Late Toxicity in Radical Radiotherapy for Bladder Cancer. Clinical Oncology. 2009;21(8):598-609.

Marshman E, Booth C, Potten CS. The intestinal epithelial stem cell. Bioessays. 2002;24(1):91-8.

McCauley, H. A., & Wells, J. M. (2017). Pluripotent stem cell-derived organoids: Using principles of developmental biology to grow human tissues in a dish. *Development (Cambridge)*, *144*(6), 958–962.

Mehta, I. S., Kulashreshtha, M., Chakraborty, S., Kolthur-Seetharam, U., & Rao, B. J. (2013). Chromosome territories reposition during DNA damage-repair response. *Genome Biology*, *14*(12). https://doi.org/10.1186/gb-2013-14-12-r135

Merritt AJ, Potten CS, Kemp CJ, Hickman JA, Balmain A, Lane DP, et al. The role of p53 in spontaneous and radiation-induced apoptosis in the gastrointestinal tract ofnormal and p53-deficient mice. Cancer Res. 1994;54(3):614-7.

Michaud DS. Chronic inflammation and bladder cancer. Urol Oncol. 2007;25(3):260-8.

Mimitou, Eleni P, and Lorraine S Symington. "DNA end resection: many nucleases make light work." *DNA repair* vol. 8,9 (2009): 983-95.

Mittal M, Siddiqui MR, Tran K, Reddy SP, Malik AB. Reactive Oxygen Species in Inflammation and Tissue Injury. Antioxid Redox Signal. 202014. p. 1126-67.

Mollà, M., Gironella, M., Miquel, R., Tovar, V., Engel, P., Biete, A., … Panés, J. (2003). Relative roles of ICAM-1 and VCAM-1 in the pathogenesis of experimental radiation-induced intestinal inflammation. *International Journal of Radiation Oncology, Biology, Physics*, *57*(1), 264–273. https://doi.org/10.1016/s0360-3016(03)00523-6

Moonen L, vd Voet H, de Nijs R, Horenblas S, Hart AA, Bartelink H. Muscle-invasive bladder cancer treated with external beam radiation: influence of total dose,overall treatment time, and treatment interruption on local control. Int J Radiat Oncol Biol Phys. 1998;42(3):525-30.

Moorefield E, Eric Blue R, L. Quinney N, Gentzsch M, Ding S. Generation of renewable mouse intestinal epithelial cell monolayers and organoids for functional analyses. 2018.

Nakamura T. Recent progress in organoid culture to model intestinal epithelial barrier functions. Int Immunol. 2019;31(1):13-21.

NICE. (2015). NICE Guidelines, Bladder cancer: diagnosis and management. *NICE Guidelines*, (February), 101.

Pastula A, Middelhoff M, Brandtner A, Tobiasch M, Höhl B, H. Nuber A, et al. Three

Dimensional Gastrointestinal Organoid Culture in Combination with Nerves or Fibroblasts: A Method to Characterize the Gastrointestinal Stem Cell Niche2016. p. 1-16.

Ooft, S. N., Weeber, F., Dijkstra, K. K., McLean, C. M., Kaing, S., van Werkhoven, E., … Voest, E. E. (2019). Patient-derived organoids can predict response to chemotherapy in metastatic colorectal cancer patients. *Science Translational Medicine*, *11*(513).

Phan TP, Crane CH, Janjan NA, Vrdoljak E, Milas L, Mason KA. WR-2721 reduces intestinal toxicity from concurrent gemcitabine and radiation treatment. Int J Pancreatol. 2001;29(1):19-23.

Plataniotis GA, Dale RG. Radio-chemotherapy for bladder cancer: Contribution of chemotherapy on local control. World J Radiol. 2013;5(8):267-74.

Platt, A. M. (2017). Immunity in the Gut Immunity in the Gut. Viral Gastroenteritis, 351(6279), 1329–1333.

Prati, F., Mallus, M. T., Imola, F., & Albertucci, M. (2013). Optical coherence tomography (OCT). *Catheter-Based Cardiovascular Interventions: A Knowledge-Based Approach*, *254*(5035), 363–375. https://doi.org/10.1007/978-3-642-27676-7_21

Reya T, Clevers H. Wnt signalling in stem cells and cancer. Nature. 2005;434(7035):843 50.

Rogler G, Andus T. Cytokines in inflammatory bowel disease. World J Surg. 1998;22(4):382-9.

Ruchinskas A, Clinton J. Protocol for the thawing, expansion, and cryopreservation of mouse small intestinal organoids. 2018.

Sanli O, Dobruch J, Knowles MA, Burger M, Alemozaffar M, Nielsen ME, et al. Bladder cancer. Nat Rev Dis Primers. 2017;3:17022.

Santivasi, W. L., & Xia, F. (2014). Ionizing radiation-induced DNA damage, response, and repair. *Antioxidants and Redox Signaling*, *21*(2), 251–259. https://doi.org/10.1089/ars.2013.5668

Sato T, Vries RG, Snippert HJ, van de Wetering M, Barker N, Stange DE, et al. Single Lgr5 stem cells build crypt-villus structures in vitro without a mesenchymal niche. Nature. 2009;459(7244):262-5.

Satoh Y, Yamano M, Matsuda M, Ono K. Ultrastructure of Paneth cells in the intestine of various mammals. J Electron Microsc Tech. 1990;16(1):69-80.

Schepers AG, Vries R, van den Born M, van de Wetering M, Clevers H. Lgr5 intestinal stem cells have high telomerase activity and randomly segregate their chromosomes. Embo j. 2011;30(6):1104-9.

Sean P. Elliott, B. S. M. (2013). Long-term urinary adverse effects of pelvic radiotherapy Sean, *31*(9), 1713–1723. https://doi.org/10.1109/TMI.2012.2196707.Separate

Sebbagh M, Hamelin J, Bertoglio J, Solary E, Breard J. Direct cleavage of ROCK II by granzyme B induces target cell membrane blebbing in a caspase-independent manner. J Exp Med. 2005;201(3):465-71.

Shadad AK, Sullivan FJ, Martin JD, Egan LJ. Gastrointestinal radiation injury: symptoms, risk factors and mechanisms. World J Gastroenterol. 2013;19(2):185 98.

Shaykhiev R, Bals R. Interactions between epithelial cells and leukocytes in immunity and tissue homeostasis. J Leukoc Biol. 2007;82(1):1-15.

Silverthorn, D. U., Johnson, B. R., Ober, W. C., Ober, C. E., Impagliazzo, A., & Silverthorn, A. C. (n.d.). *Human physiology : an integrated approach*.

Smith AB, Deal AM, Woods ME, Wallen EM, Pruthi RS, Chen RC, et al. Muscle invasive bladder cancer: evaluating treatment and survival in the National Cancer Data Base. BJU Int. 2014;114(5):719-26.

Smith JA, Jr., Whitmore WF, Jr. Regional lymph node metastasis from bladder cancer. J Urol. 1981;126(5):591-3.

Snippert HJ, van der Flier LG, Sato T, van Es JH, van den Born M, Kroon-Veenboer C, et al. Intestinal crypt homeostasis results from neutral competition between symmetrically dividing Lgr5 stem cells. Cell. 2010;143(1):134-44.

Sonis ST, Elting LS, Keefe D, Peterson DE, Schubert M, Hauer-Jensen M, et al. Perspectives on cancer therapy-induced mucosal injury: pathogenesis, measurement, epidemiology, and consequences for patients. Cancer. 2004;100(9 Suppl):1995-2025.

Stein JP, Lieskovsky G, Cote R, Groshen S, Feng AC, Boyd S, et al. Radical cystectomy in the treatment of invasive bladder cancer: long-term results in 1,054 patients. J Clin Oncol. 2001;19(3):666-75.

Tian H, Biehs B, Warming S, Leong KG, Rangell L, Klein OD, et al. A reserve stem cell population in small intestine renders Lgr5-positive cells dispensable. Nature. 2011;478(7368):255-9.

Torras N, García-Díaz M, Fernández-Majada V, Martínez E. Mimicking Epithelial Tissues in Three-Dimensional Cell Culture Models. Front Bioeng Biotechnol. 2018;6.

Umar S. Intestinal Stem Cells. Curr Gastroenterol Rep. 2010;12(5):340-8.

Van Batavia J, Yamany T, Molotkov A, Dan H, Mansukhani M, Batourina E, et al. Bladder cancers arise from distinct urothelial sub-populations. Nat Cell Biol. 2014;16(10):982-91, 1-5.

van der Flier LG, Clevers H. Stem cells, self-renewal, and differentiation in the intestinal epithelium. Annu Rev Physiol. 2009;71:241-60.

van Osch FH, Jochems SH, van Schooten FJ, Bryan RT, Zeegers MP. Quantified relations between exposure to tobacco smoking and bladder cancer risk: a meta analysis of 89 observational studies. Int J Epidemiol. 2016;45(3):857-70.

Wang S, Gao D, Chen Y. The potential of organoids in urological cancer research. Nat Rev Urol. 2017;14(7):401-14.

Wang, Linlin et al. "Self-renewal of human embryonic stem cells requires insulin-like growth factor-1 receptor and ERBB2 receptor signaling." *Blood* vol. 110,12 (2007): 4111-9. doi:10.1182/blood-2007-03-082586

Welty CJ, Sanford TH, Wright JL, Carroll PR, Cooperberg MR, Meng MV, et al. The Cancer of the Bladder Risk Assessment (COBRA) score: Estimating mortality after radical cystectomy. Cancer. 2017;123(23):4574-82.

Wright, William Douglass, and Wolf-Dietrich Heyer. "Rad54 functions as a heteroduplex DNA pump modulated by its DNA substrates and Rad51 during D loop formation." *Molecular cell* vol. 53,3 (2014): 420-32.

Wu XR, Kong XP, Pellicer A, Kreibich G, Sun TT. Uroplakins in urothelial biology, function, and disease. Kidney Int. 2009;75(11):1153-65.

Wyatt, M. D., & Pittman, D. L. (2006). Methylating agents and DNA repair responses: Methylated bases and sources of strand breaks. *Chemical Research in Toxicology*, *19*(12), 1580–1594.

Yan KS, Chia LA, Li X, Ootani A, Su J, Lee JY, et al. The intestinal stem cell markers Bmi1 and Lgr5 identify two functionally distinct populations. Proc Natl Acad Sci U S A. 2012;109(2):466-71.

Yao, Y., Xu, X., Yang, L., Zhu, J., Wan, J., Shen, L.,Hua, G. (2019). Patient-Derived Organoids Predict Chemoradiation Responses of Locally Advanced Rectal Cancer. Cell

Stem Cell.

Young, Barbara, et al. *Wheater's Functional Histology : A Text and Colour Atlas*, Elsevier, 2019. ProQuest Ebook Central,

Yu, J., Wang, Z., Kinzler, K. W., Vogelstein, B., & Zhang, L. (2003). PUMA mediates the apoptotic response to p53 in colorectal cancer cells. *Proceedings of the National Academy of Sciences of the United States of America, 100*(4), 1931–1936.

Zhang Y. Understanding the gender disparity in bladder cancer risk: the impact of sex hormones and liver on bladder susceptibility to carcinogens. J Environ Sci Health C Environ Carcinog Ecotoxicol Rev. 2013;31(4):287-304.

7. APPENDIX

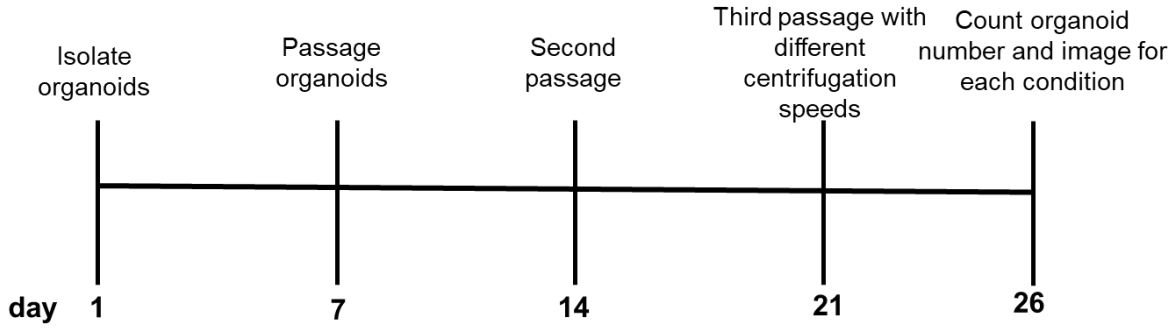

Figure S1. Timeline for centrifugation experiment

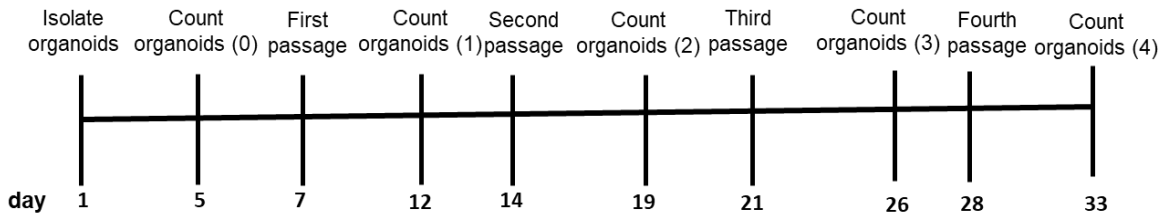

Figure S2. Timeline for expansion experiment

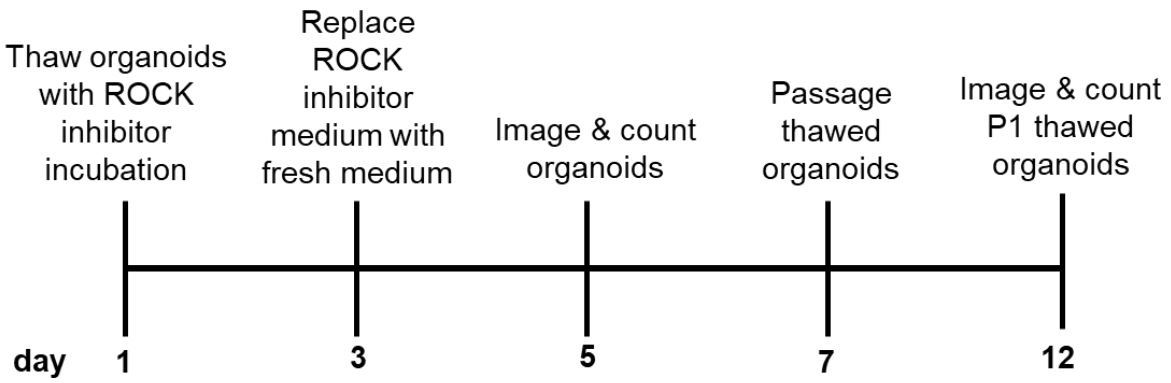

Figure S3. Timeline for cryopreservation experiment

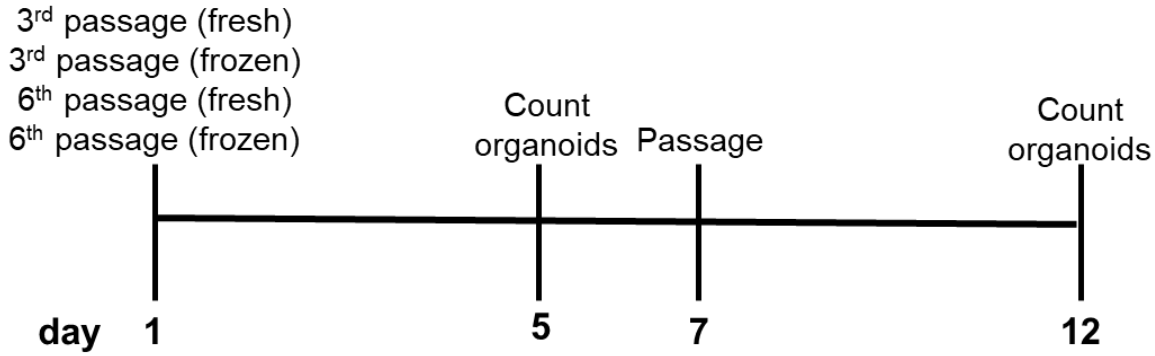

Figure S4. Timeline for frozen/fresh expansion experiment

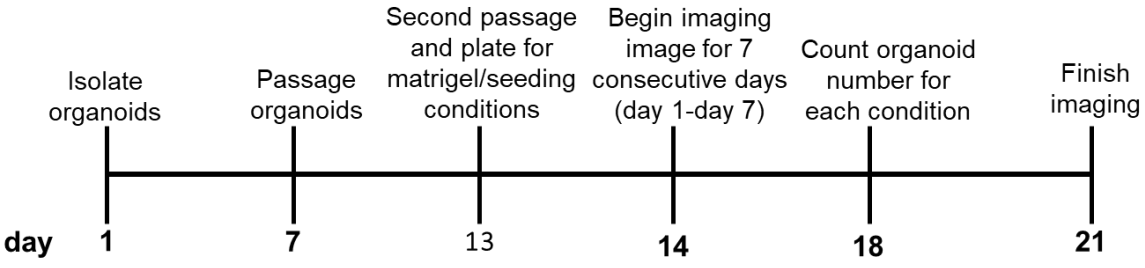

Figure S5. Timeline for organoid fragment seeding experiment

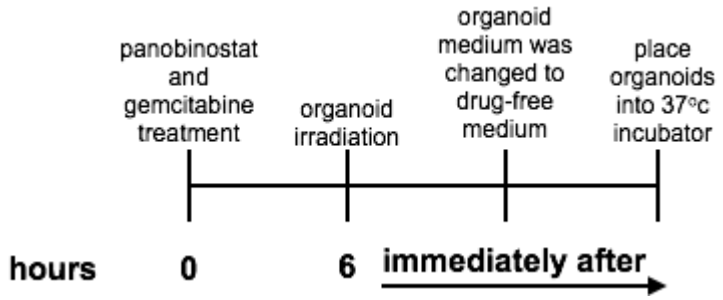

Figure S6. Timeline for chemoradiation experiment

Table S1.1. Organoid quantities for IR experiment

Organoid number		
Control	**n1**	77
	n2	48
0.5 Gy	**n1**	57
	n2	74
	n3	45
1 Gy	**n1**	67
	n2	44
	n3	56

2 Gy	**n1**	75
	n2	67
	n3	47
4 Gy	**n1**	72
	n2	58
	n3	56
6 Gy	**n1**	41
	n2	58
	n3	58

Table S1.2. Organoid size for IR experiment

Mean organoid area relative to pre-IR (%)							
Days post-IR		**0**	**1**	**2**	**3**	**4**	**5**
Control	**mean**	100	112.8	141.7	156	158.5	190
	std	0	7.6	3.5	6.6	8.5	13.6
0.5 Gy	**mean**	100	112	123	137.7	153.6	186.1
	std	0	7.3	3.9	1.5	2.5	16.6
1 Gy	**mean**	100	106.4	111.9	129.7	146.8	169
	std	0	3.9	5.3	9	5.9	14
2 Gy	**mean**	100	104.3	109.9	112.8	128.3	153.7
	std	0	6.5	11.9	6.7	6.2	3
4 Gy	**mean**	100	90.2	87	85.9	84.1	84.2
	std	0	8.1	4.1	4.6	2.7	3.2
6 Gy	**mean**	100	97.1	95.2	92.5	88.1	85.8
	std	0	4	4.5	3.6	1.7	3.5

Table S2.1. Organoid quantities for gemcitabine experiment

Organoid number				
Isolation		**1**	**2**	**3**
Control	n1	22	53	88
	n2	21	74	72
	n3	21	-	67
	n4	-	-	65
2.5 nM	n1	46	62	76
	n2	43	49	82
	n3	53	70	84
5 nM	n1	45	57	69
	n2	51	56	72
	n3	47	40	85
10 nM	n1	41	44	56
	n2	30	50	53
	n3	39	70	63
25 nM	n1	45	88	77
	n2	48	60	71
	n3	50	52	31
50 nM	n1	38	54	71
	n2	37	67	90
	n3	42	78	75

Table S2.2. Organoid size for gemcitabine experiment

Mean organoid area relative to pre-treatment (%)							
Days post-IR		**0**	**1**	**2**	**3**	**4**	**5**
Control	mean	100	129.5	149.2	160.3	172.2	183.5

	std	0	24	25.5	26	19.1	16.4
2.5 nM	mean	100	120.5	126.1	162.2	182.7	199
	std	0	13.5	16.9	47.8	52.1	53.1
5 nM	mean	100	115.1	120.8	133.4	148.5	166.1
	std	0	8.8	17.1	28	44.4	52
10 nM	mean	100	108.2	118.6	139.2	156.8	171.7
	std	0	6.4	11.8	23.5	30.1	29.3
25 nM	mean	100	99.9	90.9	92.3	86.2	82.1
	std	0	14.3	10.9	13.9	11.45	11.4
50 nM	mean	100	98.3	93.5	91	87.6	81.6
	std	0	5.2	3.1	3.8	6.8	7.9

Table S3.1. Organoid quantities for panobinostat experiment

Organoid number				
Isolation		**1**	**2**	**3**
Control	n1	22	53	88
	n2	21	74	72
	n3	21	-	67
	n4	-	-	65
6.25 nM	n1	37	51	66
	n2	30	57	62
	n3	43	57	71
12.5 nM	n1	36	58	63
	n2	27	46	62
	n3	41	53	25
25 nM	n1	28	48	63

	n2	31	49	82
	n3	45	56	100
50 nM	n1	49	48	73
	n2	26	49	66
	n3	39	59	76
100 nM	n1	44	46	67
	n2	58	51	31
	n3	59	48	76

Table S3.2. Organoid size for panobinostat experiment

Mean organoid area relative to pre-treatment (%)							
Days post-IR		**0**	**1**	**2**	**3**	**4**	**5**
Control	mean	100	129.5	149.2	160.3	172.2	183.5
	std	0	24	25.5	26	19.1	16.4
6.25 nM	mean	100	137.6	171.7	199	239.3	232
	std	0	15.7	44.8	49.7	40.67	32.6
12.5 nM	mean	100	130.2	181.5	211.5	228.8	210.7
	std	0	15	37.2	54.3	62.7	50
25 nM	mean	100	110.7	119.4	158.5	182.3	203.9
	std	0	7.8	12.24	52.6	61.9	78
50 nM	mean	100	111.5	106.4	104.1	100.1	92.7
	std	0	23	19.7	19.4	17.2	10.6
100 nM	mean	100	124.3	116.6	106.9	97.1	90.2
	std	0	44.9	37.1	27.7	16.2	13.4

Table S4.1. Organoid quantities for preliminary IR+pan experiment

Organoid number		
Control	n1	25
	n2	22
	n3	28
0.5 Gy	n1	28
	n2	48
	n3	38
1 Gy	n1	32
	n2	25
	n3	46
2 Gy	n1	29
	n2	27
	n3	26
4 Gy	n1	40
	n2	30
	n3	32
6 Gy	n1	46
	n2	37
	n3	26

Table S4.2. Organoid size for preliminary IR+pan experiment

Mean organoid area relative to pre-treatment (%)						
Radiation Dose (Gy)	**control**	**0.5**	**1**	**2**	**4**	**6**
mean	152.8	131.3	126.8	111.6	96.9	94.9
std	15	10	14.7	4.8	2.3	4.2

Table S5.1. Organoid quantities for IR+gem experiment

Organoid number			
Concentration		**10 nM**	**2.5 nM**
0.5 Gy	n1	64	84
	n2	61	66
	n3	63	47
	n4	59	61
1 Gy	n1	84	51
	n2	63	50
	n3	58	75
	n4	83	61
2 Gy	n1	70	56
	n2	86	71
	n3	53	70
	n4	51	73

Table S5.2. Organoid size for IR+gem experiment

Mean organoid area relative to pre-treatment (%)					
Radiation dose (Gy)		**control**	**0.5**	**1**	**2**
2.5 nM	mean	170.6	132.8	129.4	115.3

	std	26.2	25.1	23	13.7
10 nM	mean	170.6	130.9	122.4	112.6
	std	26.23	25	21	12.1

Table S6.1. Organoid quantities for IR+pan experiment

Organoid number			
Concentration		**25 nM**	**6.25 nM**
0.5 Gy	n1	59	55
	n2	42	62
	n3	58	67
	n4	75	50
1 Gy	n1	58	59
	n2	69	67
	n3	57	49
	n4	49	58
2 Gy	n1	81	68

	n2	79	58
	n3	71	87
	n4	68	62

Table S6.2. Organoid size for IR+pan experiment

Mean organoid area relative to pre-treatment (%)					
Radiation Dose (Gy)		**control**	**0.5**	**1**	**2**
6.25 nM	mean	170.6	131.3	124.44	108.4
	std	26.2	16.3	21	12.4
25 nM	mean	170.6	127.4	128.2	119
	std	26.2	20.3	19.9	18.2